AN ABSTRACT OF THE THESIS OF

Charles Earl Bassett, Jr. for the degree of Doctor of Philosophy
(Name of Student) (Degree)

in Mechanical and Metallurgical Engr. presented on August 8, 1974
(Major Dept.) (Date)

Title: AN EXPERIMENTAL STUDY OF FORCED CONVECTION HEAT TRANSFER TO NON-NEWTONIAN FLUIDS IN THE THERMAL ENTRY REGION OF A HORIZONTAL, UNIFORMLY HEATED, CIRCULAR PIPE

Redacted for Privacy

Abstract approved by: James R. Welty

An experimental study was made of heat transfer to the laminar flow of aqueous solutions of sodium carboxymethylcellulose (CMC) and polyethylene oxide, coagulant grade (polyox) in uniformly heated, horizontal pipes. Polymer concentration was varied such that several stages of pseudoplastic behavior were attained. A marked contrast in the variation of viscous properties with temperature occurred in the various fluids. Fluid rheology was determined using a Haake rotational viscometer, and a unique method of applying the results to conditions in the pipe flow was employed.

Velocity profiles were fully-developed prior to entry to heated sections which were 1.384 cm and 2.680 cm in diameter and 303.5 cm in length. Mass flow rates of 98.5 - 416 g/sec and heat fluxes of

1.18 - 5.24 watts/cm^2 produced local Nusselt numbers of 10.9 - 54.9 at local Graetz numbers of 225 - 38,000.

It was found that local wall shear rates control the rate of heat transfer. These shear rates increase with increasing pseudoplasticity; however, they are more substantially increased due to the temperature effect on viscous properties. Increases in the rate of heat transfer over the temperature-independent property solution of 38% at Gz_x = 625, 15% at Gz_x = 24,500, and 7% at Gz_x = 38,000 were obtained in cases where the effect of natural convection was not evident. In a case where natural convection explicitly affected the rate of heat transfer, a 62% increase over the temperature-independent property solution was obtained at Gz_x = 230.

Other evidence of the existence of secondary flow patterns was acquired. Flow patterns appeared far upstream of full thermal development, even in the most viscous fluids.

In the absence of natural convection, the correlation

$$Nu_x = 1.848\, Gz_x^{1/3 - 0.0300/\delta_x}$$

is recommended.

The effect of viscous heating on the rate of heat transfer was found to be negligible throughout the investigation. Maximum Brinkmann number was 4.22×10^{-3}.

An Experimental Study of Forced Convection Heat Transfer to Non-Newtonian Fluids in the Thermal Entry Region of a Horizontal, Uniformly Heated, Circular Pipe

by

Charles Earl Bassett Jr.

A THESIS

submitted to

Oregon State University

in partial fulfillment of
the requirements for the
degree of

Doctor of Philosophy

Completed August 1974

Commencement June 1975

APPROVED:

Redacted for Privacy

Redacted for Privacy

Professor of Mechanical Engineering
in charge of major

Redacted for Privacy

Head of Department of Mechanical and Metallurgical Engineering

Redacted for Privacy

Redacted for Privacy

Dean of Graduate School

Date thesis is presented August 8, 1974

Typed by Illa W. Atwood for Charles Earl Bassett Jr.

ACKNOWLEDGMENTS

Several people have been instrumental in bringing this research to a conclusion. Dr. James R. Welty has shown great patience while providing advice and encouragement and committing scarce funds for support.

My wife, Joyce, has somehow managed to endure without losing her patience. Not once has she complained.

Jack Kellogg provided critical advice in the construction of the apparatus. Dale Peinecke assisted in drawing the figures. Mrs. Illa Atwood typed the manuscript.

Funds which, in part, covered the costs of this investigation were furnished by the Oregon State University Engineering Experiment Station and the Oregon State University Unsponsored Research Fund.

TABLE OF CONTENTS

		Page
1.	INTRODUCTION TO HEAT TRANSFER TO STEADY, LAMINAR, HORIZONTAL PIPE FLOWS	1
	Constant Property Solution	1
	Effect of Temperature Variation of Viscosity	2
	Effect of Secondary Flow Due to Buoyancy	5
	Effects of Non-Newtonian Behavior	17
	Non-Newtonian Effects: Isothermal Tube Wall	21
	Non-Newtonian Effects: Uniform Heat Flux	23
	Buoyancy in Non-Newtonian Pipe Flows	30
	Conclusion	31
2.	OBJECTIVE AND DESIGN OF EXPERIMENT	32
	Objective of Present Study	32
	Design of Experiment	32
3.	DESCRIPTION, DESIGN, AND CONSTRUCTION OF APPARATUS	39
	Flow System	39
	Test Section Heaters	44
	Selection of Heaters	44
	Design of Heaters	49
	Construction of Heaters	52
	Heater Power Supply	56
	Measurement System	56
	Thermocouple Circuit	56
	Power and Flow Measurement	61
	Viscometer and Circulator	62
	Thermocouple Calibration System	64
4.	METHOD OF TESTING	67
	Calibration of Test Section Thermocouples	67
	Mixing of Polymers	68

TABLE OF CONTENTS (cont.)

		Page
	Test Procedure	70
	Viscometer Procedure	71
5.	REDUCTION OF DATA	73
	Temperature Data	73
	Rheological Data	76
	Development of the Constitutive Equation	76
	Application to Tube Flow	81
	Data from Other Sources	88
	Dimensionless Parameters	89
6.	RESULTS	93
	Calibration of Thermocouples	93
	Viscometry	95
	Heat Transfer	102
7.	ANALYSIS OF ERROR	121
8.	CONCLUSIONS AND RECOMMENDATIONS	129
	NOMENCLATURE	132
	BIBLIOGRAPHY	137
	APPENDICES	
	A. Axial Conduction in Tube Wall	148
	B. Effect of Heating Gaps on Wall Temperature	151
	C. Listing of Computer Programs	157
	D. Listing of Viscometer Data	169
	E. Listing of Reduced Test Data	172
	F. Listing of Parameters	180

LIST OF FIGURES

Figure		Page
1.1	Velocity profiles for isothermal, heated, and cooled flows.	3
1.2	Flow cross section showing vortices which comprise the secondary flow.	6
1.3	Typical velocity and temperature profiles for air showing the effects of secondary flow.	8
1.4	Plot showing typical findings from recent investigations of horizontal pipe flows.	11
3.1	Schematic diagram of test apparatus.	38
3.2	View of test apparatus showing pump, feed tank, tank mixer, weigh tank, and scale.	45
3.3	View of entrance piping, heat exchanger, static mixer, mixer elements, and thermocouple reference junctions with ice bath container.	45
3.4	Test sections with surrounding insulation removed.	46
3.5	Schematic diagram of heater layout for small test section.	50
3.6	Schematic diagram of heater layout for large test section.	51
3.7	Method of joining element pairs that were temporarily terminated at each thermocouple location.	55
3.8	Schematic diagram of thermocouple circuit.	57
3.9	View of instrumentation, power supplies, and viscometer.	63
3.10	Schematic diagram of test apparatus modified for wall thermocouple calibration.	65
3.11	Flanged adapters at entrance end of test section used during thermocouple calibration.	66

LIST OF FIGURES (cont.)

Figure		Page
5.1	Effect of heater gaps on wall temperature.	74
5.2	Geometry of the Couette system under consideration. Gap size is exaggerated.	77
5.3	Typical behavior of constitutive equations obtained from the viscometric data.	83
5.4	Interpolation between adjacent constitutive equations.	83
6.1	Calibration curve for bottom thermocouple located 18 inches from entrance to small test section.	94
6.2	Calibration curve for top thermocouple located 72 inches from entrance to large test section.	94
6.3	Viscometry results for 3.0% CMC solution. From the top, data were taken at 22.0, 32.3, 65.4, and 82.4 C.	96
6.4	Viscometry results for 5.4% CMC solution. From the top, data were taken at 20, 30, 40, 50, 60, 70, and 83.2 C.	97
6.5	Viscometry results for 1% Polyox solution. From the top, data were taken at 20, 30, 40, 50, 60, 70, and 83.2 C.	98
6.6	Viscometry results for 1.6% Polyox solution. From the top, data were taken at 20, 30, 40, 50, 60, 70, and 83.2 C.	99
6.7	Viscometry results for 2.4% Polyox solution. From the top, data were taken at 20, 30, 40, 50, 60, 70, and 83.2 C.	100
6.8	Viscometry results for 2.4% Polyox (degraded) solution. From the top, data were taken at 20, 30, 40, 50, 60, 70, and 84.0 C.	101

LIST OF FIGURES (cont.)

Figure		Page
6.9	Heat transfer results for 5.4% CMC and 2.4% Polyox at low mass flow rate in large test section.	104
6.10	Heat transfer results for 5.4% CMC and 2.4% Polyox at moderate mass flow rate in large test section.	105
6.11	Heat transfer results for 5.4% CMC and 2.4% Polyox at low mass flow rate in small test section.	106
6.12	Heat transfer results for 5.4% CMC and 2.4% Polyox at moderate mass flow rate in small test section.	107
6.13	Heat transfer results for 2.4% Polyox (degraded) at high mass flow rate.	110
6.14	Heat transfer results for 2.4% Polyox (degraded) at moderate flow rate and low power.	111
6.15	Comparison of results for 3.0% CMC in small test section at low flow rate with solution by Cochrane.	113
6.16	Heat transfer results for 3.0% CMC and 1.0% Polyox at low flow rate in large test section.	114
6.17	Wall temperatures (uncorrected for gap effect) for flow of 5.4% CMC solution in large test section at low flow rate.	117
6.18	Heat transfer results for all data.	118
6.19	Best correlation of data which did not show an obvious effect from natural convection.	119
A.1	Model for heat balance on tube wall segment.	148
B.1	Model of uniform heat flux with gaps (above) and its equivalent below.	152
B.2	Plot showing behavior of functions which, when superimposed, give $T_w - T_o$.	154
C.1	Flow chart.	157

AN EXPERIMENTAL STUDY OF FORCED CONVECTION HEAT TRANSFER TO NON-NEWTONIAN FLUIDS IN THE THERMAL ENTRY REGION OF A HORIZONTAL, UNIFORMLY HEATED, CIRCULAR PIPE

1. INTRODUCTION TO HEAT TRANSFER TO STEADY, LAMINAR, HORIZONTAL PIPE FLOWS

The rigorous analysis of heat transfer in the thermal entry region of viscous, horizontal, laminar pipe flows is extremely complex. The problem involves accounting for the following contributions:

1. The basic conduction mechanism at the boundary.

2. The temperature dependence of transport properties, particularly viscosity.

3. The shear rate dependence of viscosity in non-Newtonian fluids.

4. The development of a secondary transverse flow due to buoyancy.

5. A tertiary normal stress effect brought on by item 4 in viscoelastic fluids.

Constant Property Solution

An analytical solution which considers only item 1 on the above list was first obtained by Graetz (30) in 1885. Fully developed flow

was specified prior to entry to an isothermally heated or cooled section. Sellars, Tribus, and Klein (86) extended the Graetz solution to the case of a uniformly heated or cooled section. Siegel, Sparrow, and Hallman (92) obtained an improved solution of the latter case.

The asymptotic solutions to the Graetz problem applicable to the two thermal regimes are given by (43, p. 372-373):

Thermal Entry Region: $(Gz_x > 50\pi)$ $$Nu_x = C_1 Gz_x^{1/3} \quad (1.1)$$

Fully Developed Region: $(Gz_x < 2\pi)$ $$Nu_\infty = C_2 \quad (1.2)$$

where C_1 and C_2 are 1.17 and 3.656 respectively for an isothermal boundary and 1.41 and 4.364 respectively for a uniformly heated boundary.

Leveque (48) postulated that, in the thermal entry region, heat transfer depends only on transport conditions near the boundary. He obtained results identical to those of Graetz (in the thermal entry region) by using a linear velocity profile in the vicinity of the wall.

Effect of Temperature Variation of Viscosity

Most liquids become less viscous when heated. In a fully-developed isothermal pipe flow, the shear stress increases linearly from zero at the center. In non-isothermal pipe flow, the shear stress distribution remains essentially linear; however, local heating

(or cooling) near the wall changes the viscosity. The effect of heating, as shown in Figure 1.1, is to steepen the velocity profile near the wall. The opposite effect occurs during cooling. The result is to increase the rate of heat transfer during heating and to depress it during cooling.

Sieder and Tate (91) correlated data for oils heated and cooled in isothermal horizontal tubes. They added a large number of isothermal data from other investigations and suggested the correlation,

$$Nu_m = 2.0 Gz^{1/3} \left(\frac{\eta_b}{\eta_w} \right)^{0.14} \qquad (1.3)$$

where all properties except η_w are evaluated at the bulk temperature. The resulting curve falls slightly above a correlation derived from the Graetz solution (43, p. 377).

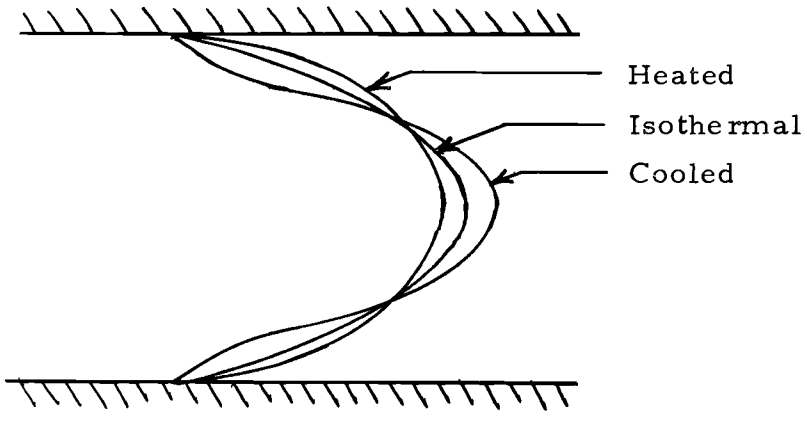

Figure 1.1. Velocity profiles for isothermal, heated, and cooled flows.

Pigford (80) obtained a solution for the flow of viscous fluids in isothermal vertical tubes by extending the Leveque solution to include the effects of variable viscosity and buoyancy. The analysis resulted in

$$Nu_m = 1.75\,\delta^{1/3} Gz^{1/3} \qquad (1.4)$$

where $\delta = \dot{\gamma}_w/8V/D$ with $\dot{\gamma}_w$ a function of Gz, $\frac{\eta_b}{\eta_w}$, and Gr. The solution given for δ was applicable to vertical flows; however, the introduction of the term has been useful in subsequent horizontal flow correlations.

Yang (107) has applied an integral technique to the problem of temperature dependent viscosity pipe flows. He obtained solutions for the cases of both an isothermal wall and uniform heat flux. His results show that the latter case has the greatest potential for divergence from the constant property solution. However, the viscosity models were apparently chosen for computational convenience in that they are not readily obtained from viscometric data.

Test (97) analyzed the same problem using a finite difference solution of the boundary layer equations. He also attempted to confirm his results by experiment. The fluid chosen for the model and the test was SAE 60 oil. The analysis showed that deviation from the constant property solution by as much as 50% was possible. The experimental data were greatly scattered; however, an attempt was

made to correlate both sets of data with

$$Nu_{\ell} = 1.517 \left(\frac{\eta_b}{\eta_w} \right)^m Gz_{\ell}^{1/3} \qquad (1.5)$$

where m = 0.05 for heating and 1/3 for cooling. Except for η_w, all properties are evaluated at the bulk temperature.

Effect of Secondary Flow Due to Buoyancy

Early investigations of natural convection in horizontal flows were all experimental. The complexity of the problem discouraged analytical investigation until the digital computer became available. A shortcoming of experimental investigations is the difficulty in isolating the contributions to heat transfer from each effect. Consequently, most of the insight regarding the effect of the secondary flow has come from recent analytical work. None of the investigators thus far has attempted to add the effects of temperature variation of viscosity or non-Newtonian flow to his model. In addition, almost all of the analytical work has been for the thermally fully developed region. There is evidence that significant secondary effects occur before leaving the thermal entry region.

Visual studies (67) of the flow of air in a uniformly heated horizontal tube for $Gr^* > 40,000$ show the presence of a pair of vortices in the cross section (see Figure 1.2). The vortices are centered symmetrically on either side of the vertical centerline and

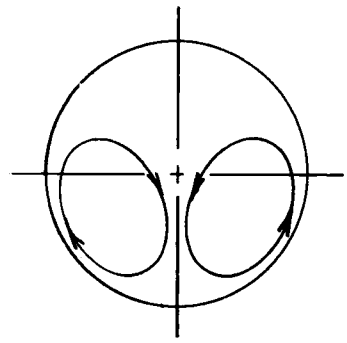

Figure 1.2. Flow cross section showing vortices which comprise the secondary flow.

somewhat below the horizontal centerline. As Gr^* is increased, the centers move down and closer to the tube wall. The interaction of the primary (axial) flow and the secondary flow result in a helical motion of the fluid about the longitudinal centerline. Although some deviation from this pattern is to be expected, the basic mechanism is similar for other fluids.

Early empirical equations by Colburn (14),

$$Nu_m = 1.75 \left(\frac{\eta_b}{\eta_{af}}\right)^{0.14} Gz_{ab}^{1/3} (1 + 0.015 Gr_{af}^{1/3}) \qquad (1.6)$$

Martinelli and Boelter (55)(for vertical tubes),

$$Nu_m = 1.75 F_1 \left[Gz_{ab} + 0.0722 F_2 \left(\frac{Gr_w Pr_w D}{L}\right)^{0.75} \right]^{1/3} \qquad (1.7)$$

$$F_1 = F_1(Nu_m, Gz_{ab})$$

$$F_2 = F_2(X/L, Nu_m, Gz_{ab})$$

Eubank and Procter (21),

$$Nu_m = 1.75\left(\frac{\eta_b}{\eta_w}\right)^{0.14}\left[Gz_{ab} + 12.6\left(Gr_{ab}Pr_{ab}\frac{D}{L}\right)^{0.40}\right]^{1/3} \quad (1.8)$$

and more recent correlations by Jackson, Spurlock, and Purdy (41),

$$Nu_{\ell m} = 2.67\left[Gz_{ab}^2 + (0.0087)^2(Gr_wPr_w)^{1.5}\right]^{1/6} \quad (1.9)$$

Oliver (71),

$$Nu_m = 1.75\left(\frac{\eta_b}{\eta_w}\right)^{0.14}\left[Gz_{ab} + 0.00056\left(Gr_{ab}Pr_{ab}\frac{L}{D}\right)^{0.70}\right]^{1/3} \quad (1.10)$$

and Brown and Thomas (6),

$$Nu_m = 1.75\left(\frac{\eta_b}{\eta_w}\right)^{0.14}\left[Gz_{ab} + 0.012\left(Gz_{ab}Gr_{ab}^{1/3}\right)^{4/3}\right]^{1/3} \quad (1.11)$$

have been improved upon by Depew and August (17),

$$Nu_m = 1.75\left(\frac{\eta_b}{\eta_w}\right)^{0.14}\left[Gz_{ab} + 0.12\left(Gz_{ab}Gr_{ab}^{1/3}Pr_{ab}^{0.36}\right)^{0.88}\right]^{1/3} \quad (1.12)$$

All of these investigators correlated large amounts of data taken during heating and cooling with isothermal walls. Depew and August claim ±40% accuracy for their correlation. Note that in most of the recent correlations, the L/D term has been dropped.

More attention has been given recently to the uniform heat flux boundary. For very long tubes with isothermal walls, the bulk temperature will approach the wall temperature, thereby shutting off the buoyant mechanism. Under the condition of uniform heat flux, a

temperature difference must always exist between the wall and the bulk flow to allow the energy at the boundary to enter. Moreover, the temperature difference increases as the flow moves down the tube (the opposite is true for the isothermal wall) thus implementing and feeding the secondary flow.

Mori et al. (68) have conducted an experimental investigation of air flowing in a uniformly heated horizontal tube. Data were taken in the fully developed region. As might be expected, the velocity and temperature profiles are similar ($Pr \approx 1$). Typical vertical distortion of the profiles is shown in Figure 1.3. They determined the

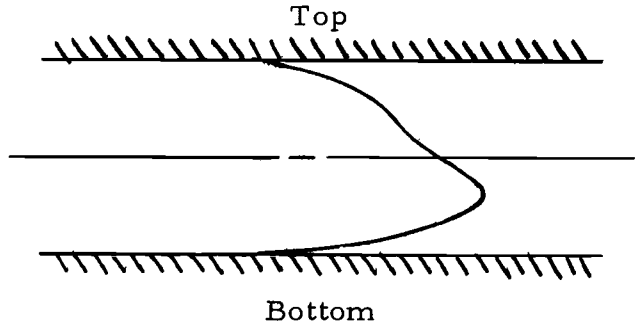

Figure 1.3. Typical velocity and temperature profiles for air showing the effects of secondary flow.

effect of buoyancy on the rate of heat transfer to appear at $Gr^* \approx 4000$ and that

$$Nu = 0.61 (Gr^*/4)^{1/5} [1 + 1.8 (Gr^*/4)^{-1/5}] \qquad (1.13)$$

correlated the data. (Nu pertains to the fully developed region and is the local value.)

McComas and Eckert (51) took data for air in and beyond the thermal entry region with uniform heat flux at the boundary. Their data show a shorter thermal entry length than predicted. They state that no appreciable heat transfer effect, due to buoyancy, occurred in the thermal entry region. However, inspection of their plots reveals a substantial secondary effect prior to full development. No correlation of the data was attempted.

Ede (19) studied the flow of water through a horizontal pipe while applying a uniform heat flux. He took data in the fully developed region and correlated it with:

$$Nu = 4.36(1 + 0.06\,Gr^{0.3})$$

or (1.15)

$$Nu = 4.36(1 + 0.032\,Ra^{0.3})$$

Shannon and Depew (88, 89) have collected data in the thermal entry region and beyond for the uniform heating of water and ethylene glycol. On one of the water runs and on all of the ethylene glycol runs shown, the data lie below the line for the constant property solution. No satisfying explanation was given by the authors. Another interesting trend of the data was observed at low values of Gz_x. Typically the value of Nu_x reached a minimum and subsequently rose rapidly as Gz_x decreased further (flow moved downstream). There was no apparent region of fully developed flow. Other data

and analytical results have indicated a region of full thermal development where the local Nusselt number is constant at a given flow and flux rate. A possible explanation is that the method of wall temperature measurement used by the authors indicated a local circumferential value rather than an average value. In any event, the correlation of

$$\left(\frac{\eta_w}{\eta_b}\right)^m (Nu_x - Nu_{xo}) \text{ vs } Ra^{1/4}/Nu_{xo}$$

scattered the data. As a criterion for defining the region of neglible buoyant effect $(Ra^{1/4}/Nu_{xo}) < 2$ was suggested. Nu_{xo} is the Nusselt number based on the constant property solution.

Petukhov and Polyakov (76, 77, 78, 79) have studied heat transfer to water in a uniformly heated horizontal pipe. They obtained a transition criterion for the onset of significant secondary flow,

$$Ra^*_{tr} = 6.37 \times 10^3 Gz_x \quad , \quad Gz_x > 460 \tag{1.16}$$

$$Ra^*_{tr} = 18000 + 83 Gz_x^{1.7}, \quad Gz_x < 460 \tag{1.17}$$

and recommended a correlation:

$$Nu_x = Nu_{xo}\left[1 + \left(\frac{Ra^*}{Ra^*_{tr}}\right)^4\right]^{0.045} \tag{1.18}$$

Their data show a trend typical of those in most of the recent investigations. The plot in Figure 1.4 shows this characteristic pattern.

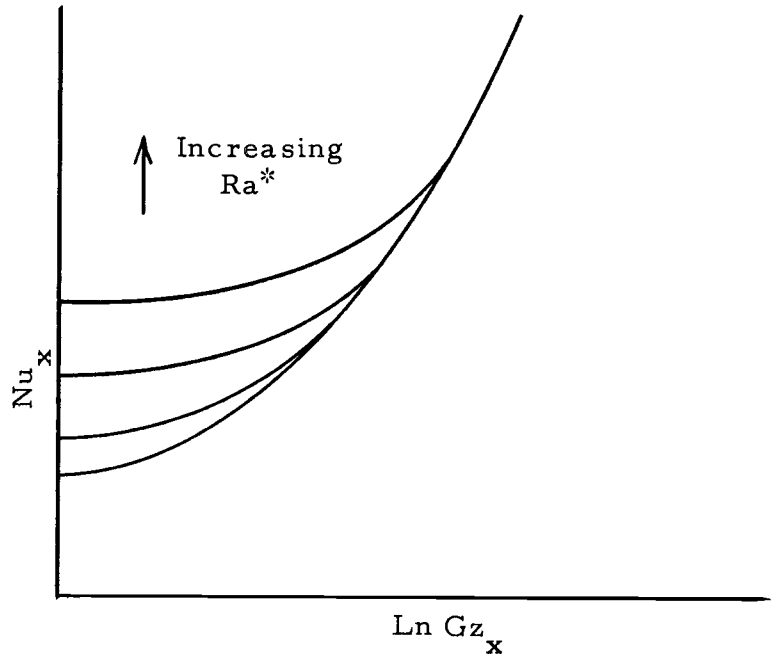

Figure 1.4. Plot showing typical findings from recent investigations of horizontal pipe flows.

The Nu_x used is an average circumferential value at a particular axial position.

Petukhov and Polyakov have also plotted separately the values of local Nusselt number at the top of the pipe and at the bottom of the pipe against local Graetz number. The data taken at the top of the pipe fall below the line for the constant property solution, while the data taken at the bottom of the pipe are above the line.

Also of interest in this investigation is a sketch of the isotherms in the cross section of a flow with Re = 960 and $Ra^* = 2.8 \times 10^7$. The coldest region is centered very close to the bottom

indicating that the temperature gradients in the vicinity of the bottom are extremely high.

In order to minimize circumferential conduction in the tube wall, Bergles and Simonds (3) used a glass tube for the heated section. The outside of the tube was coated to a nominal depth of 16 microns with a conductive material so that uniform heating could be applied via electrical resistance. The data taken for water in the fully developed region exhibit considerable scatter. The authors speculated that some of the problem probably was due to the non-uniformity of the coating on the tube. Based on their data and some previous investigations, the authors produced a "predictions plot" for heat transfer to water flowing in horizontal tubes that are uniformly heated.

Except as noted, the following papers are analytical studies of the secondary flow contribution to horizontal pipe flows with uniform heating.

Morton (69) modeled the problem by superimposing a small secondary flow on the forced flow. The perturbation parameter chosen was Ra, and the technique has validity in the region $\frac{Gr^*}{4} < 3000$ and $(Gr^*/4\,Pe) < 100$. A corrected version of the solution (67) which is confined to the fully developed region is:

$$\frac{Nu}{48/11} = 1 + (0.1036 - 0.0007\,Pr + 0.3334\,Pr^2)\left(\frac{Gr^*/4}{4608}\right)^2 + \ldots \tag{1.19}$$

Del Casal and Gill (16) have extended Morton's solution to include cases of very small Re; however, the perturbation method has validity only for values of $Gr^*/4$ at the low end of the range in which secondary flows occur.

Faris and Viskanta (22) also used a perturbation method, their parameter being $Gr^*/4Re^3$. Some very lengthy expressions for the velocity and temperature profiles were obtained which match the air data of Mori, et al. (68) quite well. A solution for the circumferential average Nusselt number in the fully developed region was also obtained:

$$\frac{Nu}{48/11} = 1.0 + \frac{Ra^{*2}}{16Re}\left[2.175 \times 10^{-8} + 1.0025 \times 10^{-7} Pr^{-1}\right] \quad (1.20)$$

The only limits mentioned were those for the case of the flow of air:

$$Gr^*/4\ Re^{1/2} < 3000 \quad (1.21)$$

Mori and Futagami (67) developed an integral solution of the boundary layer equations (for the secondary flow) valid for $Pr \approx 1$. They separated the fully developed flow into two regimes--a thin layer near the wall where viscosity and thermal conductivity control transport and a core region where they are ignored. (One might expect this model to have the greatest validity at relatively large values of $Gr^*/4$.) The heat transfer result,

$$\frac{Nu}{48/11} = C_1(Gr^*/4)^{1/5} \qquad \begin{matrix} C_1 = 0.1634 \text{ for } Pr = 0.72 \\ C_1 = 0.1929 \text{ for } Pr = 1.0 \end{matrix} \qquad (1.22)$$

matched their experimental results (68) for air; however, the solutions for the velocity/temperature profiles were a poor fit.

Siegwarth, et al. (94) also used a boundary layer model which they solved for the cases of $Pr = 1$ and $Pr \to \infty$. They based their model on the experimental observation that the isotherms in the core region are horizontal. Although a uniform heat flux was specified at the outer surface of the tube wall, no variation in circumferential temperature was allowed at the inside surface. This condition corresponds to a thick wall of high thermal conductivity. The possibility of axial conduction in the tube wall under such extreme conditions was not addressed. The solution for the case $Pr \to \infty$ in the fully developed region was found to be:

$$Nu = C_1 Ra^{*1/5} \qquad (1.23)$$

Using an approximate integral solution, the authors obtained $C_1 = 0.524$. Comparison with the data of Siegwarth and Hanratty (93) for ethylene glycol ($Pr \approx 80$) was quite good.

The experimental data of Siegwarth and Hanratty were taken to confirm the analytical approach taken above. A $2\frac{1}{2}$-inch I.D., 1-inch thick aluminum pipe was used in the experiment in order to

approach the boundary condition adopted for the model. The data and the results obtained from the analysis agree quite well. Some of the findings of this investigation were:

1. At a relatively small heating rate where $T_w - T_b = 0.05$ F and $Ra^* = 35,800$, the computed Nusselt number was found to be twice the classic value of 48/11.

2. The secondary flow had very little effect on the axial velocity profiles. Distortion from the classic parabolic form was minor. The profiles from the data exhibited maximums that were slightly above the horizontal plane indicating a temperature-dependent viscosity effect.

3. Using the solution of Del Casal and Gill (16), there is less than a 10% effect on the wall shear rate for $(Ra^*/Pe^2) \leq 12.8$.

In applying the results of findings by Siegwarth and co-workers to thin-wall tubes, the difference in boundary conditions must be kept in mind. The boundary condition used by these investigators results in heat transfer that is greater than for the uniform circumferential heat flux condition.

Newell and Bergles (70) obtained numerical solutions to the two-dimensional continuity, momentum, and energy equations for the fully developed region. They used water as the working fluid and applied a uniform heat flux to two different pipe wall models. The conditions of a very thick wall with high thermal conductivity, and a

tube of low thermal conductivity (glass) were modeled. Severe vertical distortion of the temperature and velocity profiles was noted for relatively modest heat input to the glass tube. Unfortunately, similar results for the high conductivity tube were not shown. Comparison of the circumferential average Nusselt number for the two kinds of wall conditions showed a definite advantage in the high conductivity wall which increased with tube radius. For example, for an applied heat flux of 1000 Btu/hr-ft^2 and a bulk temperature of 100 F, the Nusselt numbers were 9.7 and 13.5 for a $\frac{1}{4}$-inch radius and 11.3 and 23.4 for a $\frac{1}{2}$-inch radius.

Hwang and Cheng (39) used a "boundary vorticity" method and a numerical analysis to obtain results for Pr = 0.72, 1, 2, 4, 10, 100, and 500. The region of applicability is believed to be $2000 < \frac{Gr^*}{4} < 50000$. A stated purpose of the study was to develop a method to bridge the gap between the perturbation method on the low end and the boundary layer method on the high end of the $Gr^*/4$ range. A plot of $Nu/(48/11)$ against $Gr^*/4$ for the various values of Pr show asymptotic lines for Nusselt number ratios greater than about 1.1. The lines are parallel, and the spacing decreases logrithmically as Pr increases. The analysis was confined to the fully developed region.

Cheng, Hong, and Hwang (8) applied the same method to the thermal entrance region of a rectangular duct. They were unable to

handle the more complicated geometry imposed by circular tubes. A condition specified was high Prandtl number, which the authors believe to offer reasonable results for $Pr > 10$. For a square channel, the temperature profiles show vertical distortion (due to the secondary flow) far upstream of the fully developed region. For example, the minimum temperature for the cross section is located below the horizontal plane at an axial location 2/3 of the distance upstream from full development for $Ra^* = 30,000$. The plot of $Nu_x/(48/11)$ against $\pi/4Gz_x$ for $1000 < Ra^* < 300,000$ shows the same asymptotic characteristics as the plot in Figure 1.4. There was found to be no effect on heat transfer for $Ra^* \leq 1000$. Also, the effect is negligible until a certain entry value of $\pi/4Gz_x$ is reached which depends on Ra^*.

The Effects of Non-Newtonian Behavior

Flow media which depart from the well known Newtonian model, $\tau = \eta \left| du/dr \right|$, have received a great deal of attention in recent years. They are important to many industries including rubber, plastics, synthetic fibers, petroleum, soap, cosmetics, pharmaceuticals, cement, food, paper, paint, biological fluids, printing, ore processing, brewing, and distilling.

The departure from Newtonian behavior can result in peculiar phenomena. Dilatant fluids (viscosity increases with shear rate)

"shatter" with a loud crack when a critical flow rate is attained in a confined flow. Viscoelastic fluids (exhibiting elastic behavior) climb a rotating shaft due to the tensile normal stresses generated. Viscoelastic behavior in the turbulent flow of dilute polymer solutions reduces the drag even though the viscosity is greater than that of the original fluid.

Non-Newtonian behavior has been observed only in fluids where particles, bubbles, or large molecules are present in the fluid media. A change in the flow rate causes a change in the interaction between the particles resulting in non-linear behavior. For example, the macromolecules in many polymer solutions have a "pig's tail" structure. At low flow rates they are oriented in a random fashion in the flow media and tend to become greatly entangled with one another. As the flow rate is increased, the molecules tend to straighten and orient themselves more in the flow direction. At the same time degradation increases as more of the molecules are sheared or pulled apart. The result is a decrease in apparent viscosity ($\tau/\dot{\gamma}$) with the increasing shear rate, $\dot{\gamma}$ (pseudoplasticity).

The entanglement of the molecules also explains the viscoelastic behavior of most polymers. The helical-shaped molecules interact like entangled springs.

Other particle interaction mechanisms are created by electrostatic bonding of particles into chains. In still others, macro-

molecules are formed by agglomeration. The subsequent change in particle bonding under varying flow conditions causes non-linear behavior.

Dilatant behavior is a relatively rare phenomenon that has been documented in certain suspensions of particles in the 5-20 micron range. The particle concentration necessary for such behavior is usually 30-50% by volume and quite critical. A possible mechanism to explain such behavior follows. At low shear rates, the particle surfaces are well lubricated by the fluid media and slide over each other with relative ease. At progressively higher shear rates the particles interact at an increasing rate to scrape dry more and more of the surface of an adjacent particle. This results in an increase in flow resistance which appears as an increase in apparent viscosity with increasing shear rate. The range of shear rates for which dilatant behavior is exhibited is usually quite limited. Once thought to be related to volume dilatancy, Metzner and Whitlock (58) have demonstrated otherwise.

In a tube flow, pseudoplastic behavior promotes the same distortion of the velocity profile as heating does in the case of temperature-dependent viscosity. That is, the profile becomes blunt and steeper at the wall. Dilatant behavior promotes the opposite effect, analogous to cooling in the case of temperature-dependent viscosity. Thus, one would expect an increase in heat transfer as pseudoplastic

behavior becomes more severe; and conversely, a decrease in heat transfer as the degree of dilatancy increases.

An introduction to basic rheology is given by Fredrickson (27). Bird (5) has written a review of the use of various empirical models to describe flow behavior. Skelland (95) has covered the non-Newtonian flow and heat transfer state of the art from a design standpoint.

In order to accomplish analytical progress in studying heat transfer to non-Newtonian fluids, a compromise has been made. Simplicity at the expense of accuracy has been the criterion in the choice of rheological models. Any one of these models cannot begin to describe the wide range of behavior which has simply been labeled non-Newtonian. The rheologists dream, a general constituitive equation which simply and accurately describes the behavior of all fluids under a broad range of temperature and flow conditions, is not a reality. In the absence of a general equation, the engineer has had to use a patch-work of relatively simple empirical equations each of which is justified for a particular class of fluids over a limited range of temperature and flow conditions. Hence, a vast literature has been developed, each investigation embracing a particular rheological model.

Non-Newtonian Effects--Isothermal Tube Wall

Isothermal wall data have been gathered for a variety of fluids. Orr and Dallavalle (73) studied the vertical flow of water-clay, water-powdered copper, water-powdered aluminum, ethylene glycol-graphite, and ethelene glycol-aluminum. Thomas (98) studied thorium oxide-water. Charm and Merrill (7) used ammonium alginate, applesauce, and banana puree in their work.

The majority of data have been collected for polymer melts and solutions. Polymer melt data have been taken by Gee and Lyon (28), Griskey and Wiehe (32), Forsythe and Murphy (26), and Collins and Filisko (15). Polymer solution data were taken by Metzner, Vaughn, and Houghton (59) for water-CMC and water-carbopol; Metzner and Gluck (57) for water-carbopol; Hanks and Christiansen (35) and Christiansen and Craig (9) for water-CMC and water-carbopol; and Oliver and Jenson (72) for water-CMC, water-carbopol, water-polyox, and ethyl alcohol-carbopol.

Analytical studies employing the power law model,

$$\tau = K\dot{\gamma}^{n} \tag{1.24}$$

have been made by Lyche and Bird (49), Toor (99, 100, 101), Whiteman and Drake (105), Pawlek and Tien (75), and Foraboschi and de Federico (24). Hirai (37), Wissler and Schechter (106), Kumar (46),

Stephan (96), and Samant and Marner (82) obtained solutions for the Bingham plastic model:

$$\tau = \tau_o + \eta_o \dot{\gamma} \tag{1.25}$$

Shulman, et al. (90) employed a non-linear plastic,

$$\tau = \tau_o + \eta_o \dot{\gamma}^n \tag{1.26}$$

in their analysis.

None of the above analyses have included property variation with temperature. Solutions using a temperature-dependent power law are documented by Forsyth and Murphy (26), Hanks and Christiansen (35), Christiansen and Craig (9), Korayem (44), Christiansen, Jensen, and Tao (11), and McKillop et al. (53, 54). Gee and Lyon (28) used a temperature-dependent Ellis model.

$$\tau = \eta_o \frac{\dot{\gamma}}{1+K\tau^n}, \quad \eta_o = \eta_o(T) \tag{1.27}$$

and Christiansen and Jensen (10) adopted a temperature-dependent Powell-Eyring model,

$$\tau = \eta_o \dot{\gamma} e^{\Delta H/RT} + \frac{1}{C_1} \sinh^{-1}\left(\frac{\dot{\gamma} e^{\Delta H/RT}}{C_2}\right) \tag{1.28}$$

in obtaining solutions.

Non-Newtonian Effects--Uniform Heat Flux

Lyon (50) has developed equations for the case of uniform heat flux at the wall which can be used with any temperature-independent rheological model. The equations which are restricted to the thermally fully developed region include:

$$\frac{1}{Nu} = 2 \int_0^1 \frac{d\xi}{\xi} \left[\int_0^\xi \frac{u}{V} Z \, dZ \right]^2 \tag{1.29}$$

where Z is a dummy variable and $\xi = 2r/D$.

Sestak and Charles (87) extended Lyon's solution to include radial-dependent heat generation. For the special case of viscous dissipation using the power law model, for the fully developed region they obtained:

$$Nu = \frac{B(n)}{1 - \frac{nB(n)}{8(3n+1)} Br'} \tag{1.30}$$

where B(n) is the solution by Bird (4)(shown below) and others for the case without viscous dissipation, and Br' is the modified Brinkmann number.

Bird (4) has obtained asymptotic solutions (in addition to a series solution) for large and small values of the dimensionless axial coordinate. Using the power law model, Bird obtained

$$Nu_x = 1.412 \, \delta^{1/3} Gz_x^{1/3} \tag{1.31}$$

for the thermal entry region. For power law fluids, $\delta = (3n+1)/4n$ and for $\frac{4}{\pi}\delta Gz_x > 100$ the error is less than 1% compared to the series solution. Except for the $\delta^{1/3}$ term which corrects for the non-Newtonian effect on the shear rate, the solution is the same as for the constant property Newtonian case.

For the fully developed regime, Bird obtained:

$$Nu = \frac{8(n+1)(n+3)(n+5)}{n^3+13n^2+43n+31} \tag{1.32}$$

A solution for the Ellis model also appears in this paper. All of the solutions were restricted to the condition of temperature-independent properties.

Grigull (31) obtained the same solution as Bird for the fully developed region using the power law model. Temperature variation of properties was not included.

Gill (29) added the possibility of viscous dissipation to the model and obtained a series solution. As with most of the series solutions, the eigenvalues are functions of the rheology parameters (in this case, n). Consequently, a new set of eigenvalues must be obtained for each new n.

Michiyoshi and Matsumoto (61) solved the same problem substituting uniform heat generation in lieu of viscous dissipation. Some results were obtained for $Gz_x < 25\pi$.

McKillop (52) used the power law model and a numerical solution of the continuity, momentum, and energy equations for two-dimensional flow to get results for pseudoplastic fluids. Temperature variation of properties was not allowed, and both fully developed and uniform entry velocity profiles were specified. For the case of fully developed entry flow, Nu_x showed a 7.5% increase when n was changed from 1 to 0.5 at $Gz_x = 100\pi$. At the same Gz_x, for a change in n from 1 to 0, a 119% increase in Nu_x was observed.

Other power law solutions include those by Inman (40) for the fully developed region and circumferentially varying heat flux, and by Deyoung and Scheele (18) for flow in a vertical pipe. In neither case is the rheology temperature dependent.

The Bingham plastic model was used by Michiyoshi (60) and Michiyoshi, Matsumoto, and Hozumi (62) to investigate, first the fully developed region, and then a short way into the thermal entry region ($Gz_x < 12.5\pi$). Both investigations include internal heat generation.

Matsuhisa and Bird (56) used a δ based on the Ellis model to modify Bird's previous thermal entry region solution. The Ellis model was then applied to the Lyon solution to obtain results for the fully developed region. Ellis model solutions for isothermal flow and isothermal walls were also presented.

Mitsuishi and Miyatake (63) also obtained solutions for the Ellis

model. They solved both the isothermal wall and the uniform heat flux problem. Eigenvalues for 5 values of the model parameter, n, are given for each solution.

Schenk and Van Laar (85) investigated the flow of Prandtl-Eyring fluids,

$$\tau = C_1 \sinh^{-1}\left(\frac{\dot{\gamma}}{C_2}\right) \tag{1.33}$$

where C_1 and C_2 are empirical constants. Provision for specifying the external (outside tube surface) Nusselt number was made. Only cooling was allowed and results were obtained for flows with and without viscous dissipation. The cases investigated included infinite, finite, and zero external Nusselt number. Typical of other eigenvalue solutions, the results are limited to relatively small values of Gz_x (near the end of thermal entry region).

In other papers, Schechter and Wissler (83) and Henning and Yang (36) have obtained solutions for the flow of Bingham plastics in tubes with insulated walls. Both analyses include internal heat generation, and the latter paper gives experimental data on the Joulean heating of aluminum-sulfuric acid slurries.

The investigations described so far have been conducted with the restriction of temperature-independent transport properties. Mizushina et al. (66) derived a solution using the power law with temperature-dependent consistency, K. They modified Bird's

asymptotic solutions by applying a correction term $(K_b/K_w)^{0.1/n^{0.7}}$. These solutions were supported by data taken using glycerol (Newtonian) and aqueous solutions of CMC. The data include the region $10 \leq Gz_x \leq 300$ which covers the end of the developing region and the beginning of full development. Significant scatter suggests the possibility of buoyant effects which are not accounted for.

Using a temperature-dependent power law, Mitsuishi and Miyatake (64, 65) paralleled Pigford's work. In their derivation a uniform shear rate is specified all along the pipe wall. To compensate for this inaccuracy, the authors evaluate δ_x at the axial mean wall temperature up to that point. Plots of δ as a function of dimensionless heat flux (which includes the temperature dependence parameter for the rheology) and $1/n$ are presented. The solution differs from Bird's only in the method of evaluating δ.

Experimental data taken in a vertical pipe for aqueous solutions of CMC are also presented. The flow behavior indices (n) of the fluids were 0.735, 0.667, and 0.606. Natural convection effects were not considered. The approximate range of local Graetz numbers covered were $25 < Gz_x < 1500$.

Cochrane (12, 13) investigated the thermal entry region for temperature-dependent power law flows by solving the boundary layer equations numerically. The results show a 3, 7.5, and 19% increase in heat transfer over the Newtonian case for $n = 0.75$, 0.50, and

0.25 respectively (with no temperature variation of viscosity). Using a rheological model,

$$\tau = K(\dot{\gamma}e^{\Delta H/RT})^n \tag{1.34}$$

where ΔH is the so-called activation energy and R is the universal gas constant, he obtained results for both heating (12) and cooling (13). For dimensionless flux, $\phi = q''D/kT_o = 2.0$, $n = 1$, $Pr_o = 1000$, and $\Delta H/RT_o = 5$, the increase in Nu_x is 5% at $Gz_x = \frac{\pi}{4} \times 10^5$ and 14% at $Gz_x = \frac{\pi}{4} \times 10^2$ compared to the constant property solution. For $\Delta H/RT_o = 10$ and other conditions the same, the increase is 7 and 27% respectively. In the case of cooling, the magnitude of ϕ imposed was low (0.25). However, of interest is the comparison of the relative changes in Nu_x from the constant property solution. The relative decrease in Nu_x was almost twice as great during cooling as the relative increase during heating.

Bader, McKillop, and Harper (1) also solved the boundary layer equations for entrance region flow of temperature-dependent power law fluids. The results are compared with data taken on aqueous hydroxyethylcellulose and sucrose and aqueous HEC alone. The flow condition on entry to the heated section was one of uniform velocity. Results for entrance Prandtl numbers from 144 to 270 are reported for the two fluids with $n = 0.85$ and 0.62. The results are not presented in terms of the usual Nu_x against Gz_x and are difficult

to interpret. In addition, the paper is brief and further weakened by the unavailability of the back-up reference.

Khabakhpasheva, Popov, and Perepelitsa (42) and Kutateladze et al. (47) report what is apparently the same set of data on the flow of a 1% aqueous solution of Polyacrilamide. The fluid is viscoelastic; however, for fully developed, steady, laminar flow in circular tubes (in the absence of natural convection) no elastic effects emerge. The data are presented in terms of $Nu_x \chi^{-1/3}$, where χ is a factor evaluated from an uncommon rheological model (at least in Western literature). In addition, the local Nusselt numbers have been "reduced to quasi-isothermal conditions by extrapolating to zero values of the heat flux." These factors make it virtually impossible to interpret the data.

Etchart (20) took rheological data for several non-Newtonian fluids from the literature and obtained heat transfer results for them. He used a temperature-dependent Powell-Eyring model and solved the boundary layer equations numerically.

Forrest and Wilkinson (25) chose a temperature-dependent non-linear plastic and the momentum and energy equations without the radial velocity terms to model the problem. The equations were solved numerically, and results were obtained for both heating and cooling. Additional results were also obtained showing the effects of viscous dissipation.

Buoyancy in Non-Newtonian Pipe Flows

The only attempts to account for buoyancy effects in non-Newtonian horizontal pipe flows have been made by Metzner and Gluck (57) and Oliver and Jenson (72). Both of these studies were experimental and involved isothermal wall conditions.

Metzner and Gluck correlated results obtained from aqueous solutions of carbopol and the data of Charm and Merrill (7) for aqueous ammonium alginate, applesauce, and banana puree. The correlation,

$$Nu_m = 1.75\,\delta^{1/3}\left(\frac{K_b}{K_w}\right)^{0.14}\left[Gz_{ab} + 12.6\left(Pr_w Gr_w \frac{D}{L}\right)^{0.4}\right]^{1/3} \quad (1.35)$$

scattered the data appreciably, but was an improvement over other correlations which ignored buoyancy effects.

Oliver and Jenson took data on the heating and cooling of aqueous solutions of carbopol, polyox, and CMC and ethyl alcohol-carbopol. They found that their data were better correlated by

$$Nu_m = 1.75\left(\frac{K_b}{K_w}\right)^{0.14}\left[Gz_{ab} + 0.0083\,(Gr_w Pr_w)^{0.75}\right]^{1/3} \quad (1.36)$$

than by the Metzner and Gluck equation. However, they agreed with Metzner and Gluck that the wall conditions control natural convection in non-Newtonian horizontal flows. They show that buoyancy can have a greater effect on the rate of heat transfer than either the

non-Newtonian or temperature-dependent viscosity effects. Based on their results, they claim that heat transfer can be increased as much as 100% for less viscous non-Newtonian fluids.

At this time, no work has been reported on the effect of viscoelasticity in laminar pipe flows which have developed secondary flows.

Conclusion

Heat transfer to laminar, non-Newtonian, horizontal pipe flows has been well investigated for the case of isothermal walls. Although the effects of buoyancy can be important under certain circumstances for the isothermal wall, it is of greater importance in flows with uniform heat flux at the boundary. Unfortunately, the lumped parameter correlations developed for the isothermal wall are of little use for the uniform heat flux case where local values are of interest.

Exclusive of the effects of buoyancy, the case of uniform heat flux has received a great deal of analytical attention. However, only Newtonian fluids have been investigated to determine secondary flow effects. Even those studies are not exhaustive. The experimental data for non-Newtonian flows in uniformly heated (or cooled) horizontal pipes are sparce and poorly documented.

2. OBJECTIVE AND DESIGN OF EXPERIMENT

Objective of Present Study

The objective of this investigation is to gather experimental data on the uniform heating of pseudoplastic fluids in laminar flow in horizontal, circular tubes so that the effects of non-Newtonian behavior, temperature-dependent viscosity, and buoyancy on the rate of heat transfer can be interpreted.

In order to assist in the interpretation of the results, comparison with and utilization of existing theory and analyses will be attempted. A lumped parameter correlation accounting for the various effects will be sought.

Design of Experiment

It was obvious from the outset that the entire thermal entrance region could not be investigated. Full development for flows without appreciable natural convection occurs for Graetz numbers in the vicinity of 10. Either very low flow rates or very long heated sections are necessary to obtain this value. The maximum test section length that could be accommodated in the available facilities was 10 feet. This allowed room for a flow development section not to exceed 5 feet. It was deemed undesirable to turn the flow after entering the flow development section and before leaving the test section.

The working fluids chosen were dilute aqueous solutions of the polymers sodium carboxymethylcellulose (CMC) and polyethylene oxide (polyox). These fluids have been used extensively by others who have conducted non-Newtonian investigations and their characteristics are well known. Their behavior is pseudoplastic, and the degree of behavior increases with increasing concentration. Aqueous CMC produces flow behavior indices (n) as low as 0.6 to 0.7, and aqueous polyox as low as 0.3 to 0.4. Behavior is maintained over a wide range of shear rates. The fluids are non-toxic; and the properties, other than viscosity, are essentially equal to those of water. Their cost is not prohibitive.

A dilatant flow system of ethylene glycol and corn starch was also considered. This system has been investigated extensively by Griskey and Green (33, 34), Roberts (81), and earlier by Fisher (23, p. 194). It was not found possible to duplicate their results over a significant range of shear rates, and plans for its use were abandoned.

Test section diameters of 0.5 and 1.0 inches were selected primarily due to their popular use in practice. In addition, smaller sizes have a larger wall thickness to diameter ratio increasing the possibility of significant heat conduction in the wall. Smaller sizes also discourage buoyancy since the buoyancy parameter Gr^* varies directly with D^4. Larger diameters drop the wall shear rate and

lower the heat flux input possible for a given flow. Large diameters also increase heater costs and construction time.

Based on flange design, plastic pipe wall strength, pumping losses, and the possibility of viscous dissipation, the maximum allowable pressure drop along the entry and test sections was set at 100 psi. Using viscometric data obtained on the most viscous fluid to be tested, a maximum flow rate of 1 ft^3/min was calculated. This calculation was made on the assumption of a 5-ft long flow development section.

The maximum wall shear rate expected for this flow rate was calculated and found to be within the capability of the available viscometer. The maximum hydrodynamic entry length based on the least viscous fluid to be tested was found to be 2.4 ft. This was calculated using the Newtonian model (which is conservative):

$$L_e = 0.0575\, D\, Re \qquad (2.1)$$

The maximum Reynolds number expected was 500. To assure full development of the flow, an entry length of 5 ft was chosen for both test sections.

In order to minimize the possibility of heat transfer to or from the fluid in the entrance section, an entry temperature of 70 F was chosen. To stay well away from the boiling point, a maximum wall temperature of 180 F was selected. Using the constant property

Graetz-type solution, the maximum power input necessary to achieve this temperature for a number of flow rates from 0.1 to 1.0 ft^3/min was determined. This figure was scaled up approximately 50% to account for an increase in heat transfer due to property variation with temperature. The maximum design power was thereby set at 7500 watts.

Using the results of the above solution, axial positions at which wall temperatures were to be recorded were chosen. Positions were chosen at 10 F changes in the wall temperature in order to space the data conveniently. The initial position was chosen at 3 inches from the entrance to the test section. This was the closest position to the entrance at which axial conduction was calculated not to exceed 2% of the input heat flux. Other positions chosen were 9, 18, 30, 48, 72, 96, and 117 inches from the entrance of the test section. To provide for the possibility of the presence of buoyancy, it was decided to monitor the temperature at the top and bottom of the tube wall at each axial location.

With these design criteria in mind, it was planned to run flow rates of 0.1, 0.5, and 1.0 ft^3/min for each fluid and each test section. Two or 3 concentrations of each polymer would be used to cover the range in flow behavior indices from 0.3 to 1.0. In each case, the power necessary to bring the maximum wall temperature

to 180 F would be applied. As a result, a large amount of local heat transfer data would be collected for $100 < Gz_x < 40,000$.

3. DESCRIPTION, DESIGN, AND CONSTRUCTION OF APPARATUS

A schematic diagram of the entire test apparatus is shown in Figure 3.1. Fluid was drawn from the feed tank by the pump through a short span of 2 in. piping. It was pushed through $1\frac{1}{2}$-inch piping to the tube side of the heat exchanger where it was cooled by water on the shell side. From there the fluid passed through more $1\frac{1}{2}$-inch piping to a static mixer where temperature gradients were destroyed. It then flowed through a 10-inch long viewing section just prior to having its bulk temperature measured. The flow was then routed to one of two entrance sections which were flanged to the test sections. Once in the test section, the fluid was uniformly heated by electrical resistance heaters located on the walls. Thermocouples located at various axial positions along the test section monitored the wall temperatures. At the exit to the test section another static mixer prepared the fluid for a bulk temperature measurement. Upon leaving the mixer, the fluid was transported via $1\frac{1}{2}$-inch piping to a weight tank atop a beam balance scale. From there it was dumped back into the feed tank. A tank mixer kept the fluid supply to the pump at uniform temperature and provided mixing capability in preparing the working fluids.

A wood framework was used to support the apparatus and provide a means of inclosing the test sections. The inclosure extended

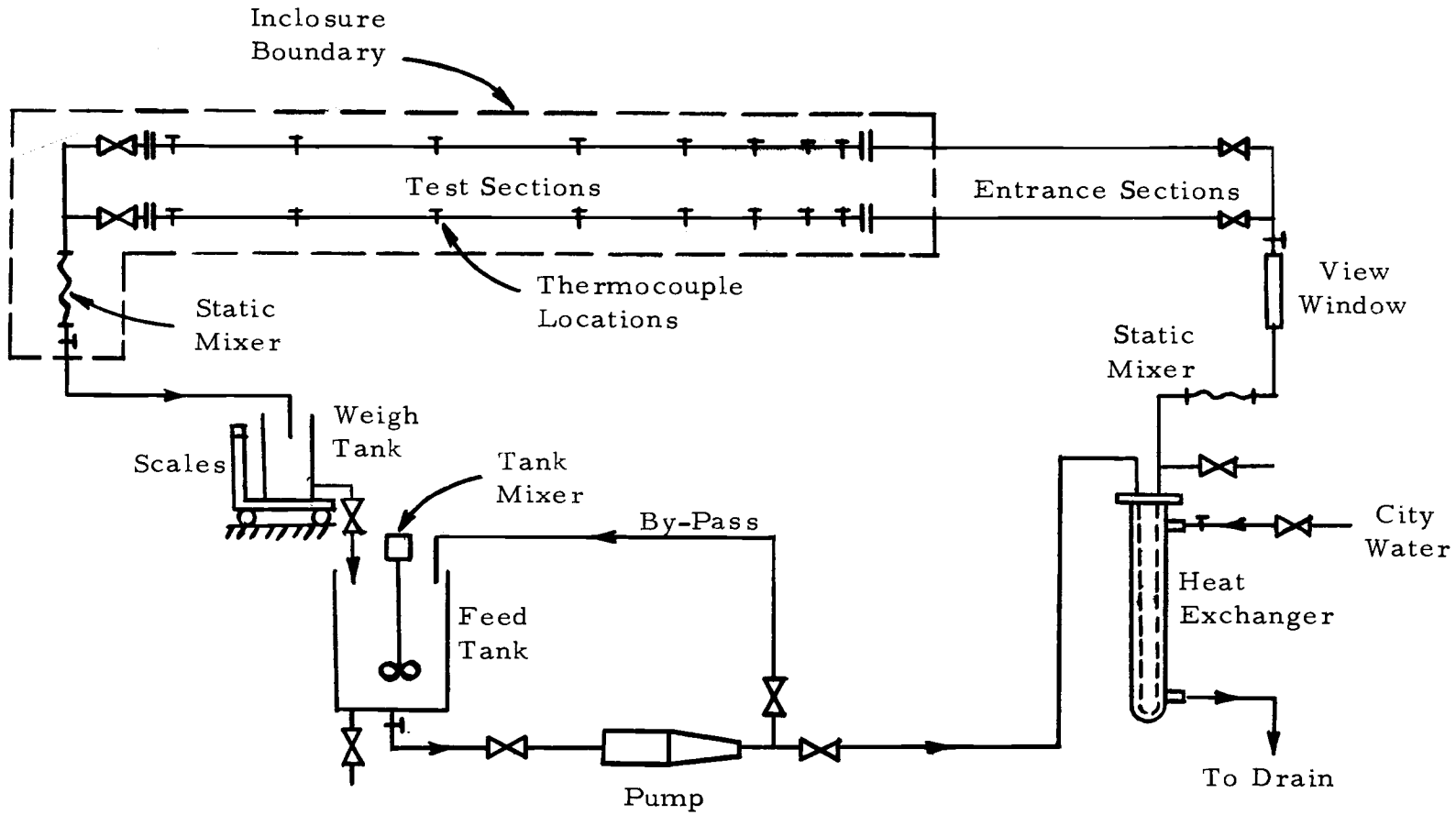

Figure 3.1. Schematic Diagram of Test Apparatus.

from a point 1 ft upstream of the inlet flanges to the end of the static mixer beyond the outlet of the test section. It was filled with loose, vermiculite insulation. It was 24 inches wide and 18 inches deep. The purpose of using loose insulation in lieu of a wrap type was to eliminate the problem of getting around obstructions within the inclosure. A disadvantage encountered with the loose insulation was difficulty in its handling. Removal and replacement were tedious, and in the process, a choking dust filled the room.

Flow System

A 55-gal steel drum was used for the feed tank. The bottom was removed, the drum inverted, and the 2-inch fitting (once at the top) was used as the exit.

The tank mixer was driven by a 240 volt DC motor, rated at 1/3 HP at 1750 rpm, through a 5 to 1 gear reduction unit. Power was provided by a 110 volt variable transformer coupled to a 2:1 step-up transformer and a full wave bridge rectifier. A 4-inch diameter, 3 blade, paddle stirrer was scaled up from a design recommended by Union Carbide Corp. (102, p. 5) for the mixing of water-soluble polymers.

The pump was a Moyno, 2L4, "progressing cavity" type with a tool steel rotor and a Buna N rubber stator. It was selected to provide a steady, almost positive displacement, flow with less shearing

action than a gear pump or a centrifugal pump. The rotor was 18 in. long and $1\frac{1}{2}$ in. in diameter. It performed much like a screw conveyer. As the rotor turned within the stator, the fluid was pushed along in a cavity that progressed downstream. Increasing pressure and/or increasing viscosity reduced the capacity. However, the process was the next best thing to positive displacement.

The pump was rated by the manufacturer at 24 gpm at 1200 rpm for fluids with viscosity in the range 1-1000 centipoise and moderate exit pressure. Output dropped to 9 gpm at 450 rpm for a viscosity of 2500-5000 cp. These outputs decreased to 22 gpm and 6.7 gpm respectively when the exit pressure was increased to 80 psig.

The pump was driven by a 240 volt DC motor rated at 2 HP at 1750 rpm. Speed reduction was accomplished by V-belt and sheaves. The sheaves had pitch diameters of 2.65 and 8.0 inches resulting in a 3.06:1 speed reduction.

Power was supplied to the motor armature using a 220 volt variable transformer and a full wave bridge rectifier. Rectifier output was smoothed with 2000 μf of capacitance. Power to the field was supplied from 208 line voltage and a full wave bridge rectifier. Smoothing was provided by 20 μf of capacitance.

The shell and tube heat exchanger had 2 tube passes and approximately 20 ft^2 of heat transfer area. The tubes were 3/4 inch in diameter and 5 ft.long. The shell side inlet was connected to city

water by a rubber hose. A rubber hose at the exit led to a drain. According to the design specifications for the experiment, the area was more than adequate.

Construction of the static mixers was based on a design patented by Kenics Co. (74). The mixer consisted of a series of "bow tie" elements that were fabricated from 0.10 inch, annealed aluminum sheet. Rectangular pieces, 1.939 inches wide and 3.25 inches long, were held at one end while the other end was twisted 180^{o}. Equal numbers of clockwise and counter-clockwise elements were made, the ends notched, and joined at right angles with epoxy glue. Element twist directions were alternated in the joining process. The idea of the design was to split, develop, and turn the flow with each new element. For N elements, the flow would be divided into 2^{N} strata, and the size of each strata would be $D/2^{N}$.

Ten elements were coated with epoxy paint and inserted into a 2-inch, "hi-temp" PVC pipe 30 inches long. The ends were capped with reducing couplings to retain the elements and provide coupling to $1\frac{1}{2}$-inch pipe.

The entrance section ahead of the small test section was $\frac{1}{2}$-inch, schedule 80, PVC pipe (0.840-inch OD and 0.546-inch ID) with a length of 5 ft. Plastic pipe, with its low thermal conductivity, was used to limit conduction losses from the test section. The large test section was preceded by 5 ft of 1 inch, schedule 40, PVC pipe

(1.315-inch OD and 1.049-inch ID).

The entrance sections were flanged to the test sections. The flange for the small entrance section was fabricated from $\frac{1}{2}$-inch PVC flat stock. Its outside diameter was $3\frac{1}{4}$ inches. Four 3/8-inch diameter holes were drilled on a 2 inch bolt circle, and the center of the flange was drilled and tapped for $\frac{1}{2}$-inch pipe. The entrance pipe was threaded and screwed into the flange to within 1/8 inch of the bearing face.

A standard 1-inch, 150 psi, PVC flange was used for the large entrance section. It was a slip-on type secured with PVC cement. The end of the pipe was butted against a lip on the flange 1/8 inch from the bearing face.

The small test section was fabricated from a 10 ft-7/8 inch long piece of 5/8-inch OD, hard drawn, copper tubing. Wall thickness was 0.040 inch giving an inside diameter of 0.545 inch. A 1-1/8-inch OD, 0.035-inch wall copper tube of the same length was used for the large test section. It had an inside diameter of 1.055 inch.

The flanges on both test sections were fabricated from $\frac{1}{4}$-inch carbon steel plate. They matched the dimensions of the corresponding flanges on the entrance sections except that 5/16-inch bolt holes were drilled. The flanges were silver-soldered to the test sections leaving a 1/8-inch lip at each end.

Assembly to the entrance sections was made using 1/16-inch thick rubber gaskets and 5/16-inch steel bolts. The lip on each test section was a snug fit inside the corresponding entrance section flange. When the sections were mated, the edge of the test section was within 1/16 inch of the edge of the entrance section.

The test sections were supported vertically and horizontally at the entrance by inserting the flange bolts through a $\frac{1}{2}$ inch thick piece of plywood which was in turn bolted to the supporting structure. The reaction from the pressure drop in the entrance and test sections was taken here. The small test section was given additional vertical support at two midspan locations and at the opposite end using light construction from wood and PVC. The large test section was given additional support at the mid-point and at the opposite end in a similar manner. The materials used and the care taken to minimize the heat transfer area limited the conduction losses from the supports.

The small test section was located with its center axis 5 inches from the inside wall of the inclosure and 9 inches from the bottom. The large test section axis was 9 inches from the opposite side and 9 inches from the bottom.

The flanges which mated the test sections to the exit piping were identical in size to those at the entrance. They were composed of CPVC "hi temp" (chlorinated PVC) material for operation at the

higher temperatures at the outlet. The exit piping, from test section to weigh tank, was also of the same material. Exceptions were the Celcon gate valves near the test section exits.

The weigh tank was constructed from a 17-gallon steel drum. The side fitting was used in attaching $1\frac{1}{2}$-inch piping and a Celcon gate valve.

A photograph of the apparatus in which the pump, feed tank, tank mixer, weigh tank, and scale are prominent is displayed as Figure 3.2. The stirrer is unattached from the mixer and sitting along side the motor.

The static mixer used upstream of the test sections is shown in Figure 3.3. Two elements are displayed in the foreground. The thermocouple reference junctions and ice bath container are on the left, and the heat exchanger is in the background.

A view of the test sections in place with the loose insulation removed from the inclosure is shown in Figure 3.4. The white conduit between the test sections contained the thermocouple wires and provided a surface for running the heater hookup wire.

Test Section Heaters

Selection of Heaters

Several methods of uniformly heating pipe flows have been used. They include:

Figure 3.2. View of test apparatus showing pump, feed tank, tank mixer, weigh tank, and scale.

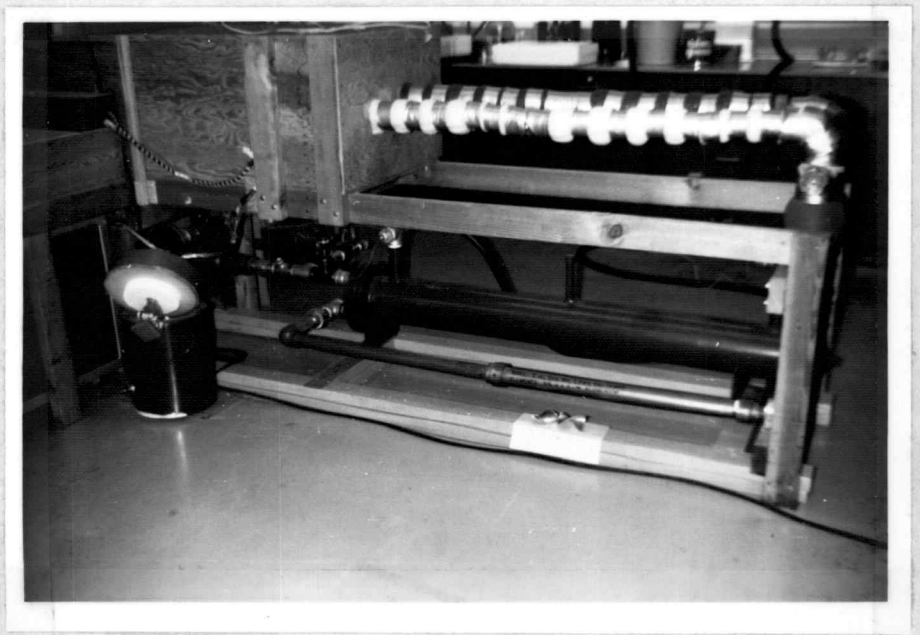

Figure 3.3. View of entrance piping, heat exchanger, static mixer, mixer elements, and thermocouple reference junctions with ice bath container.

Figure 3.4. Test sections with surrounding insulation removed.

1. Joulean heating of the pipe wall.

2. Coating a non-conducting pipe with a thin conductive layer.

3. Wrapping the pipe with nichrome wire or ribbon.

4. Applying longitudinal strips of nichrome wire or ribbon to the pipe wall.

All of these methods incorporate electrical resistance heating of the conductive media.

In evaluating these methods for possible use in this investigation, the following factors were considered:

1. Heat losses from lead wires.

2. Uniformity of heat distribution.

3. Effect of temperature on heating elements and insulators.

4. Effect of method on wall temperature measurement.

5. Power supplies available.

6. Availability of materials.

7. Construction complexity.

Joulean heating of the pipe wall by simply supplying an electric current to it was an attractive possibility. The advantages are simplicity of construction, easily available materials, and the absence of insulating materials (which might overheat). The best material from a resistivity standpoint is stainless steel. Tubing is readily available in a variety of sizes. The tolerances are no worse than for wire or ribbon and are better than those on thin conductive films. However, in order to keep a reasonable tolerance, the limit on wall thickness is about 10 mils (0.010 in.).

For a design I.D. of 0.5 and 1.0 in., very high currents would be needed to dissipate the maximum design power of 7500 watts. A power supply capable of delivering approximately 500 amps would be required. In addition, the high currents would require large lead wires through which substantial heat losses would occur. Another problem is introduced in measuring the wall temperature. If the thermocouples are fastened directly to the wall, the measurement system must operate above ground, creating a shock hazard. If the

thermocouples are insulated from the wall with a thin strip of film, a sizable measurement error can occur.

Coating a non-conductive tube with a conductive layer is also attractive for its simplicity of construction (provided someone else does the coating). However, film thickness must be on the order of 10 microns, and the control is not very good. Users have reported large uncertainties. Another negative factor for this method is the relative high cost of meeting the design criteria.

Wrapping the pipe with nichrome wire or ribbon is a low cost alternative. The element size can be matched to almost any power requirement, and low currents can be used. Though the concept is simple, construction problems are more formidable. Each wrap must be insulated from the pipe wall as well as its immediate neighbors. The insulation must be thin enough to prevent the heater element from attaining temperatures which would destroy the insulation integrity, yet it must be strong enough to resist puncture.

A serious problem peculiar to the wrapping method is the possibility of local hot spots due to element expansion. Although temperatures are moderate, the relatively long length of heater element comprising the wrap can expand substantially. If the expansion localizes, the heater element will pull away from the wall and subsequently overheat. Such overheating is not so much a danger to the element as to the insulation which is sensitive to high temperatures.

Application of longitudinal nichrome wires or ribbons to the pipe wall has advantages similar to wrapping but with a lower risk of developing local hot spots. Shorter element lengths and element layout discourage the localization and diminish the magnitude of the expansion. This method requires the most construction time; however, the materials are inexpensive. Since this method was able to satisfy our requirements and more closely match our capabilities, it was chosen.

Design of Heaters

Initially the task of design and construction of the heaters was turned over to Electrofilm Corporation. Their design entailed the use of nichrome wire elements which ran longitudinally along the tube. The elements were spaced 0.1 inch and were held in place in a silicon rubber medium bonded to the tube wall. Unfortunately, cold regions between the elements made the test sections unsuitable for use in this investigation.

Design and construction were then undertaken in the laboratory using closely spaced longitudinal elements of nichrome ribbon. The design criteria formulated were:

1. Heater element area equal to the inside area of the tube.

2. Overall heater resistance in the range $2.1 < R < 12$ ohms, with a target of 7-8 ohms.

The second criterion was dictated by the size of the available power supply.

In trying to cover the maximum possible area and for ease of construction, it was desirable to minimize the number of elements. However, larger widths required reduced thicknesses, not only to meet resistance specifications, but also to conform to the tube wall. Availability decided the issue, and a 1/8-inch wide, 35 BWG, 0.93 ohm/ft ribbon was chosen. The design for each test section was developed around this choice of ribbon and the two design criteria.

A schematic diagram of the layout of the heater elements for the small (0.545-in I.D.) test section is shown in Figure 3.5. The solid lines are individual elements, and the dashed lines are lower resistance connections and lead wires. The design consisted of 7 pairs of elements running the length of the test section (10 ft, nominal). The elements in each pair were at the same potential, and no attempt was made to isolate them from each other.

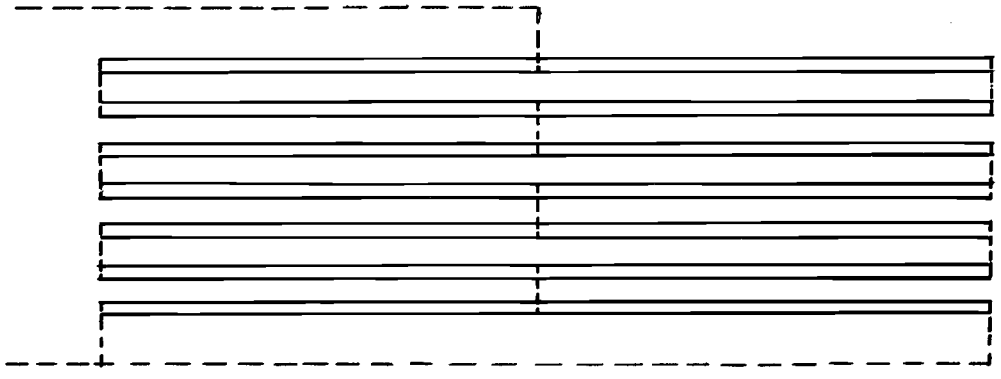

Figure 3.5. Schematic diagram of heater layout for small test section.

Connections at the ends and midpoint were made such that one might think of the design as 35 ft of paired elements at the front end in parallel (electrically) with the 35 ft at the other end. The resistance is 8.14 ohms for such a model, and the heater area is 102% of the inside wall area.

A schematic diagram of the layout of the heater elements for the large (1.055-in. I.D.) test section is shown in Figure 3.6. The design consisted of 13 pairs of elements running the length of the test section. In order to determine the resistance of this design, one might think of it as equivalent to three 43.33-ft. pairs (each end and the middle) in parallel with one another. The resistance is 6.72 ohms, and the heater area is 98.1% of the inside wall area.

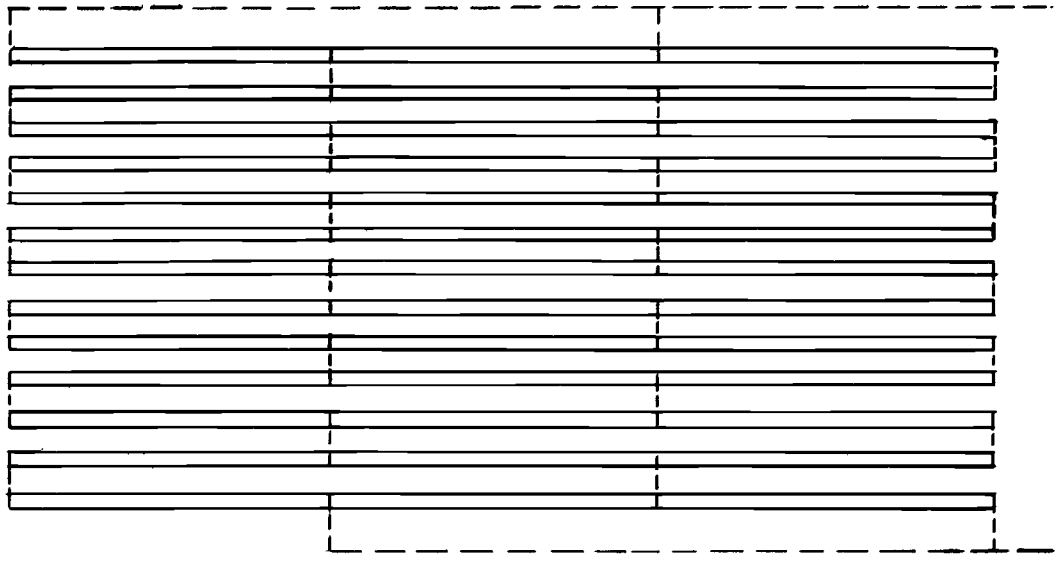

Figure 3.6. Schematic diagram of heater layout for large test section.

Construction of Heaters

Construction of the heaters, placing, and securing them on the test sections presented some formidable problems. First of all, it was necessary to isolate the elements electrically from the tube wall. This requirement created a new problem in that a temperature drop across the insulation would be necessary to drive the heat flux. Thus, the insulation thickness was limited by the maximum temperature it could sustain without losing its integrity.

Secondly, the elements had to be held temporarily in place so that the critical spacing between each pair could be accomplished. The design spacing was about 50 mils on the small test section and about 20 mils on the large test section. Very often in the construction the elements had to be removed and re-applied to accomplish the correct spacing.

In an initial attempt to solve these problems, a 1-mil mylar-backed tape with 1 mil of acrilic adhesive on each side (total thickness of 3 mils) was tried. The working temperature of the tape was limited by the adhesive to 130 C. Although the backing was quite tough, electrical continuity developed between the heater elements and the tube wall during construction. This apparently resulted from the presence of metal fragments under the elements which punctured the tape backing.

Subsequently, one layer of the mylar tape was applied

longitudinally in lengths not exceeding 2 ft. The tape width was 1 inch. Thus, 2 strips were a perfect fit on the small test section, while 3 and a large fraction covered the large test section. A 4-mil fiberglass backed tape with 3 mils of silicon adhesive on one side was then wound, adhesive side out, without overlap, on top of the mylar tape. This tape was limited by its adhesive to operation below 180 C. However, silicon adhesives do not conduct when charred as other adhesives do, leaving some margin beyond 180 C. The total insulation thickness of 10 mils with thermal conductivity estimated at 0.10 Btu/hr-ft-F, could be expected to induce an 85 C temperature difference between the elements and the wall of the small test section when 7500 watts was dissipated. Since the largest wall temperature was planned to be 85 C, the total of 170 C was less than the critical temperature.

Another area of concern was that of providing electrical connection between heater elements. The nichrome alloy could not be soldered; and since the desirable time to make the connections was during application to the test section, silver soldering, welding, or brazing were not good alternatives (due to possible damage to the insulating tape). The problem was solved by using a portable electric spot-welder to fasten 1/8-inch wide, 5-mil thick, brass strips to the elements where connections were needed.

Attachment of leads was accomplished by soldering to a brass

strip that was spot-welded to the appropriate element. The lead was then rolled up in the strip tightly against the element and further soldered to prevent a hot spot from developing on the strip. Wire used for the leads was #12 BWG, stranded copper. Hook-up wire was #10 BWG, stranded copper.

The final problem to be addressed was the need to work the heaters around the thermocouples attached to the test section wall. It was necessary to attach the thermocouples before mounting the heaters to avoid overheating the insulating tape. (A great deal of heat was required to solder the thermocouples to the copper wall.) It was decided to temporarily terminate each element pair just prior to each thermocouple location. Although only the elements in line with the thermocouples needed to be routed around them, all of the element pairs were treated in the same manner to avoid non-uniformity. Figure 3.7 shows how each pair was temporarily terminated and spliced by spot-welding to a brass strip. Thus, a 3/16-inch square area was available to circumvent the thermocouple. Heating was diminished at a distance of 1/8 inch on either side of the thermocouple by the presence of the brass strip across the element pair. The local effect from this gap in the heating on the wall temperature is addressed in Chapter 5 and Appendix B.

An added incentive to temporarily terminating the element pairs was the avoidance of a nightmarish tangle of 10-ft long ribbons.

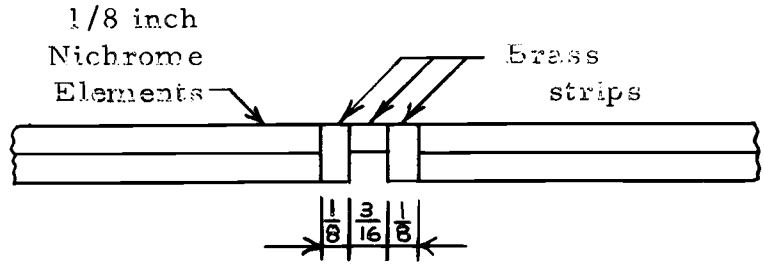

Figure 3.7. Method of joining element pairs that were temporarily terminated at each thermocouple location.

Construction of the heaters by section greatly eased the handling and spacing problems.

Thus, after laying the insulation on each section, the ribbons were cut to the appropriate length. The elements in each pair were then fastened together by spot-welding a brass strip across them at each end. One end was spot-welded to its temporarily terminated mate, and the pair were pressed down on the adhesive. When all the pairs were hooked up, laid down, and properly spaced for a given section, fiberglass tape (the same as used beneath the elements) was wound tightly around the outside, with a slight overlap, up to the next thermocouple location. When the test section was completed, an extra wrap of fiberglass tape was applied. Epoxy glue was applied to the lead attachment regions to strengthen those areas. Finally the whole test section was given a coat of polyurethane insulating spray. Particular attention was given to the regions around the thermocouples to insure isolation from the heater elements.

Heater Power Supply

Power to the heaters was provided by a Sorensen model DCR 300-35A, regulated DC supply. The rated output was 0-300 volts and 0-35 amps. Voltage output was regulated to the greater of ±0.10% or ±60 mv. If current regulation was chosen, it was controlled to ±70 ma.

Measurement System

Thermocouple Circuit

A schematic diagram of the thermocouple circuit is shown in Figure 3.8. Forty-two copper-constantan thermocouples, taken from the same spool, were used in the investigation. The wire size was #24 BWG, the insulation was vinyl, the wires were paired, and the grade was precision. Two reference junctions were formed using each leg of the thermocouple and a length of #24 BWG solid, copper hookup wire. An Omega 16-position thermocouple switch was wired to each of the 16 thermocouples attached to the wall of a test section. Another identical switch was used for the other test section. The output pair from each switch was fed to the input terminals of a third switch. The latter was a 12 position type leaving 10 input pairs for other thermocouples. The output pair from the last switch was connected across the input of a Leeds and Northrup, model K-3,

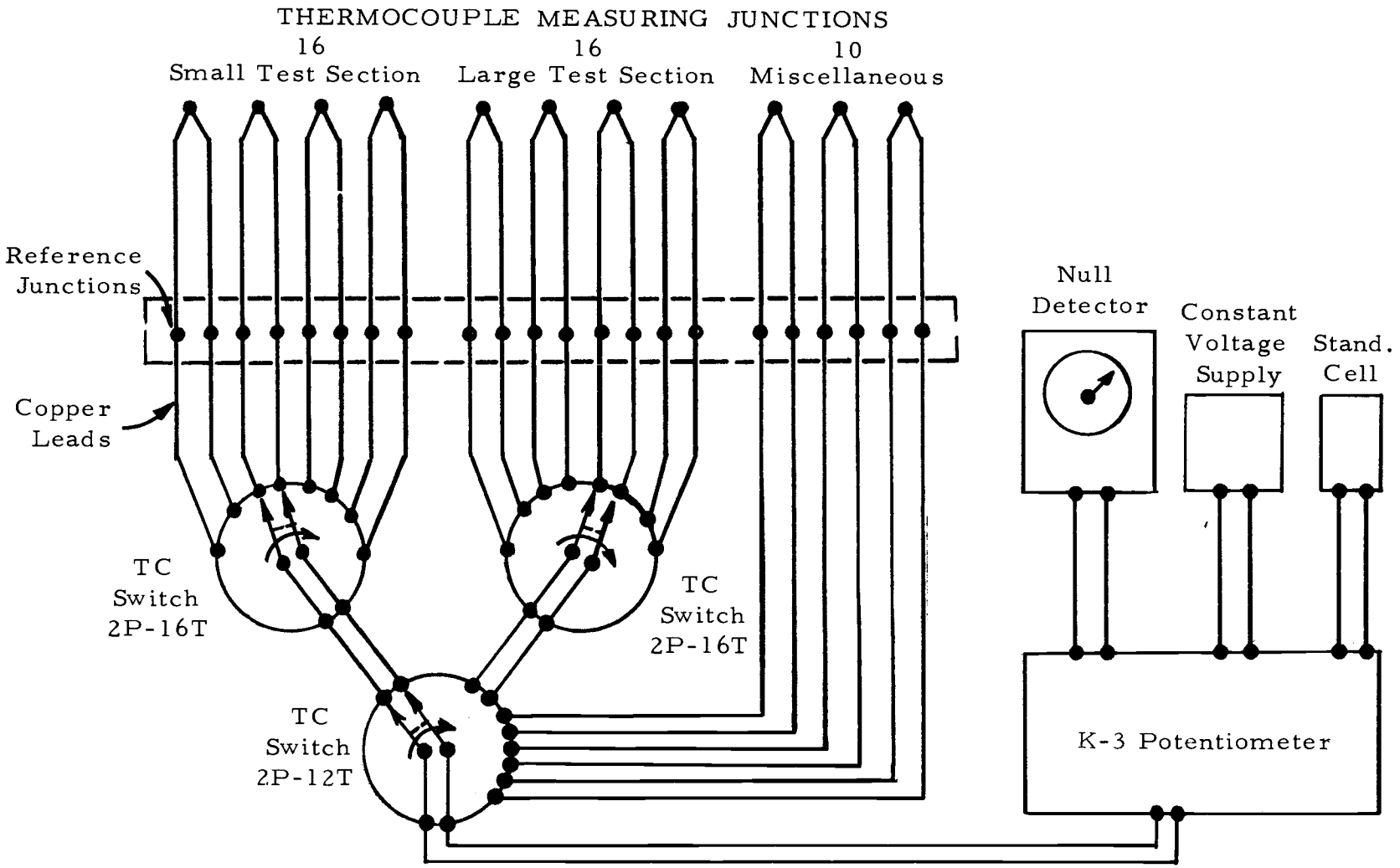

Figure 3.8. Schematic Diagram of Thermocouple Circuit.

potentiometer. A #9834 null detector, a #099034 constant voltage supply, and a standard cell from the same manufacturer were used in conjunction with the potentiometer.

This precision type circuit, recommended by Benedict (2, p. 67-75), was used to reduce uncertainties in measurement. It was used in lieu of a more simple circuit in which the reference junction is switched into each thermocouple loop. The latter practice places switches, terminals, and instruments in the loop between the measuring junction and the reference junction. The effect is the creation of another thermocouple which, if a temperature gradient exists across it, adds an emf to the true value. Benedict estimates these uncertainties are commonly on the order of 1-2 F for each piece of hardware so placed in the circuit. The precision measuring arrangement eliminates the hardware from the loop between the two junctions.

The thermocouple junctions were formed with an electric arc thermocouple welder using an argon environment. The reference junctions (84 in number) were isolated from one another by pushing them through a PVC block 2-3/4 inches square, $\frac{1}{2}$ inch thick, and drilled $\frac{1}{4}$ inch between centers. The junctions extended 1/8 inch from the block.

The 16 test section thermocouples were located at axial positions 3, 9, 18, 30, 48, 72, 96, and 117 inches from the inside (non-bearing) surface of the inlet flange. Two thermocouples were

soldered, top and bottom, at each position. The site was prepared by pitting the surface to a depth not exceeding 15 mils with a 1/16-inch drill. The surface was heated, the bead located in the pit, and a layer of solder, deep enough to cover the bead, applied. The area was dressed with a file so that a solder button, 1/8 inch in diameter and approximately 1/32 inch deep, was left around the junction. Epoxy glue was applied to the bare leads which emerged from the solder, and a 1 inch piece of "spaghetti" insulation was pushed down over the outside of the thermocouple to complete the isolation from the surroundings. The leads were cut approximately 1 ft from the measuring junction.

During the installation of the heaters, 4 of the thermocouples on the small test section broke near the solder button. Thermocouples at 9 (top), 18 (top), and 96 inches (top and bottom) were replaced by using an adhesive of 1 part epoxy glue and 3 parts copper powder. A button of the same size as the solder was fashioned.

After the test sections were installed, the corresponding legs to the reference junction were spliced into the wall thermocouples. These were contained in a 1-inch PVC conduit which was centered between the two test sections. The thermocouples were not wrapped around the test section, but emerged at right angles from the test section wall and went directly to the conduit.

An ice bath at the reference junctions was contained in a 4 liter

stainless steel vessel. The vessel was approximately 7 inches in diameter and 8 inches deep. It was surrounded with $2\frac{1}{2}$ inches of foam insulation. All this was contained in a larger pail. A top of $\frac{1}{2}$ inch thick plywood and 3 inches of styrofoam was fabricated and drilled to accept the $1\frac{1}{4}$-inch diameter bundle of wire.

Thermocouple probes used to measure flow temperatures were constructed by stringing thermocouple wire through a piece of $\frac{1}{4}$-inch copper tubing, $4\frac{1}{2}$ inches in length. The measuring junction was then soldered into a hole in a copper button which in turn was soldered to the end of the tube. The end was then dressed up and the probe inserted through a Swagelok male connector. Nylon farrules were used so that when the connector was loosened, the probe could be easily adjusted. These probes were located in the main flow at the outlet of the feed tank, just prior to the entrance sections, and just after the outlet mixer. Another probe was situated at the inlet to the shell side of the heat exchanger. A final one was used in an auxilary capacity to measure, among other things, the ambient air temperature in the vicinity of the entrance sections.

Thermocouples were also glued to the top of the outside surface of each entrance section, 6 inches upstream of the inlet flange. Others were glued 1 inch downstream of the last wall thermocouple on the outside wrap of each test section. The final thermocouple was glued on the thermocouple conduit near the entrance end.

Power and Flow Measurement

Shunts, rated 50 mv/30 amp, were placed in both legs of the heater circuit for the large test section. An identical shunt was also placed in the parallel leg of the heater circuit for the small test section. It was desired to monitor the relative input to each section of the heater in operation. Any change in relative values would offer a better indication of local problems than the total input values would. These shunts were monitored by 2 Fairchild digital voltmeters with 1 mv resolution. Since the purpose was only to detect changes, accuracy was not important.

A 50 mv/30 amp shunt was also placed in the main leads from the power source to the heaters. A Vidar 500 digital voltmeter with resolution to 0.1 mv on the lowest scale was connected across the shunt. Voltmeter accuracy was ±0.1% of full scale (100 mv on lowest scale). Provision was also made to switch this instrument across the output of power supply to obtain an output voltage (1000-volt scale used). Panel meters with resolution to 5 volts and 0.5 amps were mounted on the power supply providing a rough check on the output.

The scale used to weigh the fluid was a Fairbanks platform type with a range of 0-120 lb. It was calibrated with weights to the nearest ounce. The lower scale, used during test, was incremented in 1 pound intervals. Sensitivity was found to be at least 1 ounce.

Viscometer and Circulator

The instrument chosen for this investigation was a Haake Rotovisco rotating viscometer. The instrument's task was to measure the torque required to turn a rotor or cone against the viscous drag induced by the fluid sample located between it and a stationary surface (cylinder or plate). Nine choices of measuring systems were offered. Five were beaker and rotor types; 3 were plate and cone types; and the last a double gap beaker and rotor type. Discrete choices of rotational speed offered were: 3.6, 7.2, 10.8, 21.6, 32.4, 64.8, 97.2, 194.4, 291.6, and 583.2 rpm. The stationary surfaces were jacketed so that temperature control could be exercized by use of a fluid circulator. A complete description of the viscometer and its capabilities is given by Van Wazer et al. (103, p. 102-108).

Two of the measuring systems were used in this investigation. The first was a beaker and rotor type (MV-I) with diameters of 42 and 40.08 mm respectively. The second was the double-gap beaker and rotor type (NV) with diameters of 35.7 and 40.2 mm for the rotor and 35 and 41 mm for the beaker.

The circulator used for temperature control was a Haake model Fe. It was capable of controlling the circulating fluid (distilled water) to ±0.02 C. Heat was supplied by a 1000 watt element. Reservoir capacity was 2 liters, and pumping capacity was 10 liters/

min. A $\frac{1}{4}$-inch stainless steel coil in the reservoir allowed heating or cooling of the circulating fluid by an external fluid source.

Figure 3.9 shows (from left) pump motor power supply, thermocouple switches, and K-3 potentiometer. Below is the Sorensen power supply, and at the far right is the Rotovisco viscometer. Above left is the null detector, and from bottom to top, the quartz thermometer, Vidar digital voltmeter, and a Fairchild digital voltmeter used as a monitor on the heater legs.

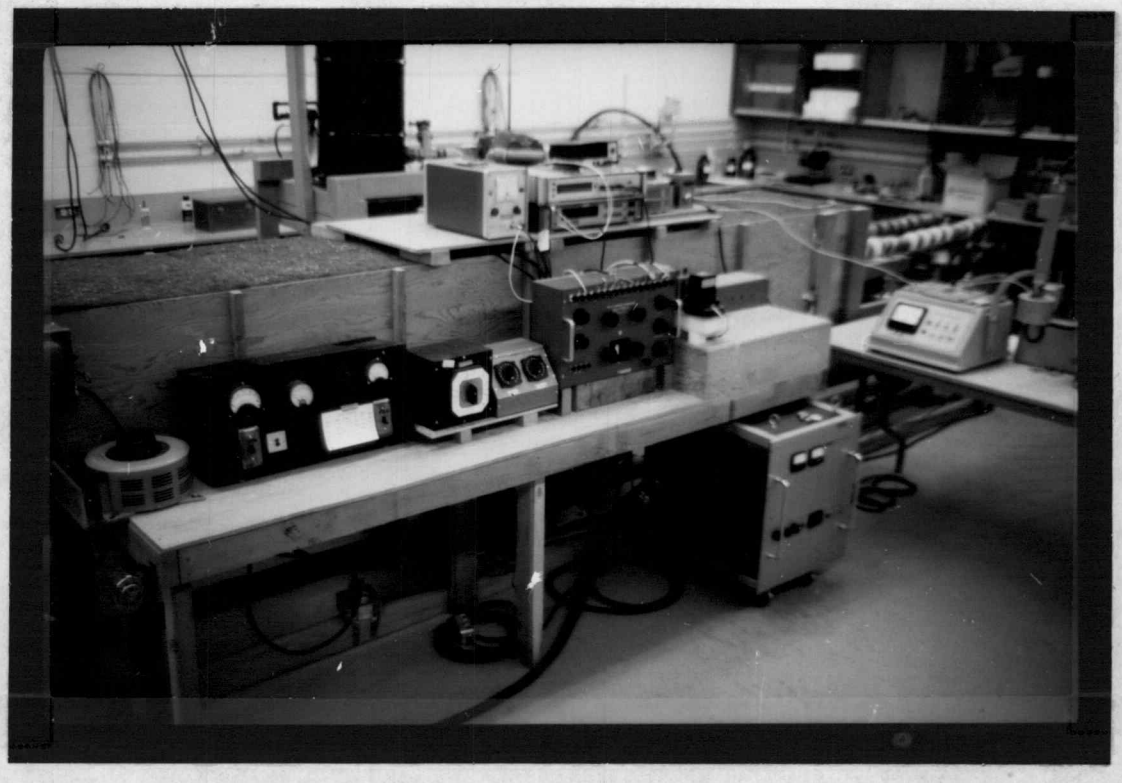

Figure 3.9. View of instrumentation, power supplies, and viscometer.

Thermocouple Calibration System

Thermocouples attached to the test section walls were calibrated after the test sections were installed. The schematic diagram in Figure 3.10 shows the calibration apparatus which was a modification of the test apparatus. The entrance sections were removed from the test sections, and flanged adapters were mounted in their place. These adapters (shown in Figure 3.11) functioned to connect the test sections, via a rubber hose, to the outlet of a small Dunham Bush C4A-5 centrifugal pump powered by a 1/8-HP motor. The suction side of the pump was connected to the outlet of the feed tank.

The weigh tank was removed and the flow re-routed directly to the feed tank by a short piece of rubber hose. The feed tank was covered, top and sides, with 3 inches of foam type insulation. A 5-ft long coil of 3/8-inch copper tubing was placed in the tank, one end connected to a low pressure (60 psi) steam line and the other to a drain line. Another coil, 10 ft in length, was connected to the Haake circulator (described in conjunction with the viscometer). This coil was also placed in the tank.

The sensor to a Hewlett Packard 2801A quartz thermometer replaced the thermocouple probe at the outlet bulk temperature station. The quartz thermometer had an accuracy of ± 0.01 C over the range 0-100 C. The instrument operated on the basis of the

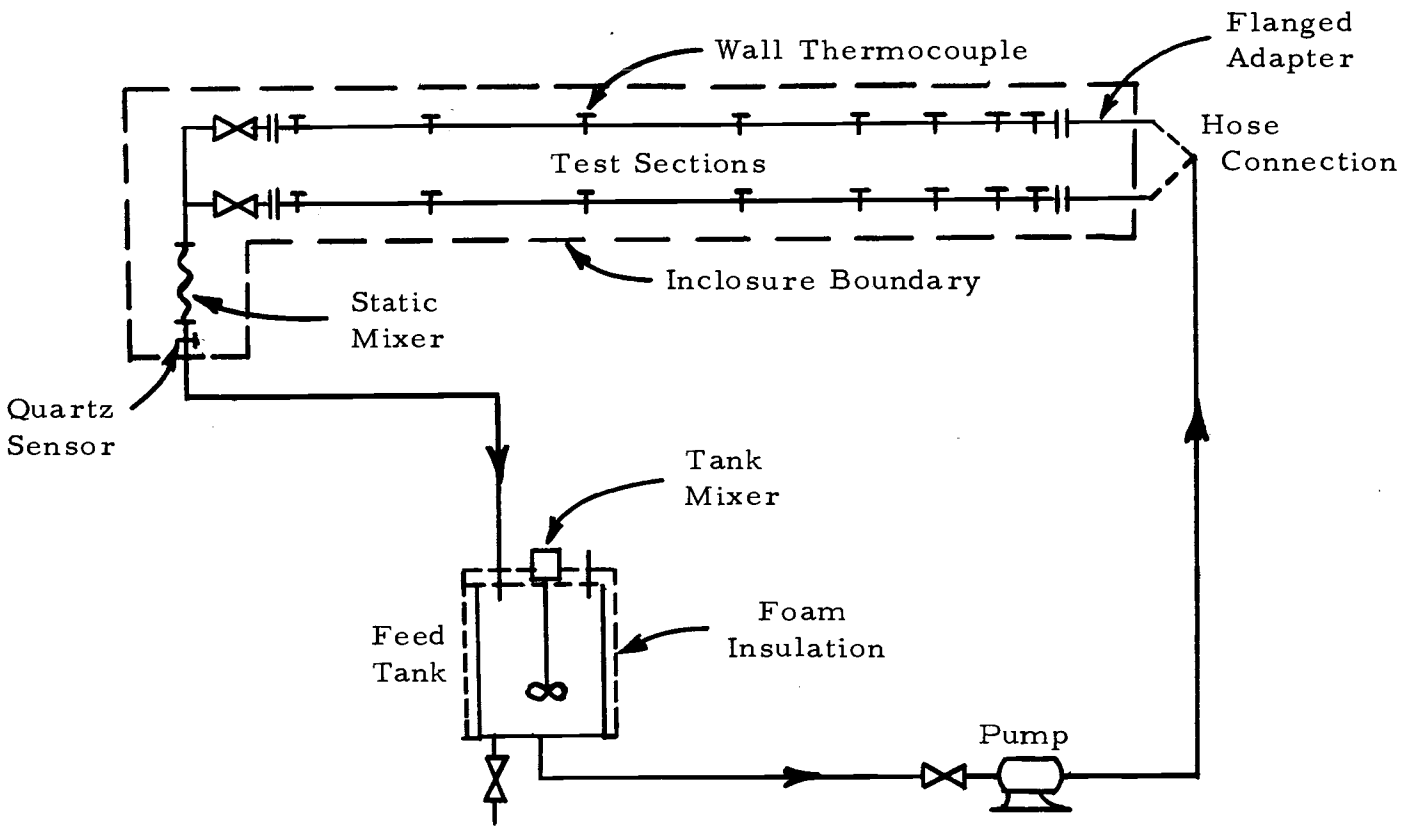

Figure 3.10. Schematic Diagram of Test Apparatus Modified for Wall Thermocouple Calibration.

Figure 3.11. Flanged adapters at entrance end of test section used during thermocouple calibration.

temperature dependence of the frequency response of a quartz crystal located in the sensor. This response, which was essentially linear over a limited range, was approximately 1000 hz/C. Conversion to temperature units (C) was made by the instrument and indicated on a digital display. A choice of resolution to 0.01, 0.001, and 0.0001 C was offered.

4. METHOD OF TESTING

Calibration of Test Section Thermocouples

At least 14 data points at temperatures in the neighborhood of room temperature, 30, 40, 50, 60, 70, and 83 C were taken for each test section thermocouple.

Water was used as the calibration fluid. Approximately 30 gallons, close to test temperature, was placed in the tank for each run. Only one test section was used during a test. The pump circulated the water at a rate of approximately 8 gal/min. At temperatures of 50 C and below, the circulator was able to maintain equilibrium over long periods of time. Above 50 C it was necessary to use the steam heating system. The circulator was also used at these higher temperatures to obtain more precise control.

The system was allowed to run at temperature at least one hour before data were obtained. During a run, readings for all the wall thermocouples, the ambient air temperature, and the thermocouples located on the thermocouple conduit and the heater wrap were taken. The latter were taken for possible use in the diagnosis of the results. All of the data for a run were usually gathered in 5 minutes.

Mixing of Polymers

Initially, the polymers were mixed in amounts that corresponded to earlier viscometric results. However, it was found that after the fluid had been circulated for several hours through the test section considerable degradation had occurred. It was often necessary to add more polymer to a batch some time after its initial mixing to obtain the desired degree of pseudoplasticity. A set of runs for a particular fluid took from 1 to 2 days, and it was desirable to obtain a rheological condition that would persist over this interval. The alternative would have been to gather complete viscometric data for each run. This alternative was hardly realistic in that a complete viscometer run often took twice as long as a data run.

As a consequence of obtaining a stable rheology, the lowest flow behavior index was only a bit below 0.4. At this stage, the fluid was so viscous that addition of more polymer would have increased the pressure drop in the test section beyond the design value.

Thus, early in the investigation, the polymers were carefully blended into the water, the process sometimes taking an hour or more. Batch sizes of 30 gallons were prepared using water from the tap. With the tank mixer set at 100 rpm, the polymer was sifted into the fluid by hand through a #30 standard sieve. Regardless of the amount of care taken, lumps always appeared in the fluid.

Subsequently, when it became apparent that degradation was unavoidable, less care was taken in adding the polymer. The fluid was circulated through the bipass circuit at rates up to 1 ft^3/min in order to speed the mixing and blend in the lumps. A 14 mesh, 20 mil wire screen was installed in the exit of the bipass to assist in this task. With this procedure it became possible to test a batch as soon as 24 hours after initially adding the polymer. Formerly, the process took about 3 days.

The CMC obtained for use in this investigation was a commercial grade from Dupont used primarily in laundries. Since the rheology of the mix was determined during the test, the presence of impurities was not of concern. The polyox, coagulant grade, supplied by Union Carbide was of considerably higher quality than the CMC. If a lower grade had been available, it would have been used.

Table 4.1 shows the composition of the fluids which were prepared for test. The higher concentrations were obtained by adding

Table 4.1. Composition of Test Fluids

Polymer Type	Polymer Amount, lb	Water Amount, gal	Nominal % Polymer
CMC	7.5	30	3.0
CMC	13.5	30	5.4
Polyox	2.5	30	1.0
Polyox	4.0	30	1.6
Polyox	6.0	30	2.4
Polyox*	6.0	30	2.4

* Severely degraded form of previous batch.

more polymer to the previous batch. The last entry in the table is a severely degraded version of the previous batch. It was run several weeks later, and water was added to compensate for that lost due to evaporation.

Test Procedure

Data were obtained on the first 5 fluids in Table I at flow rates in the vicinity of 0.2 and 0.6 ft^3/min. Each fluid was run at these flow rates in each of the test sections. Only one test section was used during a run. Power input to the heaters was adjusted such that the highest indicated wall temperature was approximately 83 C.

Data were obtained on the last fluid at flow rates in the vicinity of 0.6 and 0.9 ft^3/min. The lower flow rate runs were made in each test section using about half the power input that would have brought the maximum wall temperature to 83 C. The higher flow rate runs were made, first using a conservative heat input to each test section of approximately 6000 watts, and then applying enough power to bring the test sections to a maximum wall temperature of 83 C. Hesitation to run the last condition was brought on by concern that the tape insulation might become overheated (it did not).

Usually about an hour was required to bring the system from start-up to steady state. An inlet temperature near ambient was maintained. At the start and at the end of each run, flow rate data

were acquired using the classic stop watch and beam balance method. At the lowest flow rate, 10 lb of fluid was timed. At the medium and high flow rates, 15 and 20 lb of fluid respectively were timed. The average time for 3 trials was recorded.

Also recorded at the start and finish of a run were the ambient, coolant inlet, thermocouple conduit, heater wrap, entrance section wall, tank outlet, inlet bulk, and outlet bulk temperatures. During the run, test section wall temperatures were taken. If bulk or wall conditions changed more than 0.1 C during a run, the run was repeated. Each run took about 20 minutes. During this time, the power input to the heaters was always observed to be very stable.

Viscometer Procedure

The 4 runs required on each of the first 5 fluids were usually completed in one day. Between each run, a fluid sample was drawn from the weigh tank exit. It was loaded into the viscometer. Using the MV-I system and controlling sample temperature at 20 C, data were collected at each of the 10 speeds. At the end of the day, another sample was drawn and data were taken at temperatures of 20, 30, 40, 50, 60, 70, and 83 C. At the lower temperatures tap water was routed through the cooling coil to allow the controller to operate more effectively. During higher speed runs, viscous heating was minimized by engaging the speed control only long enough to

obtain a steady state reading (usually about 5 seconds).

The last fluid in Table 4.1 was also tested using the NV system (due to higher shear rates at 0.9 ft^3/min). Circulator fluid controlled the temperature of both stationary surfaces during the use of this system. The procedure used was the same as for the MV-I system above.

The temperature of circulating fluid in the jacket was recorded using the quartz thermometer described in the section on thermocouple calibration.

5. REDUCTION OF DATA

Temperature Data

Calibration data for each thermocouple on the test sections' walls were interpreted using a linear least squares fit:

$$\Delta E = C_1 + C_2 E_{tc} \tag{5.1}$$

where ΔE is the emf error, C_1 and C_2 are constants, and E_{tc} is the thermocouple indicated emf. The reference temperature, taken using the quartz thermometer, was converted to an emf value by interpolating the copper-constantan tables. A statistical program, SIPS, available to users of the Oregon State University CDC 3300 computer, was used in fitting the data and obtaining the constants in Equation (5.1) for each wall thermocouple.

After the emf values were corrected, temperatures were obtained by using second degree Lagrange interpolation polynomials based on key values of emf at 0, 50, 100, 150, and 200 F. One polynomial covered the range 0-100 F while the other covered 100-200 F. Using the inverse process to duplicate thermocouple tables, Benedict (2, p. 78-83) claims that the generated values do not differ from the tables by more than 1 μv at any entry.

Using these data values of wall temperature, a correction was made to account for the effect of gaps in the heaters at the

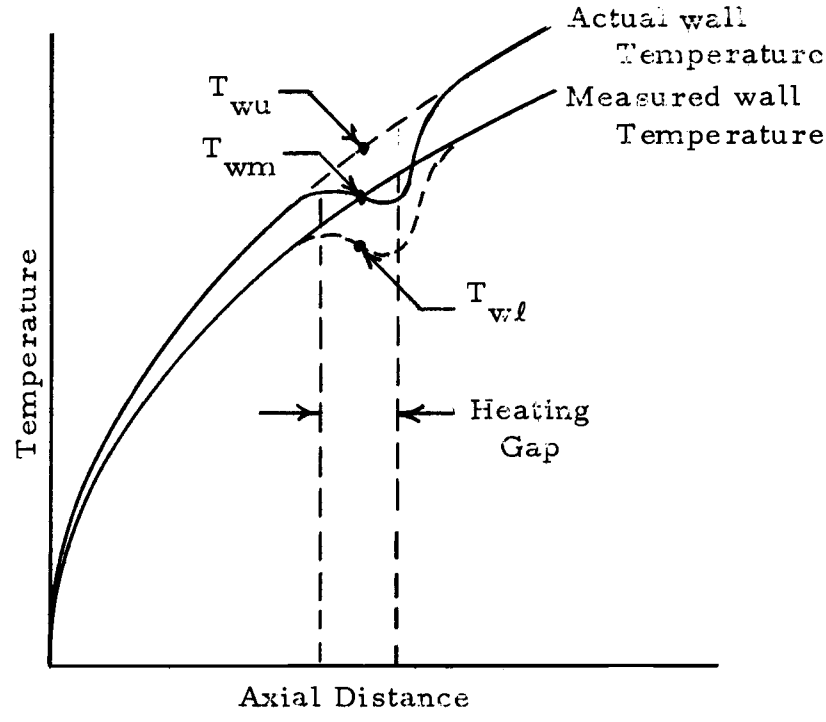

Figure 5.1. Effect of heater gaps on wall temperature.

thermocouple locations. An analysis of the problem is shown in Appendix B. The computations were accomplished using program TCOR listed in Appendix C.

Figure 5.1 shows an exaggerated view of the "gap effect." The lower curve is a line through the measured data. The upper curve shows the actual wall temperature variation along the tube, including a dip in the curve at each thermocouple location. Each dip in the upper curve passes through a measured data point, T_{wm}. The dip in the lower curve is a predicted drop using the measured data. It

was assumed that the difference, $T_{wm} - T_{w\ell}$ was equal to $T_{wu} - T_{wm}$, the actual drop. This value was added to T_{wm} as a tentative correction. Using the corrected values, an attempt was made to generate T_{wm} as a check.

In the absence of a conducting wall, the effect of the heating gaps can be remarkable. Drops on the order of 10 C are predicted. However, axial conduction in the tube wall reduced these drops to more reasonable values. It is ironic that in the heated sections, axial conduction in the tube wall was negligible; whereas, in the gaps, axial conduction played a prominent role in moderating the temperature drop. This apparent contradiction can be resolved by comparing the axial temperature gradients in each situation. Very high gradients in the gap provided the driving mechanism for a substantial flow of heat.

Bulk inlet temperatures were obtained from measured emf's by direct use of the thermocouple tables. At the controlled inlet condition of 21 to 23 C, the inlet probe was accurate to within 0.1 C. The other temperature data taken were not corrected. Their function was diagnostic only.

The input power to the test sections was assumed to be distributed uniformly over an area:

$$A_L = \pi DL \qquad (5.2)$$

where D is the inside diameter of the tube and L is the total length of heated tubing, including the gaps (119.5 inches). The local bulk temperature was then calculated using an energy balance:

$$T_{bx} - T_o = \pi D x q_o'' / \dot{m} C_p \qquad (5.3)$$

These initial computations (exclusive of the gap correction) were made using program DATRED listed in Appendix C.

Rheological Data

No viscometer has yet been devised which will measure the shear stress and the rate of shear at the same point in the flow. In the case of Newtonian fluids, the shear rate at the point of measurement of the shear stress can usually be obtained quite easily by analysis. However, in non-Newtonian cases, even if a model is adopted, the determination is usually quite tedious. If accuracy is not important, an average value of shear rate is sometimes used. If accuracy is important, one must be put to a certain amount of inconvenience in obtaining it.

Development of the Constitutive Equation

Consider the case of a rotor-beaker type of viscometer in which a Couette flow is developed between a rotating inner cylinder (rotor) and a stationary concentric outer cylinder (beaker). The

fundamental equations, developed (103, p. 51-61) from the equations of continuity and momentum under the conditions of one-dimensional, steady, laminar, incompressible, isothermal flow, are:

$$\tau r^2 = \text{constant} \tag{5.3}$$

$$\tau_1 = M/2\pi R_1 h_r \tag{5.4}$$

$$\Omega = -\frac{1}{2}\int_{\tau_1}^{\tau_2} \dot{\gamma}\,\frac{d\tau}{\tau} \tag{5.5}$$

where M is the torque applied to the rotor, h_r is the length of the rotor, Ω is the angular speed of the rotor, and R_1, R_2, and r are as shown in Figure 5.2.

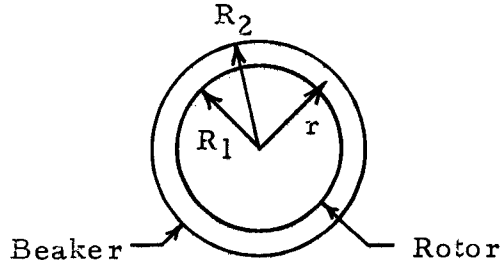

Figure 5.2. Geometry of the Couette system under consideration. Gap size is exaggerated.

From Equations (5.3) and (5.4), the shear stress at any point in the flow may be easily determined using only the geometry and the applied torque. In the Newtonian case, determination of the shear rate from Equation (5.5) is also quite easy:

$$\dot{\gamma} = 2\Omega R_2^2/(R_2^2 - R_1^2) \tag{5.6}$$

Using Equation (5.6) for other than Newtonian fluids can lead to errors of 5-10%. Using specific models, such as the power law, improves the results only to the extent that the model is able to describe the rheology of that fluid.

One popular way of solving this problem without having to assume a specific model is to use a differentiated form of Equation (5.5),

$$\frac{d\Omega}{d\tau_1} = \frac{1}{2\tau_1}(\dot{\gamma}_1 - \dot{\gamma}_2) \tag{5.7}$$

Kreiger and Elrod (45) have used the Euler-MacLaurin sum formula in conjunction with Equation (5.7) to obtain the series solution:

$$\dot{\gamma}_1 = \frac{\Omega}{\mathrm{Ln}\,\epsilon}\left[1 + \mathrm{Ln}\,\epsilon\,\frac{d(\mathrm{Ln}\,\Omega)}{d(\mathrm{Ln}\,\tau_1)} + \ldots\right] \tag{5.8}$$

where $\epsilon = R_2/R_1$. To use this solution, one must differentiate the data curve of $\mathrm{Ln}\,\Omega$ vs. $\mathrm{Ln}\,\tau_1$. Unfortunately, differentiated values taken from data curves substantially weaken the accuracy arguments for subsequent calculations.

Huang (38) has suggested a numerical scheme to solve Equation (5.5). An initial assumption is that

$$\dot{\gamma} = B_1\tau + B_2\tau^2 + B_3\tau^3 + \ldots \tag{5.9}$$

will describe the data with a reasonable number of terms. This expression, when substituted into Equation (5.7), yields:

$$\frac{d\Omega}{d\tau_1} = \frac{1}{2\tau_1}\left[B_1(\epsilon^2 - 1)\tau_1 + B_2(\epsilon^4 - 1)\tau_1^2 + \ldots\right] \qquad (5.10)$$

Using a least squares fit of the data, one obtains:

$$\frac{d\Omega}{d\tau_1} = C_o + C_1\tau_1 + C_2\tau_1^2 + \ldots \qquad (5.11)$$

where C_i are known. Thus, one can solve for B_j:

$$B_1 = \frac{2C_o}{\epsilon^2 - 1}, \quad B_2 = \frac{2C_1}{\epsilon^4 - 1}, \quad B_3 = \frac{2C_2}{\epsilon^6 - 1}, \ldots \qquad (5.12)$$

The solution is completed. The disadvantage of using the differentiated values of $\frac{d\Omega}{d\tau_1}$ is still present.

In the present investigation, a modified version of Huang's method was employed. Equation (5.9) was substituted into Equation (5.5), with the result:

$$2\Omega = B_1'(\epsilon^2-1)\tau_1 + \frac{B_2'}{2}(\epsilon^4-1)\tau_1^2 + \frac{B_3'}{3}(\epsilon^6-1)\tau_1^3 + \ldots \qquad (5.13)$$

Equation (5.13) was compared with a least squares fit:

$$\frac{2\Omega}{\tau_1} = C_o' + C_1'\tau_1 + C_2'\tau_1^2 + C_3'\tau_1^3 + \ldots \qquad (5.14)$$

The constants for the model were then,

$$B_1' = \frac{C_o'}{\epsilon^2 - 1}, \quad B_2' = \frac{2C_1'}{\epsilon^4 - 1}, \quad B_3' = \frac{3C_2'}{\epsilon^6 - 1}, \ldots \qquad (5.15)$$

The values of τ_1 were obtained from the instrument scale reading, S, using:

$$\tau_1 = C_1 S \qquad (5.16)$$

where C_1 is a constant obtained from the manufacturer's calibration of the instrument for a particular measuring system (beaker and rotor combination). Comparison with Equation (5.4) shows that the geometry and a torque conversion factor are represented by the constant, C_1. Also accounted for, since the constant was obtained by calibration, are the end effects which have been excluded from the analysis.

Each set of viscometer data taken at each temperature for each test fluid was regressed using SIPS. A sixth order polynomial was assumed as Equation (5.9), and the corresponding least squares fit, Equation (5.14), was made. Terms were dropped from the model according to an F-test at the 99% level of confidence. The remaining terms numbered from 3 to 6 when this process was accomplished. The percent error was evaluated for the model at each of the data values of τ_1. It was rarely more than 3%.

The difficult geometry of the double-gap NV measuring system prevented an analysis comparable to the MV system. Therefore, an

average shear rate (derived assuming Newtonian behavior) given by the manufacturer was recorded. This data was used only for the high flow-rate runs of the last fluid in Table 4. 1. It can be expected that viscometric data for this fluid using this measuring system is in error as much as ±5%. When using this measuring system. Equation (5. 9) was obtained directly by least squares fit of τ_1 and $\dot{\gamma}$. As in the previous case, terms were subjected to an F-test to determine if they should be dropped from the model.

It should be emphasized that neither of these measuring systems was capable of producing data accounting for viscoelastic behavior. When this behavior is present in Couette viscometers, normal stresses contribute to a secondary flow pattern in the vertical direction which can result in the fluid spilling over the top of the gap. This normal stress phenomenon is called the Weissenberg effect. Although the test fluids showed some evidence of viscoelasticity (especially polyox solutions), it did not present a problem in the viscometer.

Application to Tube Flow

In order to apply the constitutive equations, Equations (5. 9), to tube flow, the Mooney-Rabinowitch equation was used:

$$\frac{8Q}{\pi D^3} = \frac{1}{\tau_w^3} \int_0^{\tau_w} \tau^2 \dot{\gamma}\, d\tau \qquad (5.17)$$

where Q is the volume flow rate, and τ_w is the shear stress at the tube wall. Conditions imposed during its derivation (95, p. 70-72) were:

1. Steady, laminar flow.
2. Fully developed, one-dimensional flow.

The second condition is not met when the velocity profile changes due to temperature effects on viscosity. Also, it is obviously not met when a secondary flow develops due to buoyancy. Thus, use of Equation (5.17) was restricted to the inlet.

Attempts to obtain a satisfactory general constitutive relationship for each fluid that included temperature variation were not successful. It was necessary to develop an interpolation scheme using Equations (5.9). Due to the integration scheme chosen for the solution of Equation (5.17), it was possible to interpolate at a chosen shear rate. As can be seen from Figure 5.3, horizontal interpolation provided better resolution between curves, particularly as one became asymptotic.

An exponential method was chosen for the interpolation, based upon the Arhhenius relationship:

$$\eta(T) = C_1 e^{-\Delta H/RT} \tag{5.18}$$

where C_1 is a constant. Consider the two adjacent constitutive curves shown in Figure 5.4. At a particular value of $\dot{\gamma} = \dot{\gamma}_p$ and at

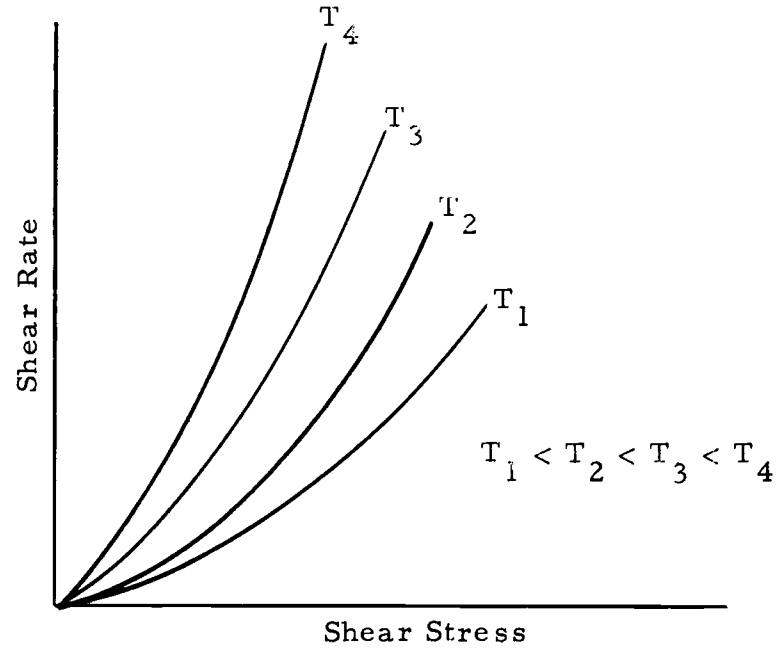

Figure 5.3. Typical behavior of constitutive equations obtained from the viscometric data.

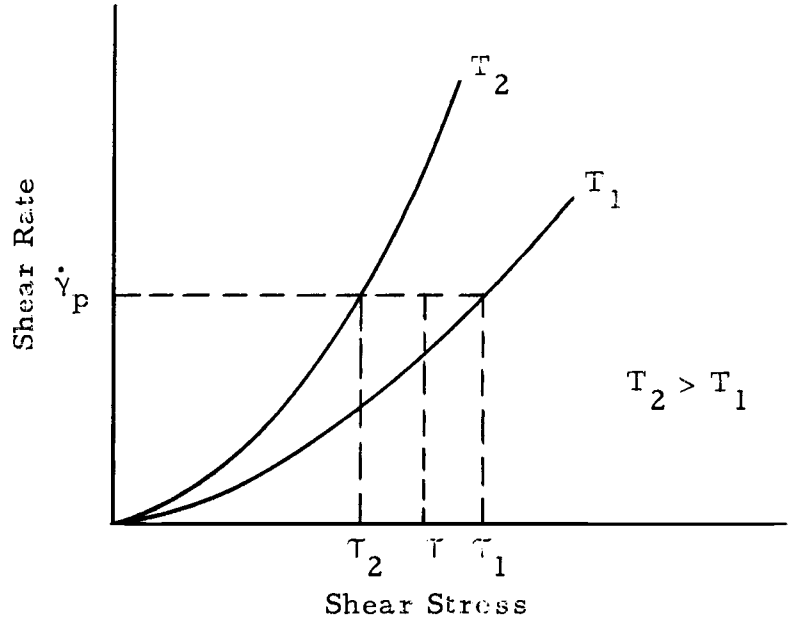

Figure 5.4. Interpolation between adjacent constitutive equations.

a temperature, T, in the range $T_1 \leq T \leq T_2$, from Equation (5.18) one obtains:

$$\tau e^{\Delta H/RT} = \tau_1 e^{\Delta H/RT_1} = \tau_2 e^{\Delta H/RT_2} \tag{5.19}$$

Assuming ΔH is constant over this small temperature range, it follows from Equations (5.19) that:

$$\text{Ln} \frac{\tau_1}{\tau_2} = \frac{\Delta H}{R}\left(\frac{1}{T_1} - \frac{1}{T_2}\right) \tag{5.20}$$

Solving Equation (5.20) for $\Delta H/R$ and substituting into Equations (5.19), yields:

$$\tau = \tau_1 \left(\frac{\tau_2}{\tau_1}\right)^{\frac{T_2}{T_1}\left(\frac{T - T_1}{T_2 - T_1}\right)} \tag{5.21}$$

Using Equation (5.21), it was possible to obtain a discrete value of τ for a particular $\dot{\gamma}$ at a temperature, T.

Since $\dot{\gamma}$ is a factor, the integrand of Equation (5.17) behaves in a manner similar to the viscosity curves. By changing the variable of integration, the accuracy of the numerical integration was improved. This was accomplished by applying integration by parts to Equation (5.17):

$$\frac{24Q}{\pi D^3} = \dot{\gamma}_w - \frac{1}{\tau_w^3} \int_o^{\dot{\gamma}_w} \tau^3 d\dot{\gamma} \tag{5.22}$$

The numerical procedure used to solve Equation (5. 22) was based on the theme of Simpson's rule. Three points at a time were considered, and the latest value was used as one of the next 3 points. Thus, it was possible to change the spacing during an integration. Knowing Q, D, T, and $\dot{\gamma} = f(\tau)$ at discrete temperatures, the right side of Equation (5. 22) was "marched along" until it matched the left side. At least 200 steps were taken for the integration.

Examination of the results of Etchart (20, p. 51-66) show that the axial pressure gradient remains constant for the entire thermal entrance region. (Some deviation occurs at low Graetz numbers, becoming more pronounced as the degree of pseudoplasticity is in-increased.) If the pressure gradient is constant, the wall shear stress (in the absence of a substantial change in momentum flux) also must remain constant.

Under the assumption of a constant pressure gradient, the wall shear stress was taken to be equal to the entrance value at every point along the heated section. Local shear rates were determined by interpolating Equations (5. 9) using the wall shear stress and the local wall temperature. Since a particular shear stress was specified, it was necessary to use vertical interpolation of the curves shown in Figure 5. 3. This was accomplished by replacing $\dot{\gamma}$ with τ in Equation (5. 21),

$$\dot{\gamma} = \dot{\gamma}_1 \left(\frac{\dot{\gamma}_2}{\dot{\gamma}_1} \right)^{\frac{T_2}{T_1} \left(\frac{T - T_1}{T_2 - T_1} \right)} \tag{5.23}$$

When the local shear rates became too high, the constitutive equations, Equations (5.9), were extended using the power law. If the value of the wall shear stress was greater than 90% of the shear stress at the highest data point on a curve, τ_{max}, that curve was extended. Values for the power law constants were obtained using computed values of shear rate at 0.5 τ_{max} and 0.9 τ_{max}. A curve was extended only when 0.9 τ_{max} was exceeded.

A "mixing cup" analogy, first suggested by Charm and Merrill (7), was used in obtaining an apparent viscosity representative of the bulk flow conditions. The relationship used was:

$$\eta_B = \frac{\int_A u \eta \, dA}{\int_A u \, dA} = \frac{2\pi}{Q} \int_0^{\frac{D}{2}} u \eta r \, dr \tag{5.24}$$

where A is the cross-sectional area, and u is the velocity. For an isothermal cross section (95, p. 71):

$$\frac{\tau}{r} = \text{Constant} \tag{5.25}$$

Using Equation (5.25), Equation (5.24) becomes:

$$\eta_B = \frac{\pi D^2}{2Q\tau_w^2} \int_o^{\tau_w} \frac{u\tau^2}{\dot{\gamma}} \, d\tau \tag{5.26}$$

To generate the required values of velocity, u,

$$\dot{\gamma} = -\frac{du}{dr} \tag{5.27}$$

was integrated. Equation (5.25) was used to change variables with the result:

$$u = \frac{D}{2\tau_w} \int_{\tau}^{\tau_w} \dot{\gamma} \, d\tau \tag{5.28}$$

Integration by parts was employed to change the variable of integration to $\dot{\gamma}$:

$$u = \frac{D}{2\tau_w} \left[\tau_w \dot{\gamma}_w - \tau\dot{\gamma} - \int_{\dot{\gamma}}^{\dot{\gamma}_w} \tau \, d\dot{\gamma} \right] \tag{5.29}$$

For the integration of Equation (5.29), the values of τ_w and $\dot{\gamma}_w$ were obtained from a solution of Equation (5.22) where the entire cross section was assumed to be at the local bulk temperature. Once the values of u were generated, together with the corresponding values of τ and $\dot{\gamma}$, it was a simple matter to integrate Equation (5.26). As a check, the generated values of u were integrated over the cross-sectional area to obtain a value which was compared with the measured value of Q.

The computational tasks for all the viscosity calculations were

performed using program VISCO, listed in Appendix C. It should be emphasized that the numerical procedures used would not be necessary in a design situation. Normally, a simple model, representative of the working fluid, would be used (such as the temperature-dependent power law). Closed form solutions for τ_w and u have been derived for such models (see Skelland (95, p. 110 and 120), for example); and a closed form, albeit lengthy, integration of Equation (5.26) is possible.

Data From Other Sources

Christiansen and coworkers (9, 35) and Oliver and Jenson (72) have found that properties (other than viscosity) of dilute, aqueous solutions of CMC and Polyox do not vary substantially from those of pure water. Heat capacity and density were found to be equal to those of pure water by Christiansen and Craig (9). They reported results from prior investigations that showed thermal conductivity to be within 1 to 3% of that for pure water.

Thermal conductivity, density, thermal expansivity, and heat capacity data for water were obtained from the Handbook of Chemistry and Physics (104, p. D-122, E-11, and F-5). Thermal conductivity data were extracted for temperatures from 7 to 97 C at 10 C intervals. Density and thermal expansivity data were obtained from the reference for temperatures of 15-85 C at 5 C intervals.

Heat capacity data for temperatures of 32 F and 40-200 F at intervals of 20 F were used from the reference.

Each set of data was regressed using SIPS. All, except the heat capacity data, were fitted by fifth order polynomials. The heat capacity data were fitted by a fourth order polynomial. The resulting functions appear at the end of the computer programs DATRED and PARGEN listed in Appendix C.

Dimensionless Parameters

A number of pertinent dimensionless parameters were generated for use in analyzing the data. The local Nusselt and Graetz numbers were computed:

$$Nu_x = q_o'' D/k(T_w - T_b) \tag{5.30}$$

$$Gz_x = \dot{m} C_p/kx \tag{5.31}$$

Properties in Gz were evaluated at the local bulk temperature. Values of Nu were generated for the cases of k evaluated at the local bulk temperature and at the wall temperature.

Prandtl numbers,

$$Pr = \eta C_p/k \tag{5.32}$$

were obtained for 4 separate conditions. Values were generated based on the entrance bulk flow conditions, the entrance wall

conditions, the local bulk flow conditions, and the local wall conditions.

Brinkmann numbers,

$$Br = 4\eta Q^2/\pi T_o D^2 k \tag{5.33}$$

were determined at the entrance wall condition.

Reynolds numbers,

$$Re = 4\dot{m}/\pi D\eta \tag{5.34}$$

were computed at the entrance and local bulk flow conditions.

Modified Grashof numbers,

$$Gr_x^* = \rho^2 \beta g D^4 q_o''/k\eta^2 \tag{5.35}$$

and modified Rayleigh numbers,

$$Ra_x^* = Gr_x^* Pr_x \tag{5.36}$$

were computed at both the local wall and the local bulk flow conditions.

Viscosity ratios, η_b/η_w and shear rate ratios,

$$\delta = \dot{\gamma}_w/(8V/D) = \pi\rho\dot{\gamma}_w D^3/32\dot{m} \tag{5.37}$$

were determined at both the entrance and local conditions.

Dimensionless flux,

$$\phi = q_o'' D/kT_o \tag{5.38}$$

was obtained locally and at entrance evaluating k at the wall temperature and at the local bulk temperature.

All of the computation was performed using program PARGEN listed in Appendix C. Data are listed in Appendix F.

The hypothesis was then formed that the parameters would obey:

$$Nu_x = C_1 X_1^{m_1} X_2^{m_2} X_3^{m_3} \tag{5.39}$$

or

$$Ln\,Nu_x = Ln\,C_1 + m_1 Ln\,X_1 + m_2 Ln\,X_2 + \ldots \tag{5.40}$$

where C_1 is a constant, and X_1, X_2, X_3, ... are the pertinent dimensionless parameters generated. The data, in log rithmic form, were then fitted to the linear model of Equation (5.40) by the method of least squares. The empirical constants C_1, m_1, m_2, m_3, ... were obtained from this fit. An F-test was performed at each stage that a variable was added to determine its statistical importance to the model.

Another hypothesis tested was:

$$Nu_x = C_1 Gz_x^{1/3\, C_2 X_1 + C_3 X_2 + \ldots} \tag{5.41}$$

or

$$Ln\,(Nu_x/Gz^{1/3}) = Ln\,C_1 + C_2 X_1 Ln\,Gz_x + C_3 X_2 Ln\,Gz_x + \ldots \tag{5.42}$$

Again a linear least squares fit was employed to determine C_1, C_2, C_3, . . . and an F-test used as a criteria in retaining a parameter in the model.

Finally, the hypothesis of:

$$\frac{Nu_x}{1.411\,\delta_o^{1/3}\,Gz_x^{1/3}} = X_1^{m_1}\,X_2^{m_2}\,X_3^{m_3} \qquad (5.43)$$

or

$$\mathrm{Ln}\,\frac{Nu_x}{1.411\,\delta_o^{1/3}\,Gz_x^{1/3}} = m_1 \mathrm{Ln} X_1 + m_2 \mathrm{Ln} X_2 + m_3 \mathrm{Ln} X_3 + \ldots \qquad (5.44)$$

was tested in a similar manner.

This statistical work was performed using the program, SIPS, from the Oregon State University computer center library.

6. RESULTS OF TEST

Calibration of Thermocouples

A plot of the calibration data obtained for the bottom thermocouple located 18 inches from the entrance to the small test section is shown in Figure 6.1. A similar plot for the large test section, Figure 6.2, displays the data taken for the top thermocouple, located 72 inches from the entrance. These plots are typical of the results of the calibration runs for the 28 thermocouples which were soldered to the walls of the test sections.

The 4 thermocouples which were broken and subsequently glued to the wall of the small test section displayed ΔE values 5 to 10 times as great as the others. This can be attributed to a higher contact resistance due to the presence of a thin layer of epoxy glue between the thermocouple and the wall. Because of this large error and because of questionable readings during the test runs later, data from these thermocouples were not correlated.

Although some scatter was evident in the calibration data, the typical range of the residuals, $\Delta E_{model} - \Delta E_{data}$, was within $\pm 3\mu v$. Extreme cases were +8, -6 μv for the bottom thermocouple, 3 inches from the entrance to the small test section; and +13, -8 μv for the top thermocouple, 3 inches from the entrance to the large test section.

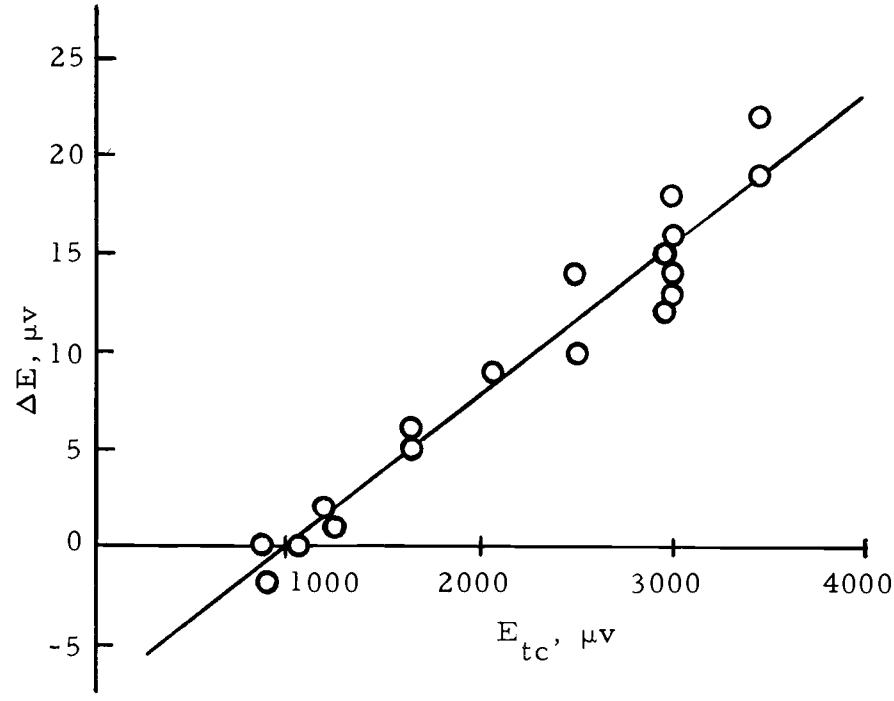

Figure 6.1. Calibration curve for bottom thermocouple located 18 inches from entrance to small test section.

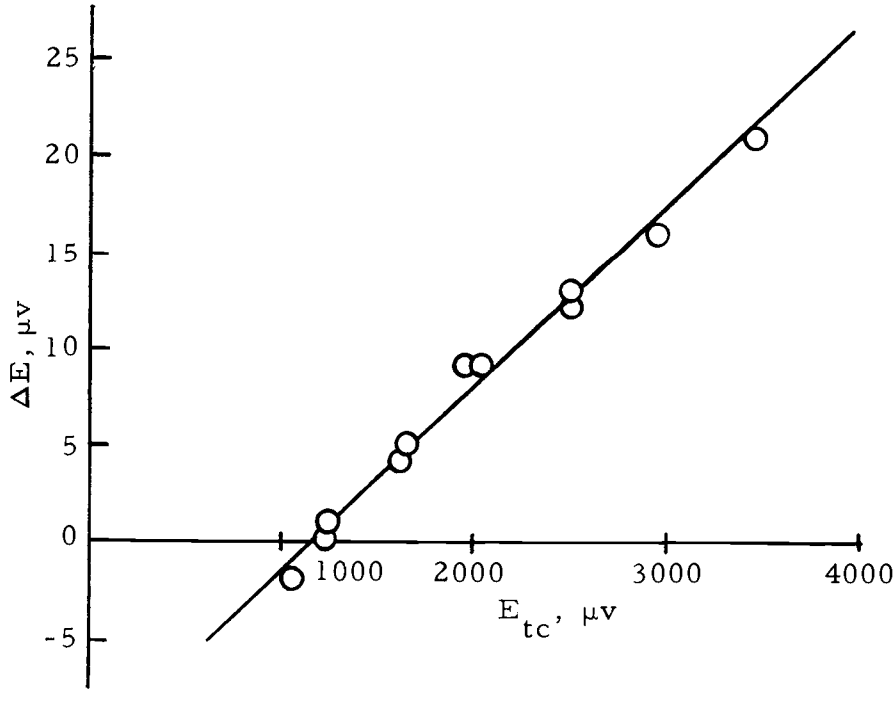

Figure 6.2. Calibration curve for top thermocouple located 72 inches from entrance to large test section.

The model estimate (using the statistical program SIPS) of ΔE for E_{tc} at an expected measured value showed a 6 μv range of uncertainty at the 99% level of confidence for the worst case for the small test section. On the large test section, a 12 μv range of uncertainty was obtained at the 99% level of confidence for the worst case. Typical uncertainty ranges for the calibration models were on the order of 4 μv.

Viscometry

Plots of the data obtained from the viscometer runs are shown in Figures 6.3 through 6.8. Although Ω, the angular speed of the rotor, is plotted along the abscissa, the trend of the data is similar to a $\dot{\gamma}$ - τ plot. Each oblique data line represents data taken at a single temperature. At the higher temperatures and lower rotor speeds, data were not always obtainable. For some of the fluids, the scale readings were too low to be meaningful. Thus, there are not 10 data points at every temperature for every fluid.

Note that the power law model (straight line on a log-log plot) might describe the CMC data quite well; however, for the polyox solutions, the range of validity appears to be quite limited. Also note the extreme difference in temperature-dependence between the 5.4% CMC solution in Figure 6.4 and the 2.4% polyox solution in Figure 6.7, particularly at higher values of Ω (corresponding to

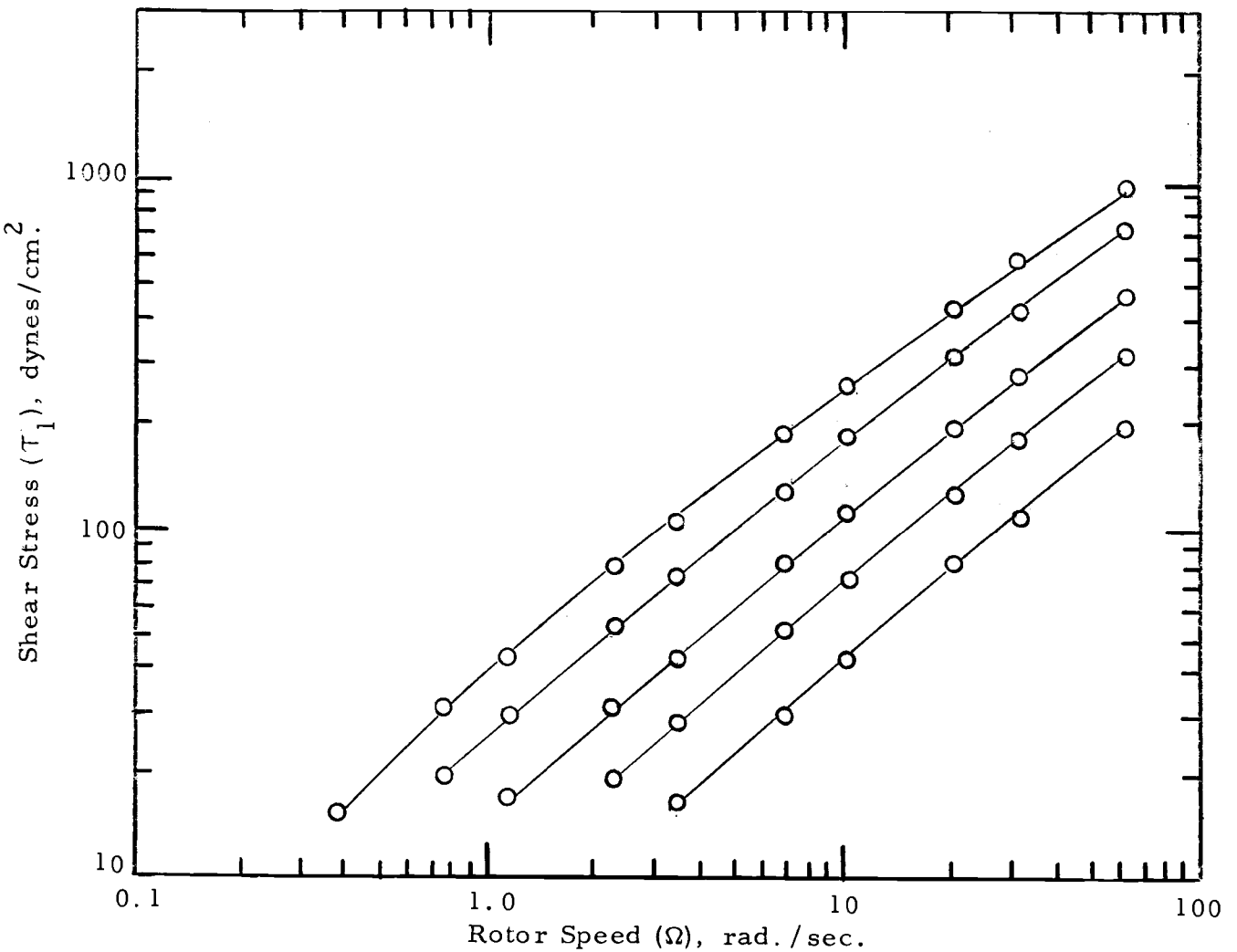

Figure 6.3. Viscometry results for 3.0% CMC solution. From the top, data were taken at 22.0, 32.3, 49.1, 65.4, and 82.4C.

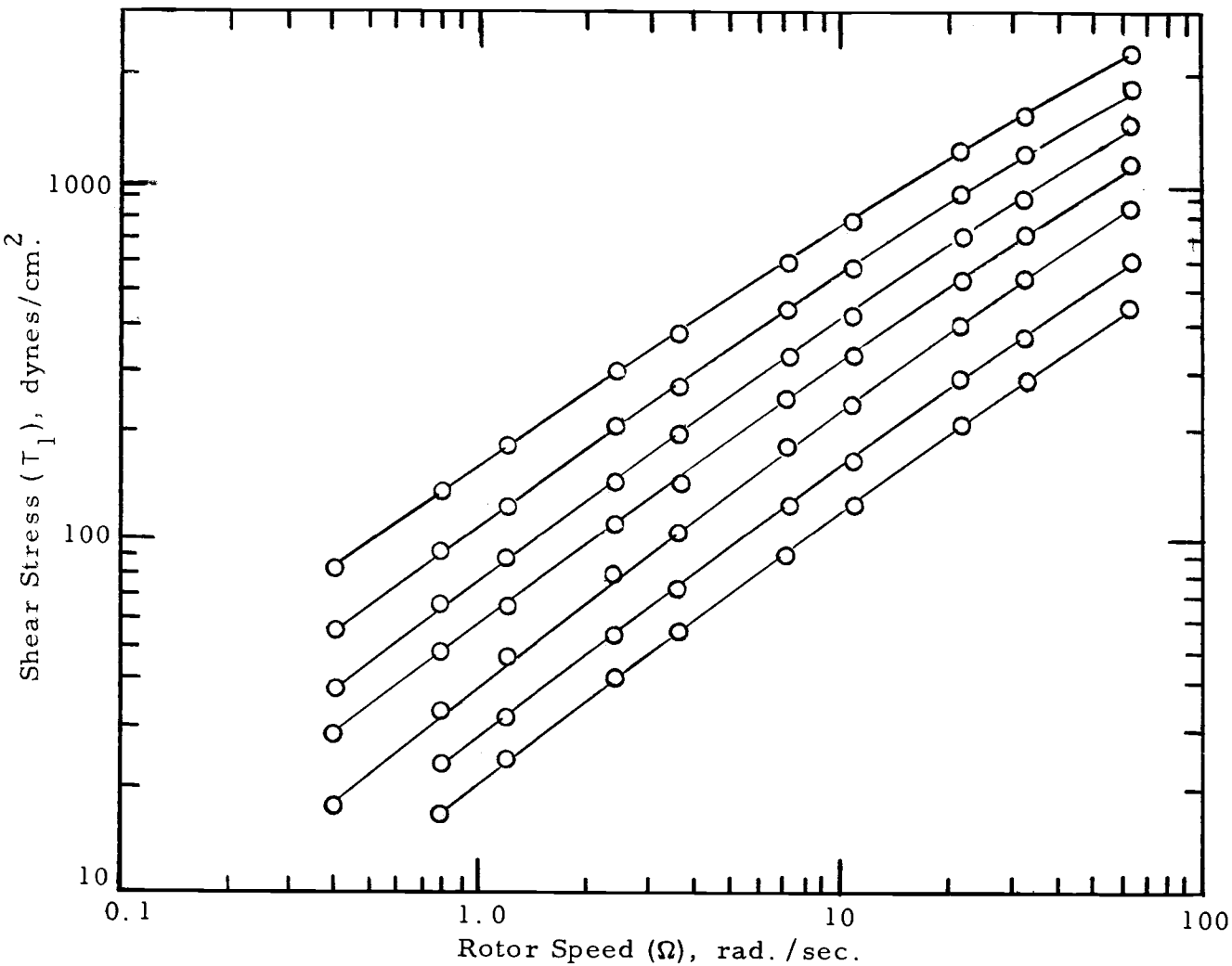

Figure 6.4. Viscometry results for 5.4% CMC solution. From the top, data were taken at 20, 30, 40, 50, 60, 70, and 83.2 C.

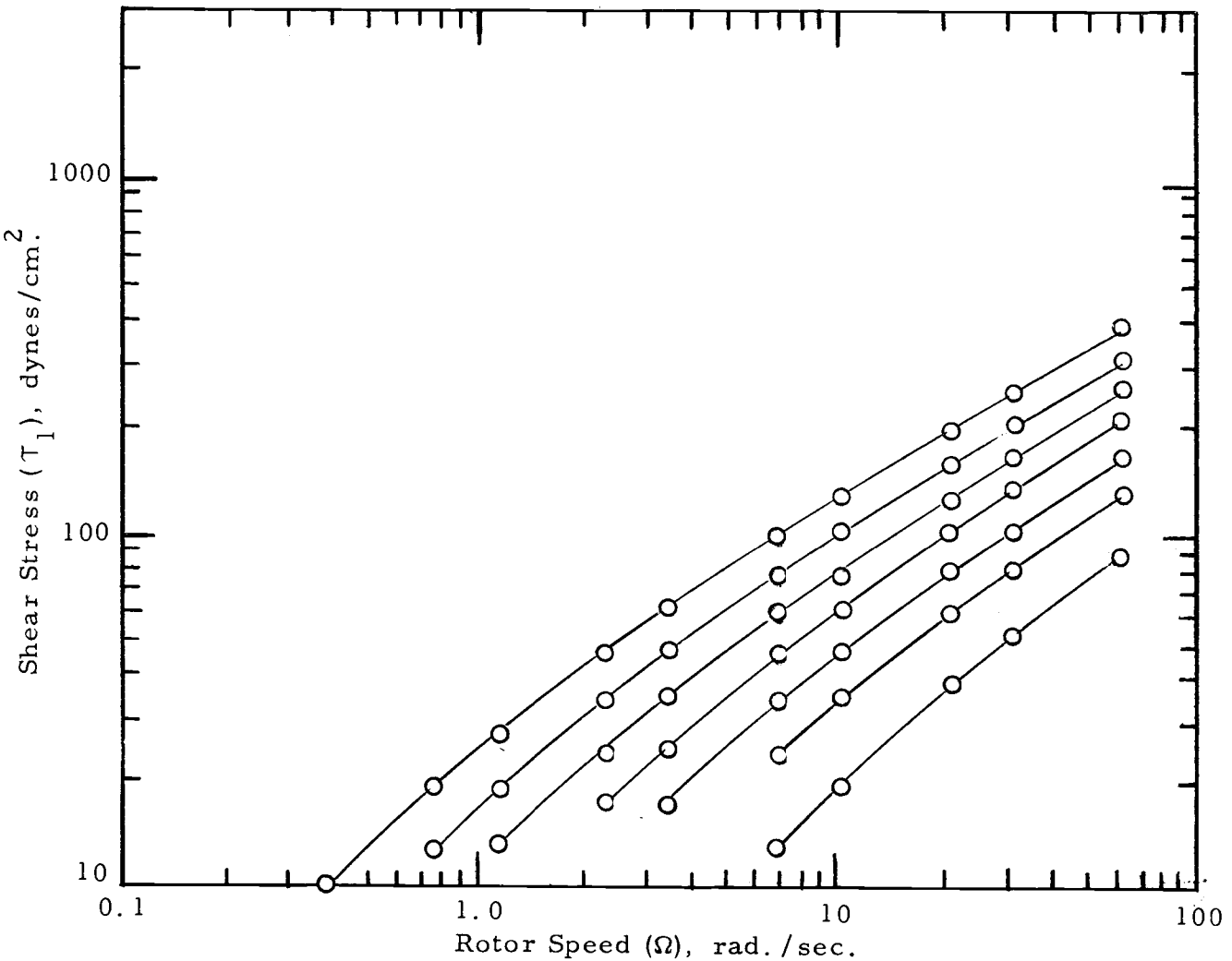

Figure 6.5. Viscometry results for 1% Polyox solution. From the top, data were taken at 20, 30, 40, 50, 60, 70, and 83.2 C.

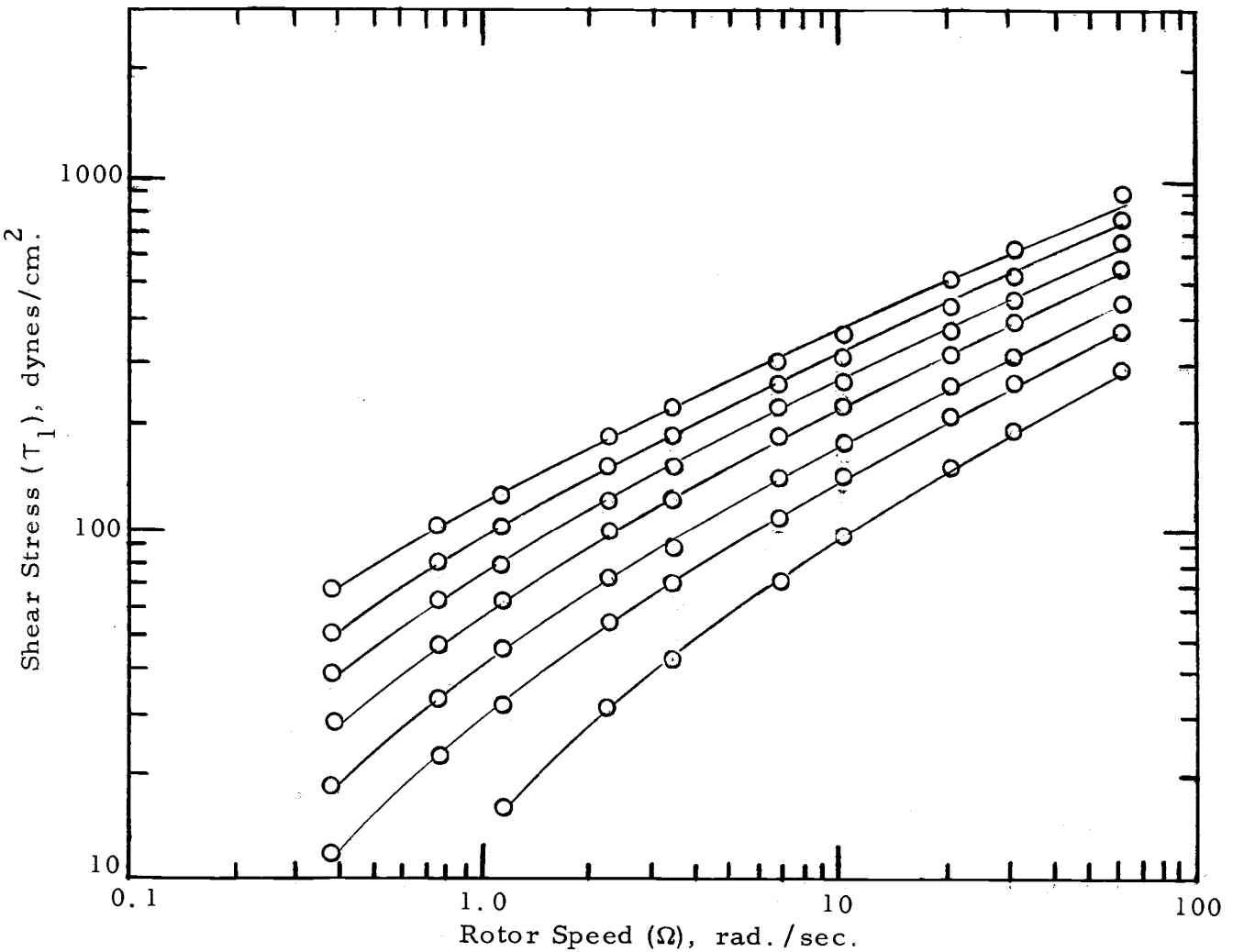

Figure 6.6. Viscometry results for 1.6% Polyox solution. From the top, data were taken at 20, 30, 40, 50, 60, 70, and 83.2 C.

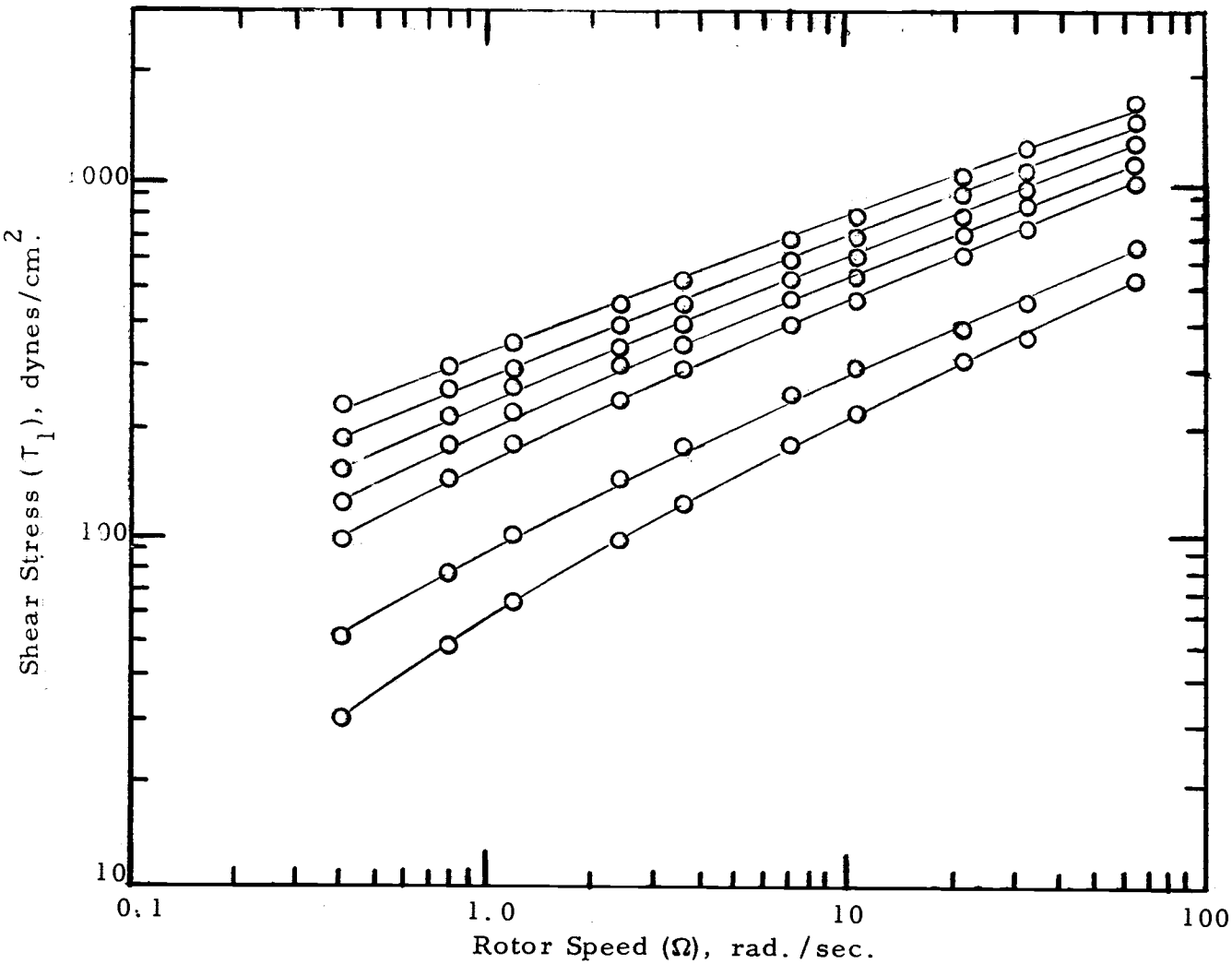

Figure 6.7. Viscometry results for 2.4% Polyox solution. From the top, data were taken at 20, 30, 40, 50, 60, 70, and 83.2 C.

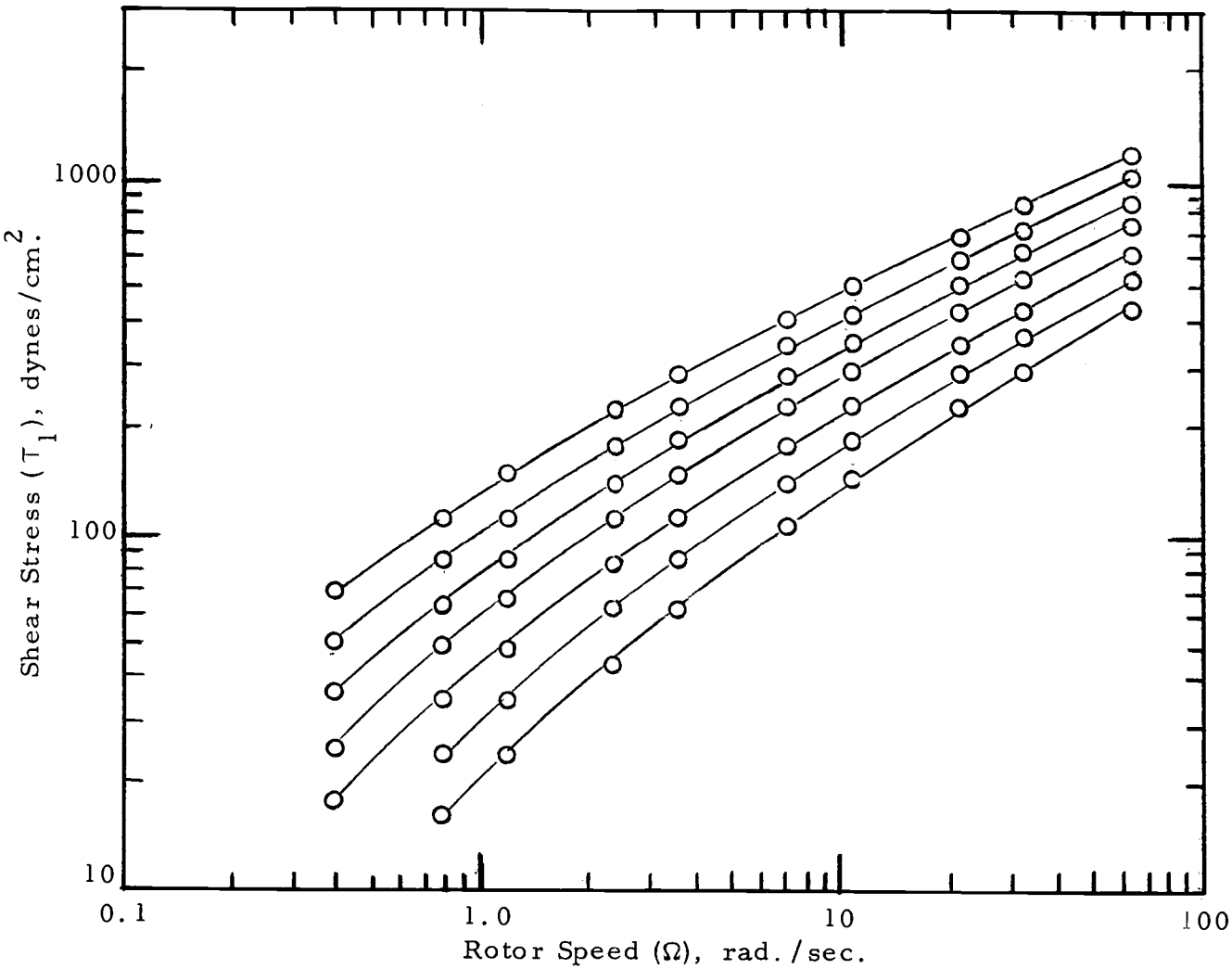

Figure 6.8. Viscometry results for 2.4% Polyox (degraded) solution. From the top, data were taken at 20, 30, 40, 50, 60, 70, and 84.0 C.

higher values of $\dot{\gamma}$). The polyox solutions appear to become less temperature-dependent with concentration, whereas the CMC solutions become more temperature-dependent with concentration.

As a final observation, there is an obvious drop in the data in Figure 6.7 between that taken at 60 C and that at 70 C. Since the problem of sample evaporation was difficult to solve, this drop might well have been a result of that problem. Another explanation might be that some of the polymer precipitated from the solution. Although precipitation should not occur prior to boiling, salt impurities lower the critical temperature. In any event, there is some question as to whether these bottom 2 curves are representative of fluid behavior in the test sections. By the time this irregularity was discovered, the sample taken during the test runs had degraded too severely to rerun the viscometer test.

A complete listing of the viscometer data is included as Appendix D.

Heat Transfer

The Nusselt number determined using k evaluated at the local wall temperature proved to correlate the data best. Its choice can further be justified on the basis that this parameter should reflect the ratio of the temperature gradient at the wall to the temperature gradient across the fluid in the pipe. The range of Nu_x evaluated in this

manner was 10.9 to 54.9 under the following range of conditions: Gz_x, 225 - 38,000; Pr_{bo}, 315 - 20,100; Pr_{wo}, 189 - 4310; Pr_{bx}, 282 - 19,600; Pr_{wx}, 28.2 - 2,260; Re_o, 1.68 - 574; Re_x, 1.73 - 633; Gr_b^*, 4.18 - 1.07×10^4; Gr_w^*, 5.40×10^2 - 2.40×10^6; Ra_b^*, 2.90×10^4 - 5.13×10^6; Ra_w^*, 4.02×10^5 - 1.05×10^8; Br_o, 8.84×10^{-5} - 4.22×10^{-3}; δ_o, 1.05 - 1.44; δ_x, 1.80 - 25.9; η_b/η_w, 2.61 - 55.7; ϕ_o, 1.75 - 3.90.

Results for 8 of the 26 runs are shown in Figures 6.9 through 6.12. The solid lines below the data represent Equation (1.31) in which all properties are evaluated at the entrance conditions for the run. This line represents the course the data might assume if the fluid properties were not temperature-dependent. The lowest line corresponds to the run with smallest value of δ_o.

Specifically compared in each of these plots are the results for the 5.4% CMC solution and the 2.4% Polyox solution under similar flow and heating conditions. Figure 6.9 compares the results at low flow rate in the large test section. Note that the Polyox run is about 8% higher than the CMC run at $Gz_x = 600$. Each is about 20% above its corresponding temperature-independent property solution at the same Gz_x. However, far upstream at $Gz_x = 9300$, the CMC run is 15% above and the Polyox run is only 7% above the temperature-independent property solution.

Figure 6.10 shows results at a higher flow rate in the same test

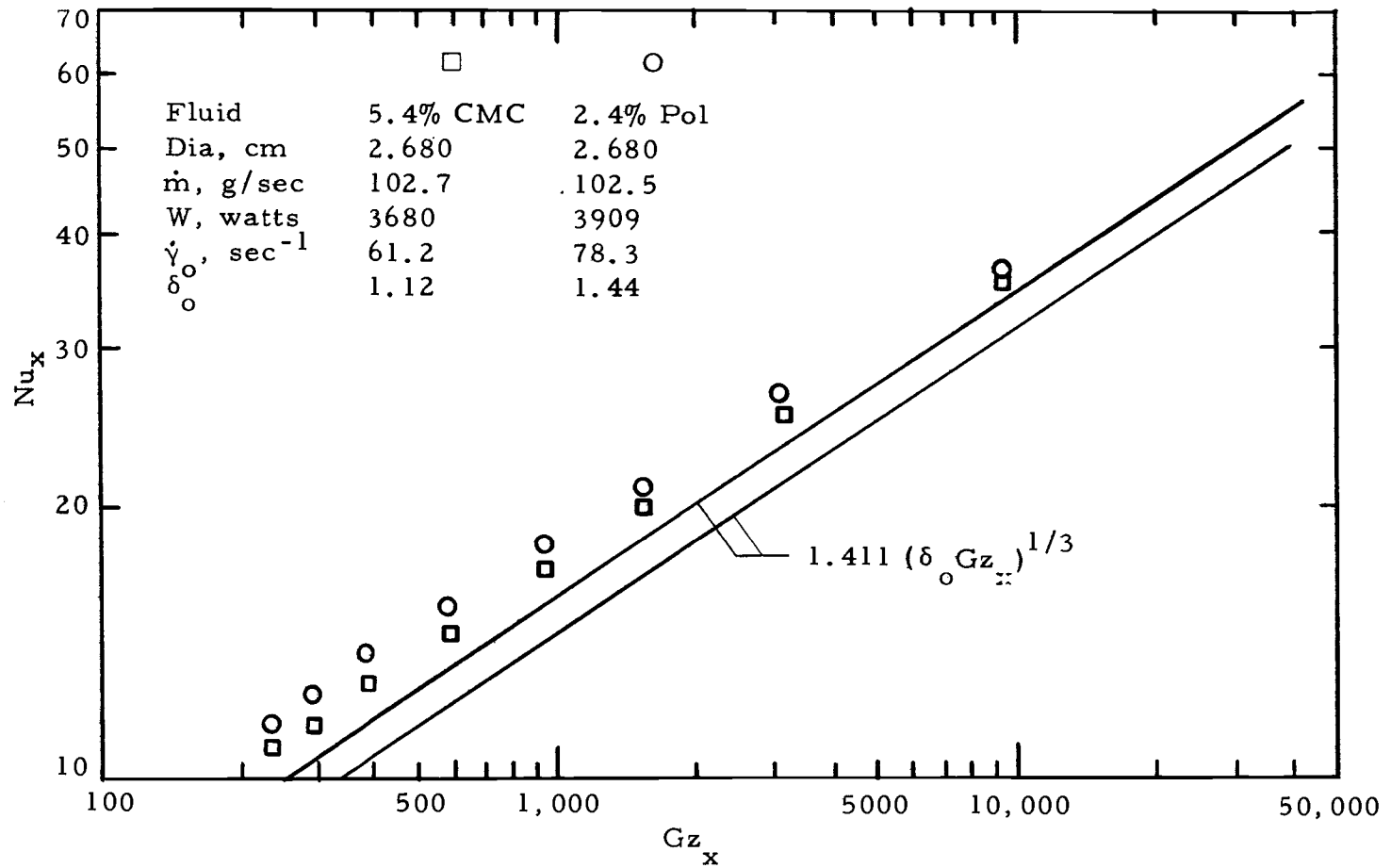

Figure 6.9. Heat transfer results for 5.4% CMC and 2.4% Polyox at low mass flow rate in large test section.

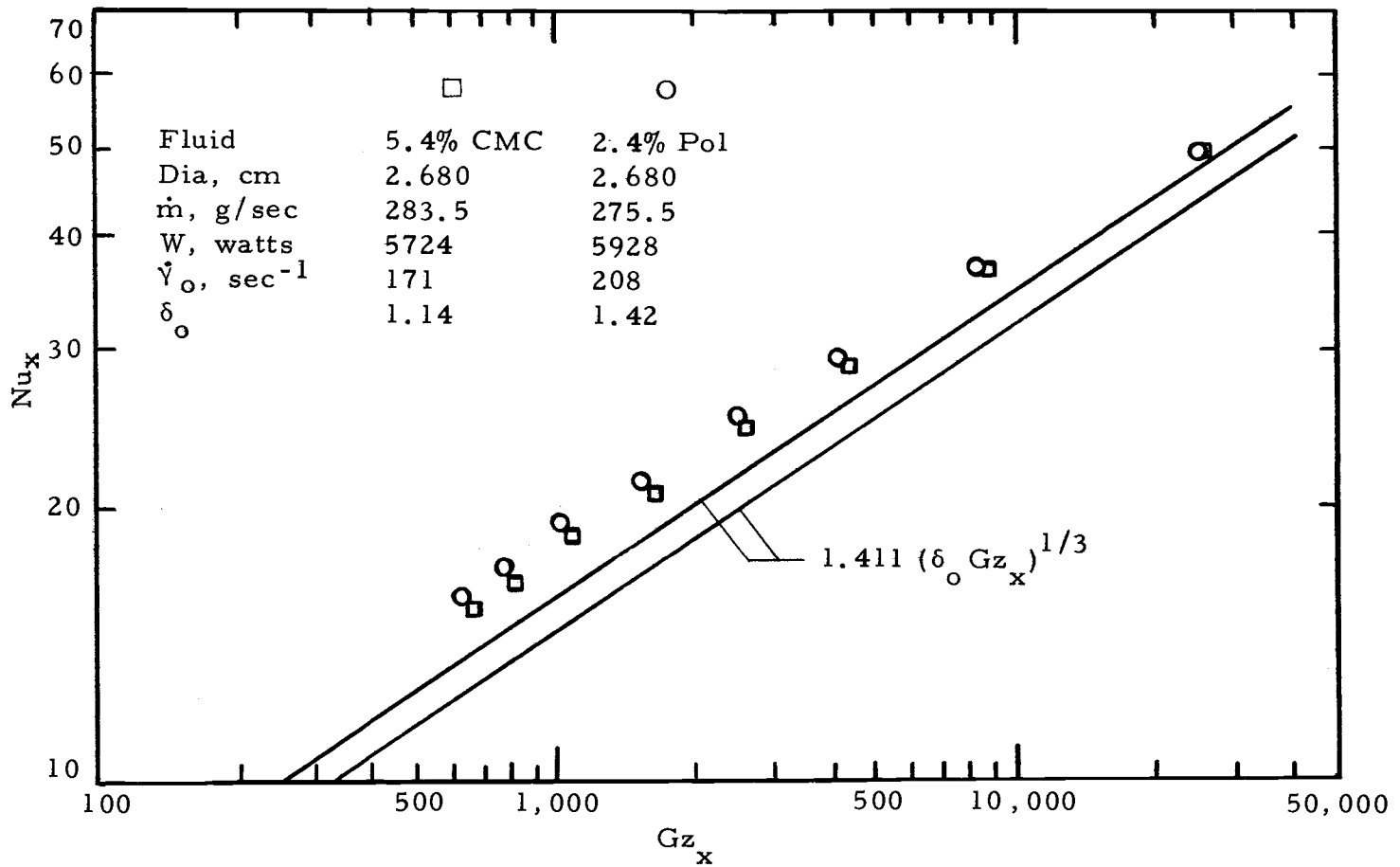

Figure 6.10. Heat transfer results for 5.4% CMC and 2.4% Polyox at moderate mass flow rate in large test section.

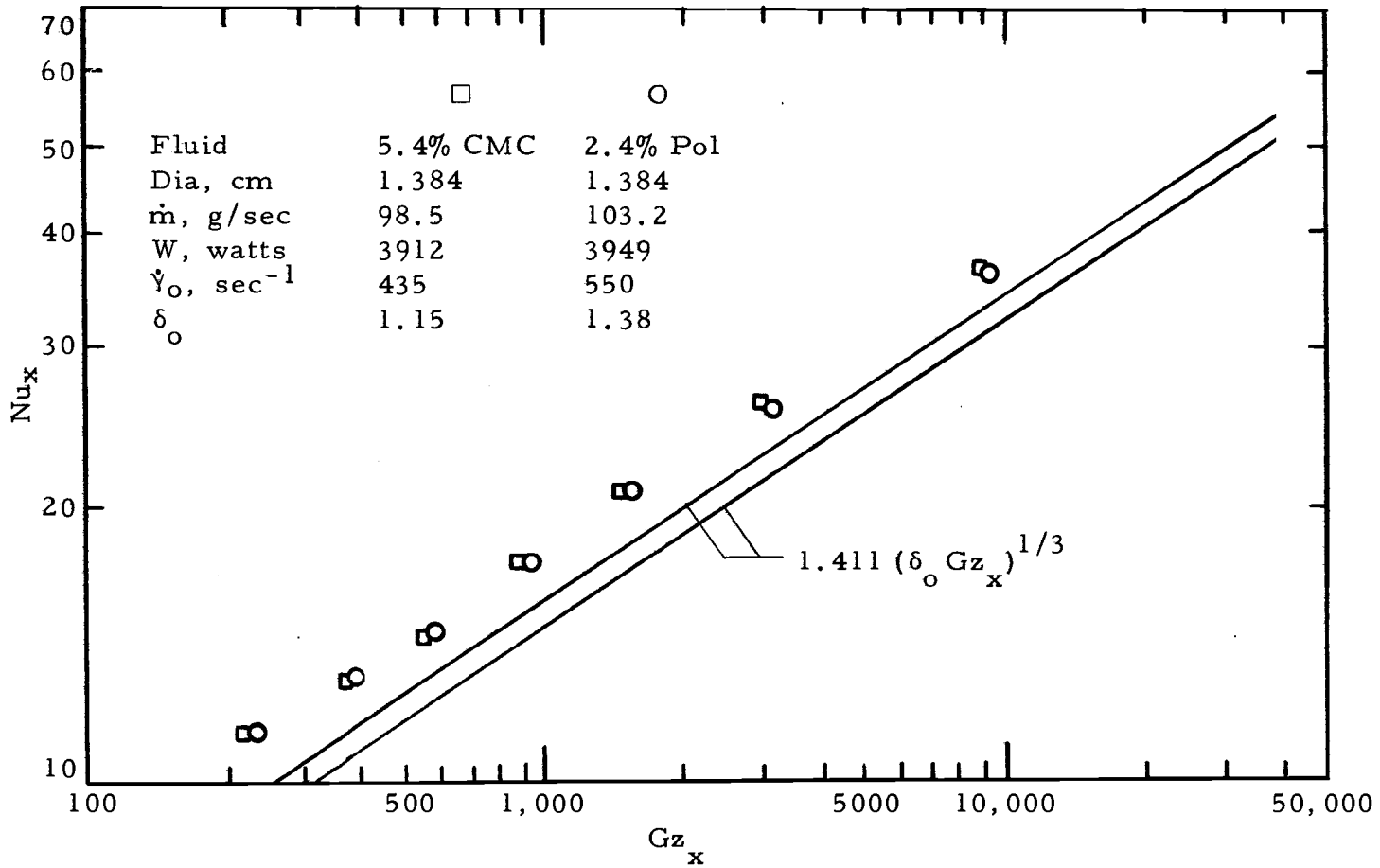

Figure 6.11. Heat transfer results for 5.4% CMC and 2.4% Polyox at low mass flow rate in small test section.

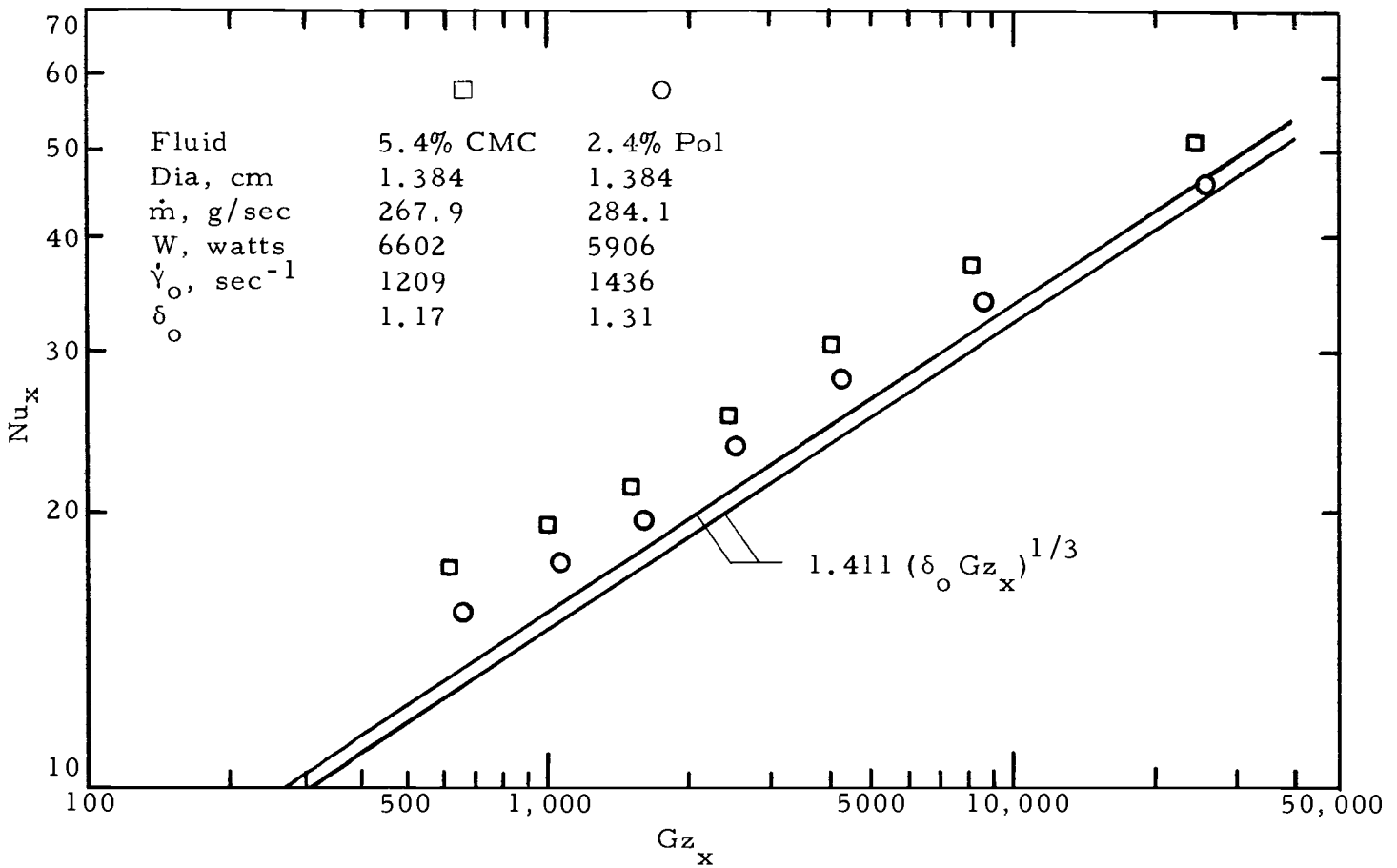

Figure 6.12. Heat transfer results for 5.4% CMC and 2.4% Polyox at moderate mass flow rate in small test section.

section. The Polyox run is just slightly above the CMC run, and proximity to the lines is maintained. In Figure 6.11, at low flow rate in the small test section, the CMC run is just slightly above the Polyox run. The CMC has maintained the same proximity to the temperature-independent property solution; however, the Polyox is closer to the solution than previously (at downstream locations). Finally, in Figure 6.12, the CMC run is 12% higher than the Polyox run at all values of Gz_x. The Polyox data has lost ground to the temperature-independent property solution and is now 15% higher at $Gz_x = 600$ and 8% higher at $Gz_x = 8600$. In contrast, the CMC data has gained on the temperature-independent property solution and is now 38% higher at $Gz_x = 600$ and 17% higher at $Gz_x = 8600$.

An explanation which synthesizes these results and is consistent with the other data obtained during this investigation focuses on the relative magnitude of local wall shear rates. Recall that the effect of increasing pseudoplasticity and the effect of heating are to increase the wall shear rate. In the case of uniform heating, the effect becomes more intense as the flow moves downstream, presumably until some maximum wall value is reached. The data is consistent in regard to these ideas.

Further, recall from Figures 6.4 and 6.7 the relative effect of temperature on the viscous behavior of these 2 fluids. For the Polyox, as the shear rate is increased, the temperature effect diminishes

sharply. For the CMC, the temperature effect is more substantial at all shear rates, and it does not diminish as sharply at higher values. Hence, at the lowest entrance value for the wall shear rate, the heat transfer to the Polyox is greater than to the CMC as the superior pseudoplastic characteristics of the Polyox offset its slightly inferior temperature-dependence characteristics. As the entrance value of the wall shear rate is increased the superior temperature-dependence characteristics of the CMC overcome the Polyox advantage in pseudoplastic behavior.

Figure 6.13 shows 2 runs made with degraded 2.4% Polyox solution at a higher flow rate and power level than for results previously shown. Although the flow rate is about 50% larger than the previous maximum, only about 15% more power could be added (maintaining the same maximum wall temperature). Data for the run in the small test section is consistently below that of the large test section. Convergence occurs near the exit, as the rate of heat transfer appears to drop off in the large test section.

Results for a moderate flow rate and a relatively low power input to the degraded 2.4% Polyox solution are shown in Figure 6.14. Wall temperatures were substantially below those maintained for the other runs. Again higher heat transfer results are achieved in the large test section. The closer proximity to the temperature-independent property solution reflects the effect of lower wall tempera-

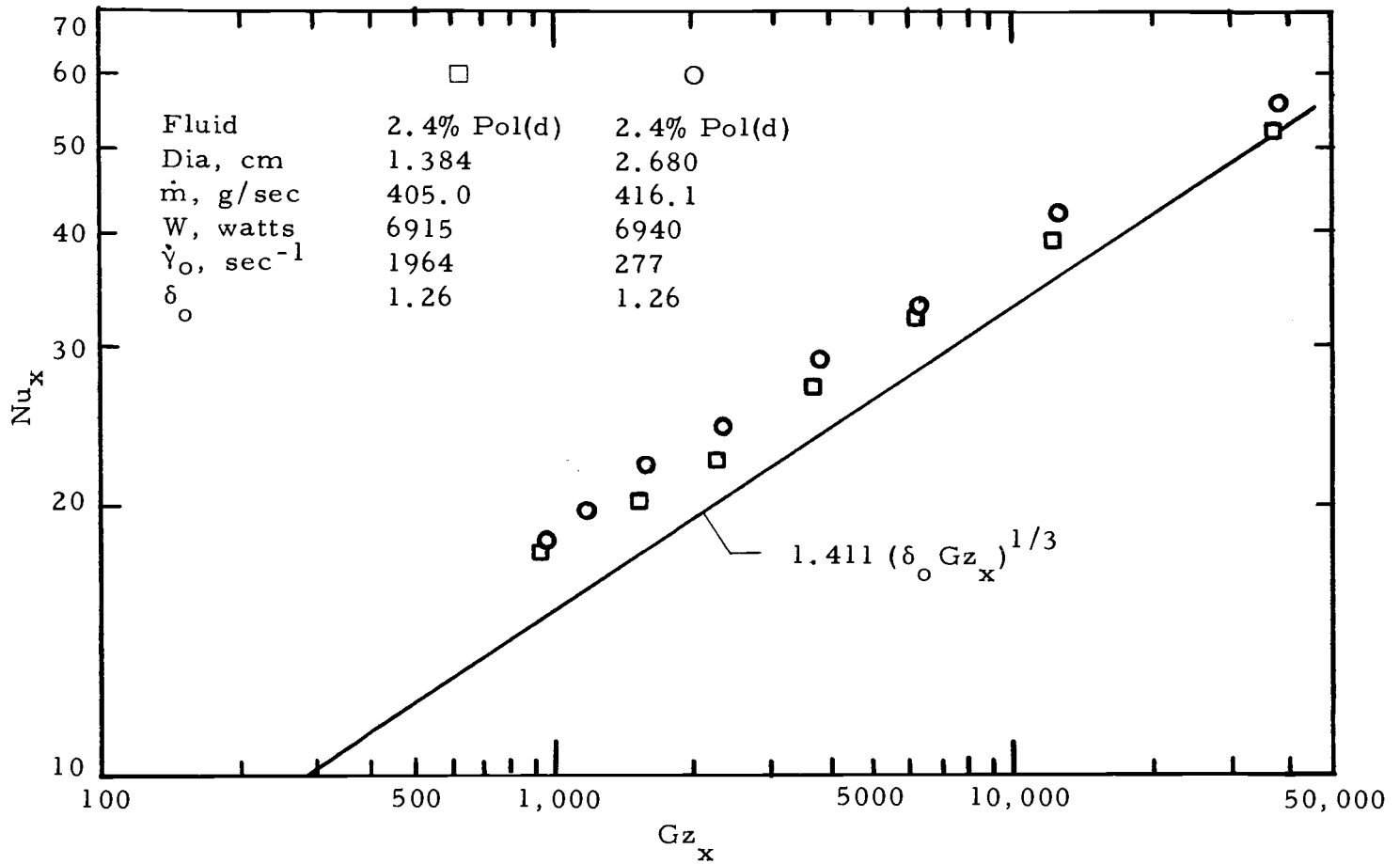

Figure 6.13. Heat transfer results for 2.4% Polyox (degraded) at high mass flow rate.

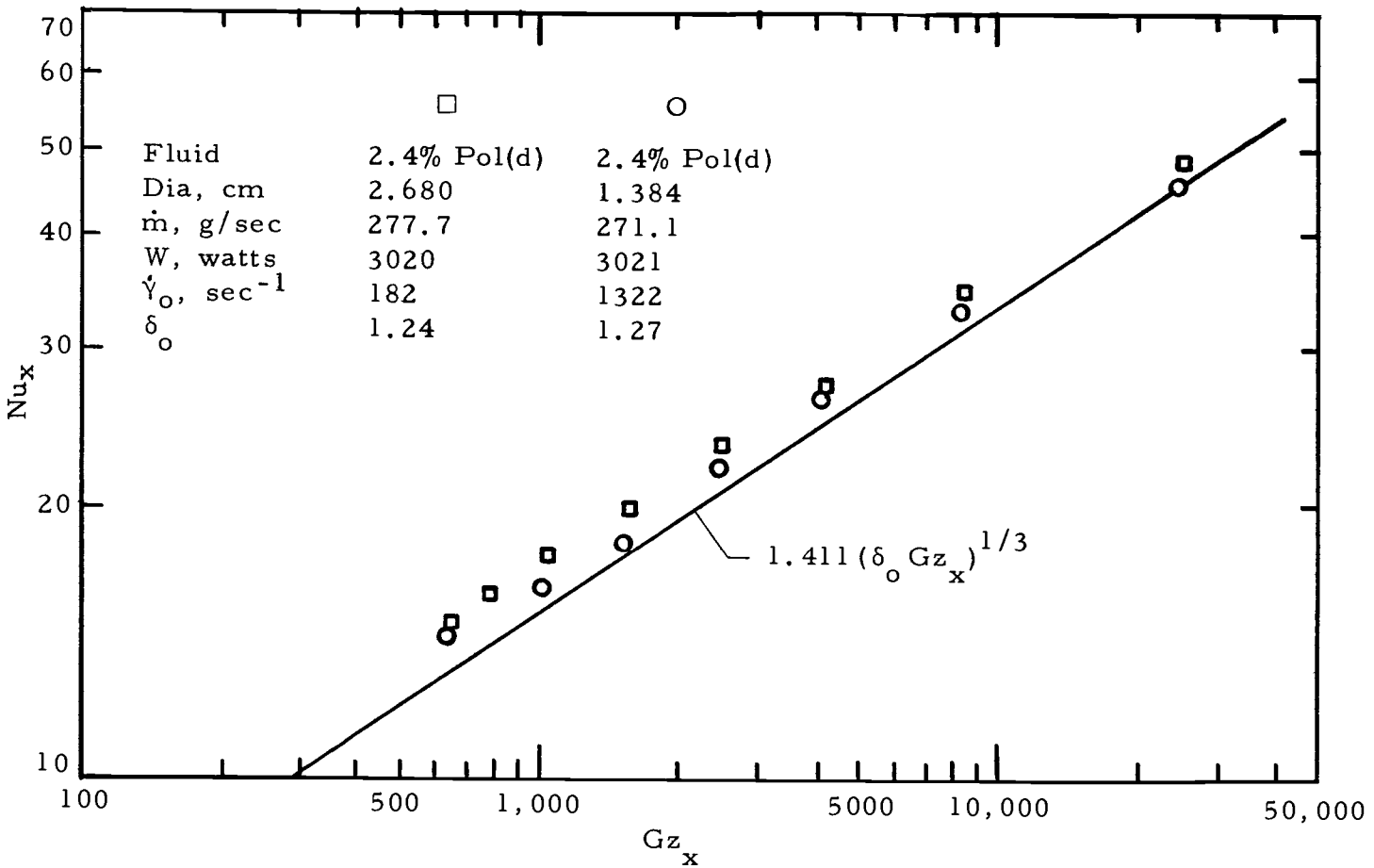

Figure 6.14. Heat transfer results for 2.4% Polyox (degraded) at moderate flow rate and low power.

tures on the fluid properties.

Comparison of a run made with the 3.0% CMC solution with one of the numerical solutions obtained by Cochrane (12, p. 37) is shown in Figure 6.15. The Cochrane solution is for a Newtonian fluid ($\delta_o = 1$) where $Pr_{wo} = 1,000$, $\Delta H/RT = 10$, and $\phi = 2$. Corresponding values for the data run were $\delta_o = 1.09$, $Pr_{wo} = 635$, $\Delta H/RT \approx 10$, and $\phi = 2.29$. Unfortunately, a reasonable match of these parameters for pseudoplastic behavior was not possible. In view of the slight difference in fluid rheology and the higher flux rate used in the run, the downstream data agree reasonably well with the Cochrane solution. However, agreement subsides at the upstream locations. The difference is 12% at $Gz_x = 9800$.

Figure 6.16 shows the only runs where natural convection had an obvious effect on the rate of heat transfer. Both runs were conducted at low flow rate in the large test section. The top data is for 1.0% Polyox, the least viscous of the fluids tested. The other data are for 3.0% CMC. The familiar contour at the downstream values of Gz_x is evident, indicating the onset of early full thermal development. The Polyox data is 62% above the temperature-independent property solution at $Gz_x = 230$. The CMC data is 38% above the solution at the same Gz_x. Moreover, if the Polyox flow is indeed fully developed, Nu_{xo} is 3.25 times the classic value of 4.364.

An insufficient amount of data exists to document a criteria for

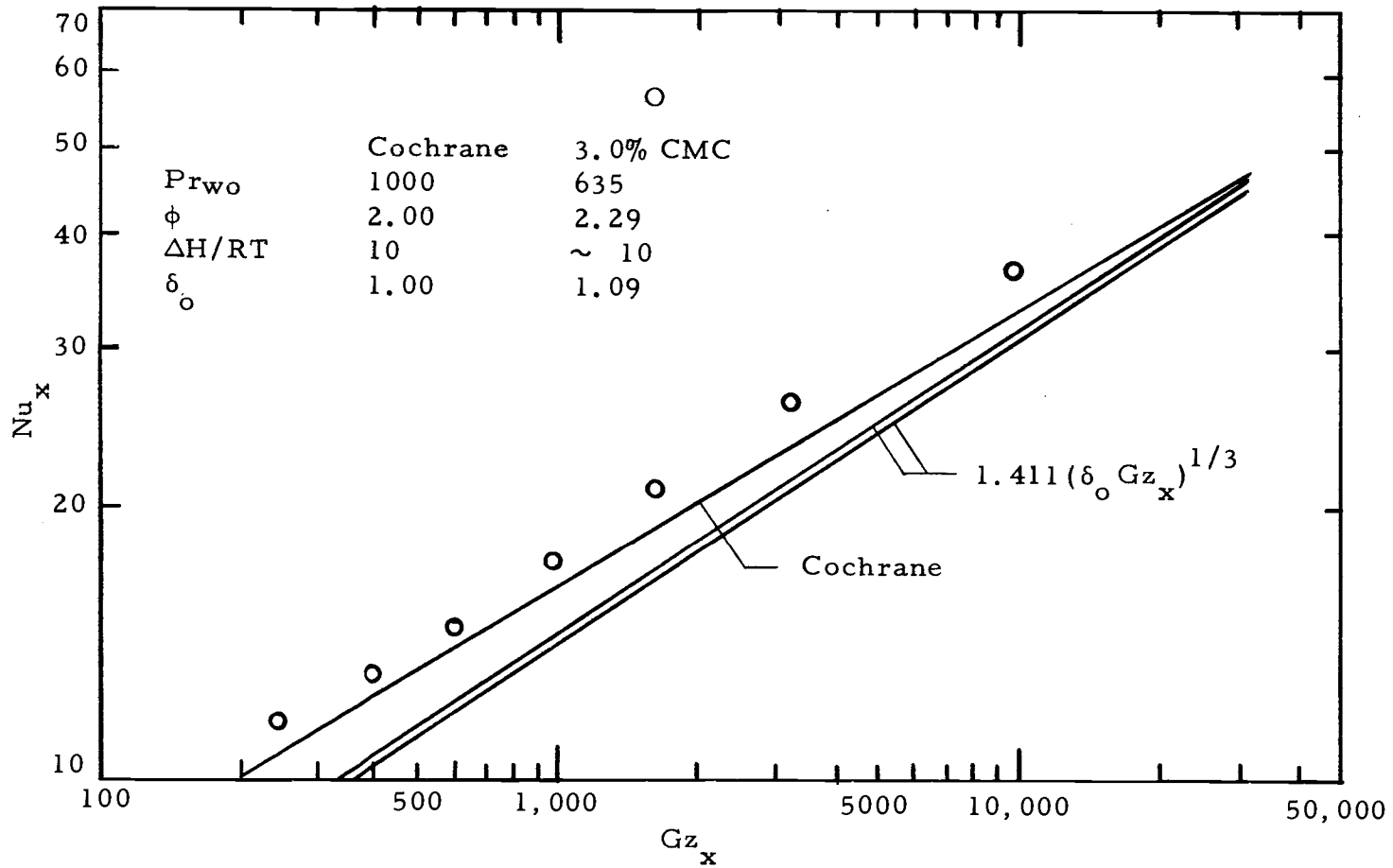

Figure 6.15. Comparison of results for 3.0% CMC in small test section at low flow rate with solution by Cochrane.

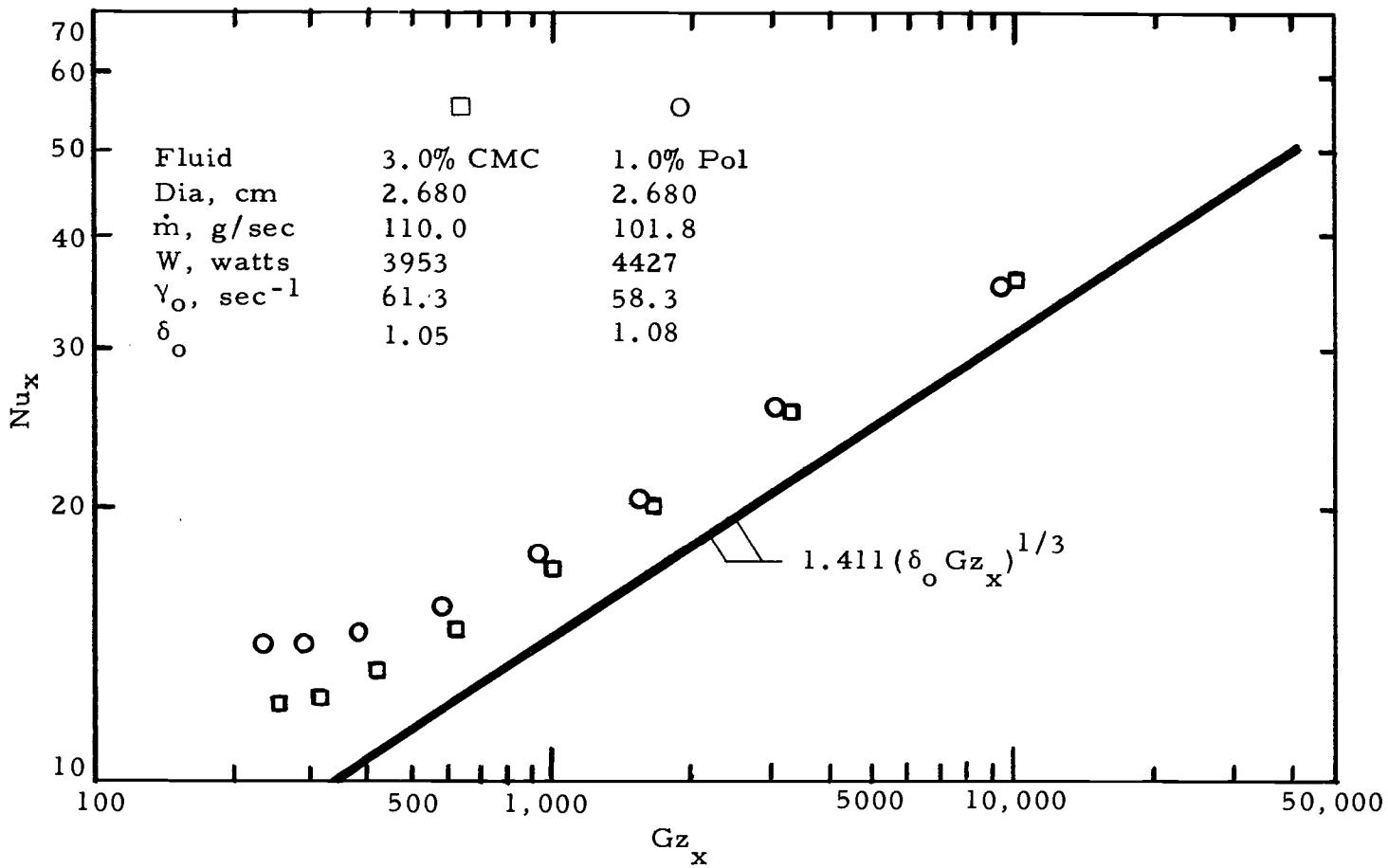

Figure 6.16. Heat transfer results for 3.0% CMC and 1.0% Polyox at low flow rate in large test section.

the onset of significant secondary flow due to buoyancy. The departure from linearity on the log-log plot appears to take place in the vicinity of 4th data point upstream of the exit ($Gz_x = 575$) for the Polyox run. At this point, $Ra^*_w = 3.47 \times 10^7$ and $Gr^*_w = 2.85 \times 10^5$. The corresponding critical point for the CMC flow appears to be in the vicinity of the 3rd data point upstream of the exit ($Gz_x = 410$). In this case, $Ra^*_w = 2.00 \times 10^7$ and $Gr^*_w = 1.36 \times 10^5$. The transition criteria of Petukhov and Polyakov (76) as given by Equations (1.16) and (1.17) predict $Ra^* = 3.66 \times 10^6$ for the Polyox run at $Gz_x = 575$ and $Ra^* = 2.31 \times 10^6$ for the CMC run at $Gz_x = 410$. Recall that their criteria was based on data obtained for water.

Evidence of the existence of secondary flow was found in other runs also. During some of the tests at moderate flow rates (about 280 g/sec in the large test section and at low flow rates (about 100 g/sec in the small test section, as well as all of the tests at low flow rates in the large test section, oscillations occurred in readings for certain of the top thermocouples. Never was an oscillation noted for a bottom thermocouple. In general, the less viscous the fluid, the further upstream the oscillations first appeared. The intensity of the oscillations was more pronounced in the less viscous fluids and increased as the flow progressed downstream.

Further evidence of the existence of secondary flow in these runs is contained in the wall temperature data. In several other

runs, differences exist between the top and bottom readings of the wall temperature at downstream locations. Wall temperature results from one of these runs is shown in Figure 6.17. The data are from a low flow rate run of 5.4% CMC solution through the large test section. The Nusselt number results for this same run (Figure 6.9) show no explicit effect from secondary flow. Due to the small temperature differences, the complication of circumferential heat conduction in the tube wall, and the uncertainties introduced by the gap in the heating no attempt was made to develop these data into a transition criteria.

Figure 6.18 shows the data for all 26 runs (195 data points). These data are contained in an envelope ± 15% from a mean line. The line beneath the data is the constant property solution for a Newtonian fluid (Equation (1.1)). The maximum deviation of the data from this line is 64%. At an extreme upstream location, $Gz_x = 38,000$, the deviation is as much as 17%.

Correlation of the data, excluding the 2 runs where natural convection was explicit, resulted in a best fit using:

$$Nu_x = 1.848\, Gz_x^{1/3} - 0.300/\delta_x \qquad (6.1)$$

The results of this correlation are shown in Figure 6.19. The spread in the data was reduced to ± 10% with a mean error of 3.57%. Other parameters tried were not as effective as δ_x, and when added after

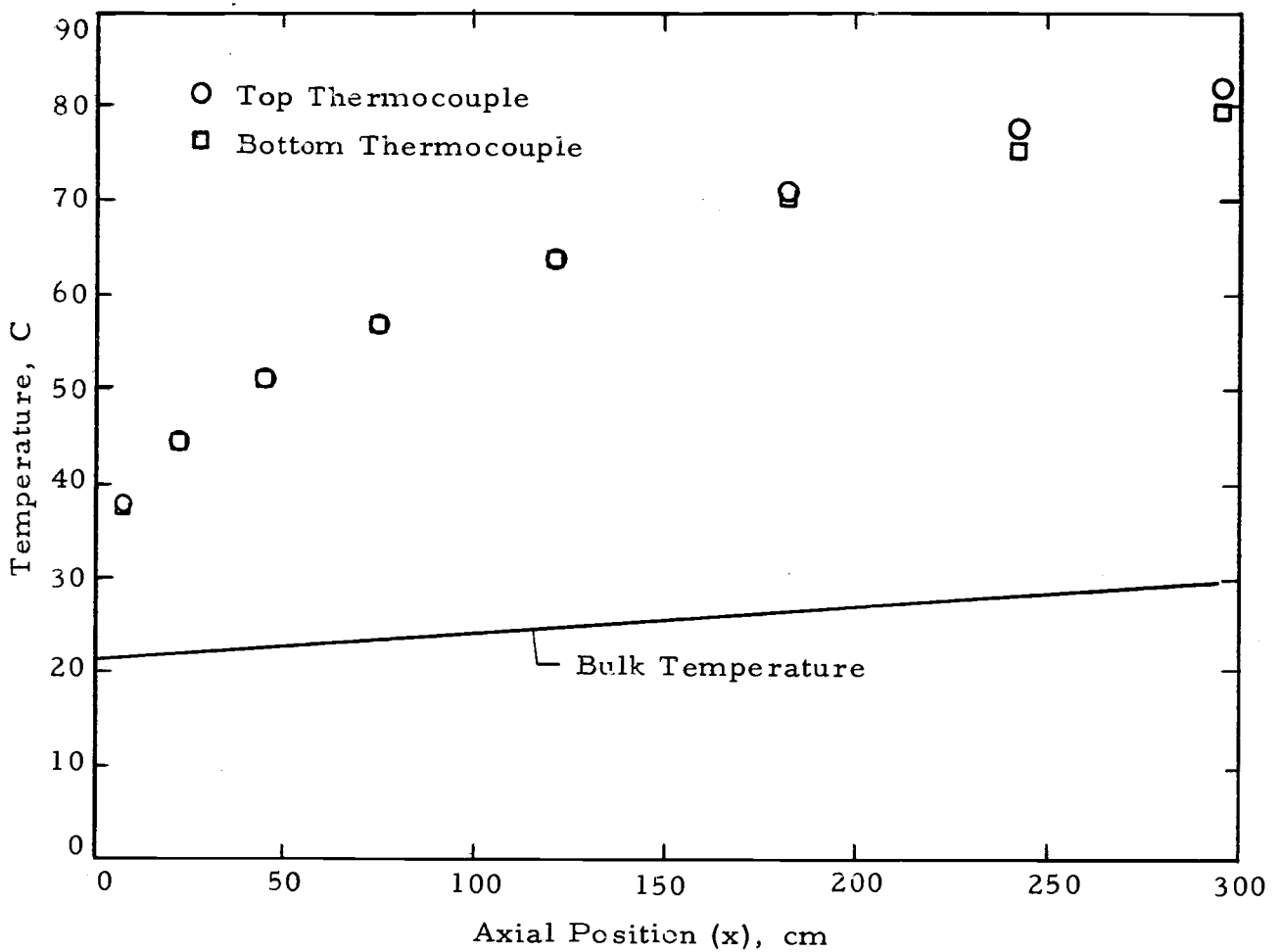

Figure 6.17. Wall temperatures (uncorrected for gap effect) for flow of 5.4% CMC solution in large test section at low flow rate.

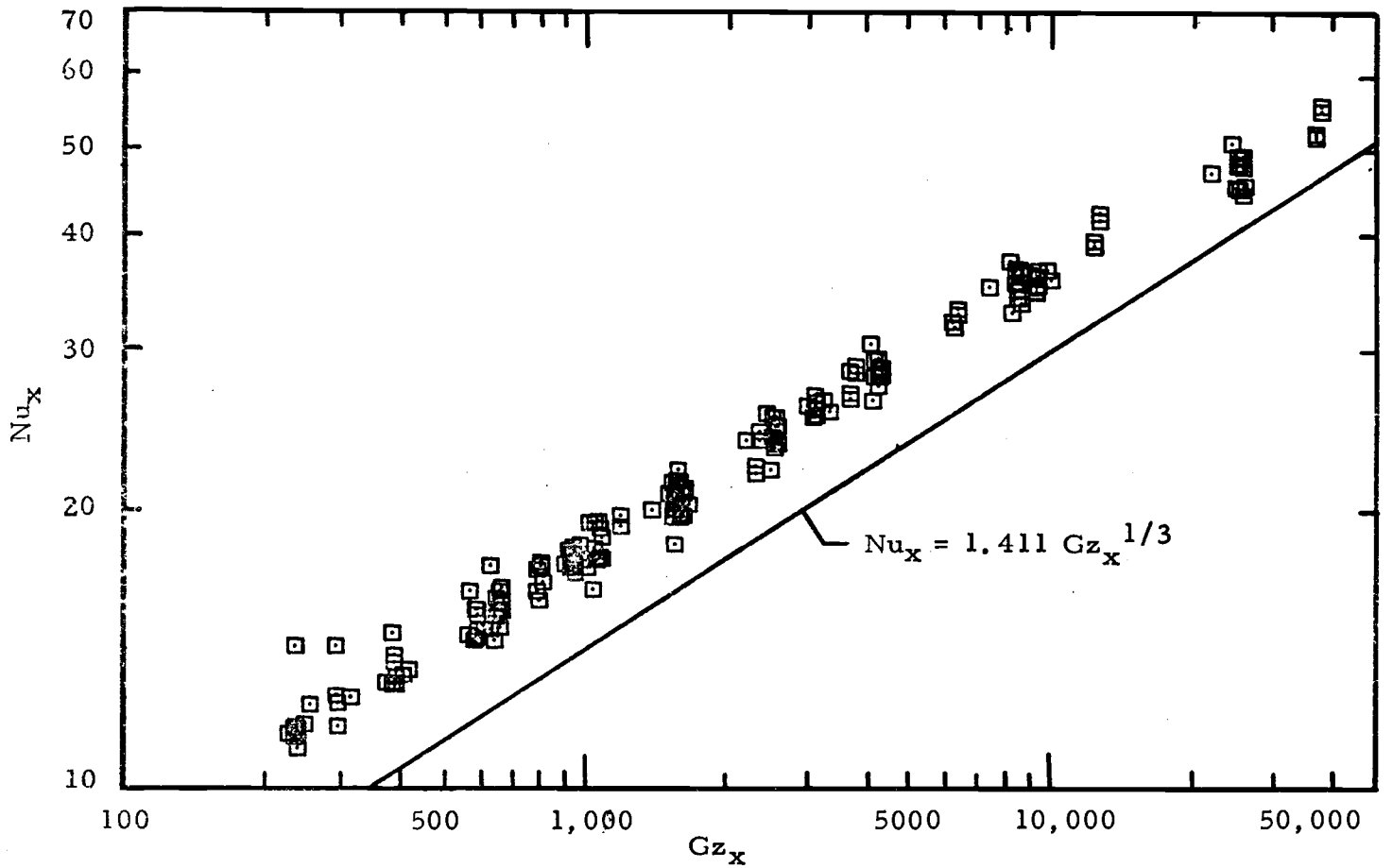

Figure 6.18. Heat transfer results for all data.

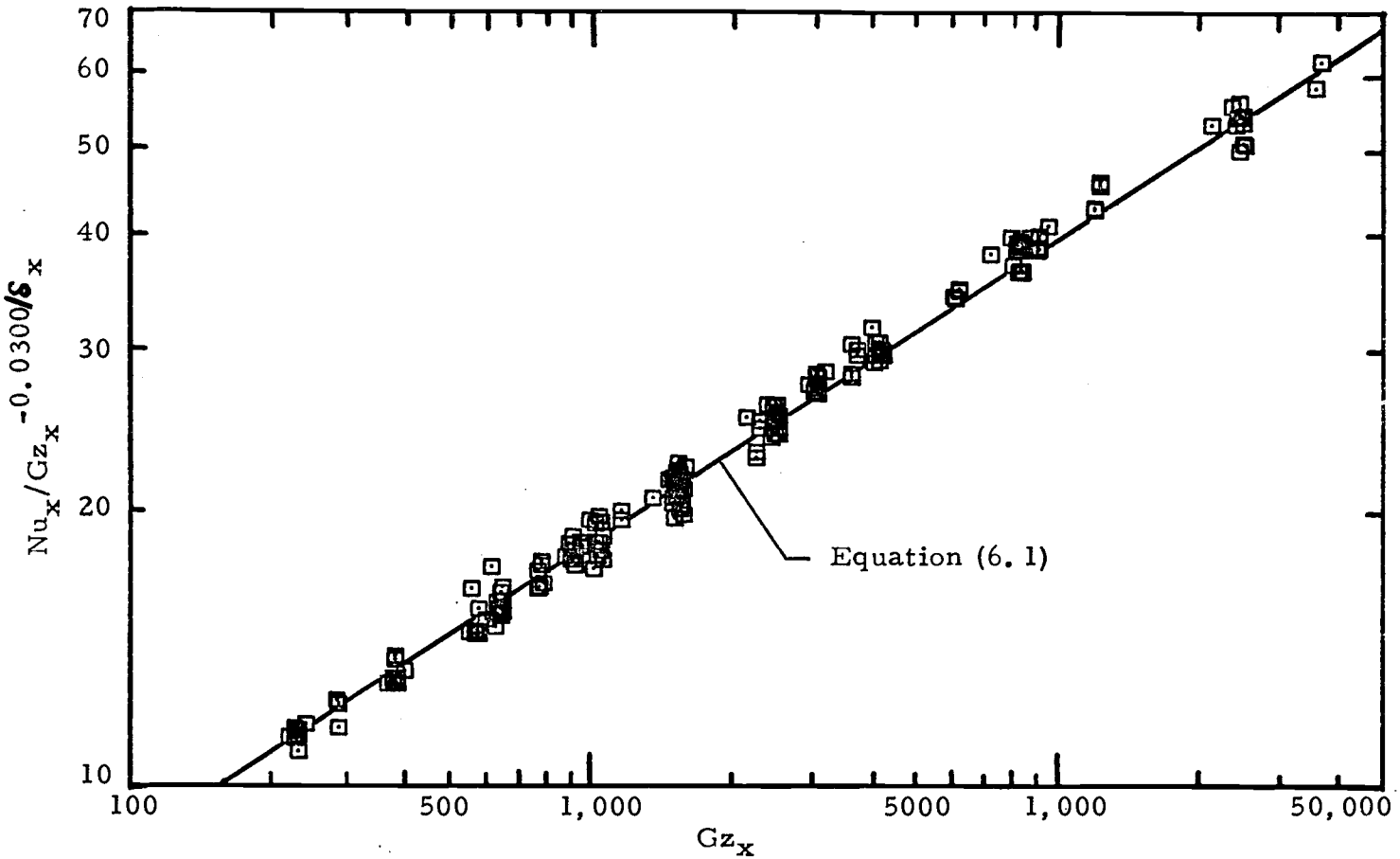

Figure 6.19. Best correlation of data which did not show an obvious effect from natural convection.

δ_x was in the model, not one proved to be significant.

Finally, it is probable that viscous heating had little or no effect on the results. Results of work by Etchart (20, p. 47) indicate that for $\phi = 1.0$ and $Br_o = 0.03$ in the flow of a 3% CMC solution, the drop in Nu_x increases from zero at high Gz_x to about 9% at Gz_x = 250. The Brinkmann numbers for the present investigation were at least an order of magnitude smaller. In addition, when the most viscous fluid tested was run through the small test section at the highest flow rate, no difference in wall temperature was observed from entrance to exit.

7. ANALYSIS OF ERROR

From Schenck (84, p. 45-53), the uncertainty interval, w_Y, for a quantity, Y, where

$$Y = f(X_1, X_2, X_3, \ldots) \tag{7.1}$$

is given by

$$w_Y^2 = \left(\frac{\partial Y}{\partial X_1}\right)^2 w_{X_1}^2 + \left(\frac{\partial Y}{\partial X_2}\right)^2 w_{X_2}^2 + \ldots \tag{7.2}$$

Here X_1, X_2, X_3, . . . are measured quantities. If $f(X_i)$ is comprised of products and quotients of the measured variables, then one obtains from Equation (7.2):

$$\frac{w_Y^2}{Y^2} = \frac{w_{X_1}^2}{X_1^2} + \frac{w_{X_2}^2}{X_2^2} + \ldots \tag{7.3}$$

Table 7.1 shows the uncertainties from various sources for the basic quantities used in generating the results. The last column shows the smallest value measured for the quantity. Entries under "Uncertainty - other sources" came from the assumption that fluid properties other than viscosity were equal to those of pure water.

Power to the heaters was directly related to heater and shunt voltage. An additional uncertainty (+0, -2%) in the power supplied to the fluid came from losses to the inclosure. Thus, the square of the relative error for the power, W, is:

Table 7.1. Uncertainties in basic quantities

*Quantity	Measurement Uncertainty	Correlation Uncertainty	Uncertainty - Other	Smallest Value
e	±0.05% ± 0.1 v			140.2 v
i	±0.05% ± 0.1 mv	±0.5 mv		32.5 mv
E_{tc}	±0.015% + 0.5 μv			1224 μv
E_{tco}	±0.015% + 0.5 μv			832 μv
M_f	±0.1 Lb			10 Lb
t_f	±0.1 sec			41.3 sec
Ω	±1.5%			
T_l	±1.5%			
T_v	±0.02 C			20 C
k		±0.1	±2%	
ρ		±0.0001%	±1%	
C_p		±0.0004%	±0.5%	
β		±0.02%	±2%	
D	±0.005 in			0.545 in
L	±1/16 in			119 1/2 in
x	±1/32 in			3.0 in

*Previously undefined terms: e - heater voltage, i - heater shunt voltage, E_{tco} - inlet thermocouple emf, M_f - mass of fluid weighed, t_f - time for M_f to flow, T_v - viscometer temperature.

$$\frac{w_W^2}{W^2} = \frac{w_e^2}{e^2} + \frac{w_i^2}{i^2} + (0.02)^2 \qquad (7.4)$$

$$= (0.0012)^2 + (0.0036)^2 + (0.0154)^2 + (0.02)^2$$

$$= (0.026)^2$$

The square of the relative error in the mass flow rate is given by:

$$\frac{w_{\dot{m}}^2}{\dot{m}^2} = \frac{w_{M_f}^2}{M_f^2} + \frac{w_{t_f}^2}{t_f^2} \qquad (7.5)$$

$$= (0.01)^2 + (0.0024)^2 = (0.010)^2$$

The inlet thermocouple reading has an additional uncertainty of ±4 μv from calibration and ±1 μv from conversion of emf to temperature. Thus, the square of the relative error is:

$$\frac{w_{T_o}^2}{T_o^2} = \frac{w_{E_{tco}}^2}{E_{tco}^2} + (0.0048)^2 + (0.0012)^2 \qquad (7.6)$$

$$= (0.00075)^2 + (0.0048)^2 + (0.0012)^2 = (0.0019)^2$$

The wall thermocouple reading, when corrected by calibration, has an additional uncertainty of ±4 μv. Conversion of emf to temperature adds an uncertainty of ±1 μv. Finally, the heating gap correction (in terms of thermocouple emf) has an uncertainty of ±10 μv. Thus,

$$\frac{w_{T_w}^2}{T_w^2} = \frac{w_{E_{tc}}^2}{E_{tc}^2} + (0.0033)^2 + (0.00082)^2 + (0.0082)^2 \qquad (7.7)$$

$$= (0.00056)^2 + (0.0033)^2 + (0.00082)^2 + (0.0082)^2$$

$$= (0.0089)^2$$

The fluid properties k, ρ, C_p, and β are related to

temperature through the use of polynomials. In each case the zeroth order term dominates the expression. Thus, the contribution to the error in the properties from the error in the temperature is severely diminished. In addition, the error in the bulk and wall temperatures is on the same order or below the maximum contribution from other sources. Thus, a negligible contribution from temperature is presumed, and the result is:

$$\frac{w_k^2}{k^2} = (0.001)^2 + (0.020)^2 = (0.020)^2 \qquad (7.8)$$

$$\frac{w_\rho^2}{\rho^2} = (0.0001)^2 + (0.010)^2 = (0.010)^2 \qquad (7.9)$$

$$\frac{w_{C_p}^2}{C_p^2} = (0.0004)^2 + (0.005)^2 = (0.0054)^2 \qquad (7.10)$$

$$\frac{w_\beta^2}{\beta^2} = (0.0002)^2 + (0.020)^2 = (0.020)^2 \qquad (7.11)$$

The sequence of calculations in which the shear rate at the inlet is obtained is also too complex to formally apply Equation (7.2). A simple (hopefully meaningful) approach is to use Equation (7.3). The uncertainty introduced in generating Equations (5.9) is ±1.5%. Another source of uncertainty is introduced when exponential interpolation is used (±3%). Finally, the use of Equation (5.22) introduces

uncertainty of ±0.1% for the integration and ±3.1% for the $24Q/\pi D^3$ term. Then,

$$\frac{w^2_{\dot{\gamma}_o}}{\dot{\gamma}_o^2} = (0.015)^2 + (0.015)^2 + (0.03)^2 + (0.001)^2 + (0.031)^2$$

$$= (0.048)^2 \qquad (7.12)$$

In specifying the wall shear rate in the test section, uncertainty of ±5% is introduced with the assumption of constant pressure gradient. The extension of the viscosity curves using the power law introduces ±5% uncertainty, and the interpolation between viscosity curves, ±3%. Thus,

$$\frac{w^2_{\dot{\gamma}_w}}{\dot{\gamma}_w^2} = (0.048)^2 + (0.05)^2 + (0.05)^2 + (0.03)^2 \qquad (7.13)$$

$$= (0.091)^2$$

Recalling the relationship for the calculation of the local bulk temperature, Equation (5.3), the square of the relative error of $T_b - T_o$ is:

$$\frac{w^2_{T_b - T_o}}{(T_b - T_o)^2} = \frac{w^2_W}{W^2} + \frac{w^2_k}{k^2} + \frac{w^2_L}{L^2} + \frac{w^2_{\dot{m}}}{\dot{m}^2} + \frac{w^2_{C_p}}{C_p^2} \qquad (7.14)$$

$$= (0.010)^2 + (0.00052)^2 + (0.020)^2 + (0.010)^2$$

$$+ (0.0054)^2 = (0.025)^2$$

Then the square of the relative error for the local bulk temperature is:

$$\frac{w_{T_b}^2}{T_b^2} = \frac{w_{T_b-T_o}^2}{T_b^2} + \frac{w_{T_o}^2}{T_b^2} = \frac{w_{T_b-T_o}^2}{(T_b-T_o)^2} \frac{(T_b-T_o)^2}{T_b^2} + \frac{w_{T_o}^2}{T_o^2} \frac{T_o^2}{T_b^2}$$

$$= (0.025)^2\left(\frac{9.3}{31.4}\right)^2 + (0.0019)^2\left(\frac{22.1}{31.4}\right)^2 = (0.0075)^2 \tag{7.15}$$

for a point near the exit. Near the entrance, $T_b \simeq T_o$, so that:

$$\frac{w_{T_b}^2}{T_b^2} = (0.0019)^2 \tag{7.16}$$

The square of the relative error in the temperature difference, $\Delta T = T_w - T_b$, is:

$$\frac{w_{\Delta T}^2}{\Delta T^2} = \frac{w_{T_w}^2}{\Delta T^2} + \frac{w_{T_b}^2}{\Delta T^2} = \frac{w_{T_w}^2}{T_w^2} \frac{T_w^2}{\Delta T^2} + \frac{w_{T_b}^2}{T_b^2} \frac{T_b^2}{\Delta T^2} \tag{7.17}$$

$$= (0.0089)^2\left(\frac{31.4}{10.4}\right)^2 + (0.0019)^2\left(\frac{21.0}{10.4}\right)^2$$

$$= (0.027)^2$$

Estimates of the uncertainties for the pertinent dimensionless parameters can now be obtained:

Nusselt number -

$$\frac{w_{Nu}^2}{Nu^2} = \frac{w_W^2}{W^2} + \frac{w_L^2}{L^2} + \frac{w_k^2}{k^2} + \frac{w_{\Delta T}^2}{\Delta T^2} \qquad (7.18)$$

$$= (0.020)^2 + (0.00052)^2 + (0.020)^2 + (0.027)^2$$

$$= (0.039)^2$$

Graetz number -

$$\frac{w_{Gz}^2}{Gz^2} = \frac{w_{\dot{m}}^2}{\dot{m}^2} + \frac{w_{C_p}^2}{C_p^2} + \frac{w_k^2}{k^2} + \frac{w_x^2}{x^2} \qquad (7.19)$$

$$= (0.010)^2 + (0.0054)^2 + (0.020)^2 + (0.010)^2$$

$$= (0.025)^2$$

Entrance shear rate ratio -

$$\frac{w_{\delta_o}^2}{\delta_o^2} = \frac{w_{\dot{\gamma}_o}^2}{\dot{\gamma}_o^2} + \frac{w_\rho^2}{\rho^2} + 9\frac{w_D^2}{D^2} + \frac{w_{\dot{m}}^2}{\dot{m}^2} \qquad (7.20)$$

$$= (0.048)^2 + (0.010)^2 + (0.028)^2 + (0.010)^2$$

$$= (0.057)^2$$

Local shear rate ratio -

$$\frac{w_{\delta_x}^2}{\delta_x^2} = \frac{w_{\dot{\gamma}_w}^2}{\dot{\gamma}_w^2} + \frac{w_\rho^2}{\rho^2} + 9\frac{w_D^2}{D^2} + \frac{w_{\dot{m}}^2}{\dot{m}^2} \qquad (7.21)$$

$$= (0.091)^2 + (0.010)^2 + (0.028)^2 + (0.010)^2$$

$$= (0.096)^2$$

Modified Rayleigh number -

$$\frac{w^2_{Ra^*}}{Ra^{*2}} = 4\frac{w^2_\rho}{\rho^2} + \frac{w^2_\beta}{\beta^2} + 9\frac{w^2_D}{D^2} + \frac{w^2_W}{W^2} + \frac{w^2_L}{L^2} + \frac{w^2_{c_p}}{c_p^2} + 4\frac{w^2_k}{k^2} + \frac{w^2_\eta}{\eta^2} \quad (7.22)$$

$$= (0.0002)^2 + (0.020)^2 + (0.028)^2 + (0.010)^2 + (0.020)^2 + (0.00052)^2 + (0.0054)^2 + (0.040)^2 + (0.091)^2$$

$$= (0.108)^2$$

(The uncertainty in η is assumed to be no worse than that in $\dot{\gamma}_w$.)

The relative errors in the Nusselt and Graetz numbers reflect conditions at the first local position, 3 inches from entrance. It is an extreme case. Most of the calculations at this position, as well as downstream, have far less uncertainty. The errors in local shear rate ratio and modified Rayleigh number reflect conditions far downstream of the inlet. However, δ_x is never any better than δ_o, and Ra^* is never any better than $\dot{\gamma}_o$

8. CONCLUSIONS AND RECOMMENDATIONS

This experimental study has provided the first comprehensive set of data for heat transfer to pseudoplastic fluids in the thermal entry region of uniformly heated, horizontal pipes. In addition, an improved method of applying data from rotational viscometers to conditions in a pipe flow has been successfully employed.

From the heat transfer results, it can be concluded that for the laminar flow of pseudoplastic fluids in the thermal entry region of uniformly heated, horizontal pipes:

1. The local rate of heat transfer for a temperature-dependent fluid is greater than that of a temperature-independent fluid at local Graetz numbers as high as 38,000. Further, the difference increases as the flow progresses downstream (Gz_x decreases).

2. In the absence of natural convection effects, the difference in the rate of heat transfer to temperature-dependent fluids as compared to temperature-independent fluids can be 38% at $Gz_x = 625$, 15% at $Gz_x = 24,500$, and 7% at $Gz_x = 38,000$.

3. In general, temperature-dependence in fluid rheology is more important in regard to the rate of heat transfer than the degree of pseudoplasticity.

4. Secondary flows due to buoyancy can have a substantial effect on the rate of heat transfer far upstream of the usual onset of

full thermal development. The point at which this effect becomes evident moves upstream for less viscous fluids.

5. The effect of the secondary flow coupled with the effect of temperature-dependence of viscous properties can increase the rate of heat transfer as much as 62% for $Gz_x = 230$. For full thermal development, the increase can be 225% over the classic constant-property value of 4.364.

6. Secondary flow patterns which have no obvious effect on the rate of heat transfer can exist far upstream of full thermal development in fluids with Prandtl numbers as high as 20,100 at the entrance.

7. The relative value of the local wall shear rate governs the magnitude of the rate of heat transfer. The relationship, Equation (6.1), determines the rate of heat transfer within ± 10%, with a mean error of 3.57%, for flows without significant natural convection effects.

8. No significant contribution to the rate of heat transfer is obtained due to viscous heating for the flow of fluids with entrance values of Brinkmann number as high as 4.22×10^{-3}.

It is recommended that further study be given to:

1. The determination of the flow patterns characteristic to secondary flows in pseudoplastic fluids.

2. The determination of the onset of significant effect of the

secondary flow on the rate of heat transfer for pseudoplastic fluids.

3. The effect of viscoelasticity when secondary flow is present.

4. Heat transfer to dilatant fluids in uniformly heated, horizontal pipes.

5. The interesting possibility of discretely placed heating gaps in a flow with otherwise uniform heating so that more energy may be transfered to the fluid without exceeding a critical wall temperature.

NOMENCLATURE

a	Distance from test section inlet to upstream edge of heating gap
A	Cross-sectional area
A_L	Lateral area
b	Distance from test section inlet to thermocouple location
B_1, B_2, B_3	Empirical constants
B_1', B_2', B_3'	Empirical constants
B(n)	Local Nusselt number defined by Equation (1.32)
Br	Brinkmann number, $4\eta_w Q^2/\pi T_o D^2 k$
Br'	Modified Brinkmann number, $D T_w^{1+1/n}/q_o'' K^{1/n}$
c	Distance from test section inlet to downstream edge of heating gap
C_p	Heat capacity
C_0, C_1, C_2, C_3	Empirical constants
C_0', C_1', C_2', C_3'	Empirical constants
d	Distance from test section inlet to a point downstream of heating gap
D	Inside diameter of pipe
e	Heater voltage
E	Thermal emf
E_{tc}	Indicated thermocouple emf
$F(\lambda)$	Function defined by Equation (B.11)

g	Gravitational acceleration
$G(\lambda)$	Function defined by Equation (B.12)
Gr	Grashof number, $\rho^2 \beta g D^3 (T_w - T_b)/\eta^2$
Gr^*	Modified Grashof number, $\rho^2 \beta g D^4 q_o''/k\eta^2$
Gz	Graetz number, $\dot{m}C_p/kx$
h	Thermal convective conductance
h_r	Viscometer rotor length
ΔH	Activation energy
i	Heater shunt voltage
k	Thermal conductivity
k_w	Thermal conductivity of tube wall
K	Empirical constant in the power law model or Ellis model
L	Test section heated length
L_e	Hydrodynamic entry length
m	Empirical constant
$m_1, m_2, m_3, \ldots$	Empirical constants
$\dot{m}$	Mass flow rate
M	Torque
M_f	Mass of fluid weighed
Nu	Nusselt number, hD/k
Nu_{xo}	Local Nusselt number from constant property solution (92)
Nu_∞	Local Nusselt number in thermally fully developed region

Pe	Peclet number, $RePr = 4\dot{m}C_p/\pi kD$
Pr	Prandtl number, $\eta C_p/k$
Pr_o	Prandtl number evaluated at inlet wall conditions
q_g	Energy into fluid from heating gap portion of wall
q_i	Energy into fluid from tube wall
q_o	Energy crossing outside surface of tube wall
q_w	Energy conducted axially in tube wall
q''	Heat flux
$\Delta q''$	Heat flux difference, $q''_o - q''_g$
q''_g	Heat flux into fluid from heating gap portion of wall
q''_o	Heat flux applied at outside surface of pipe, q_o/A_L
q''_w	Axial heat flux in pipe wall
Q	Volume flow rate
r	Variable in radial direction
R	Universal gas constant
R_1	Viscometer rotor radius
R_2	Viscometer beaker radius
Ra	Rayleigh number, $GrPr = \rho^2\beta gD^3C_p(T_w - T_b)/k\eta$
Ra^*	Modified Rayleigh number, $Gr^*Pr = q^2\beta gD^4q''C_p/k^2\eta$
Ra^*_{tr}	Modified Rayleigh number at onset of significant secondary flow
Re	Reynolds number, $4\dot{m}/\pi D\eta$
S	Viscometer scale reading

t	Pipe wall thickness
t_f	Time for M_f to flow
T	Temperature
ΔT	Temperature difference, $T_w - T_b$
T_o	Inlet temperature
T_v	Viscometer temperature
T_{w2}, T_{wm}, T_{wu}	Temperatures defined in Figure 5.1
T'_{wb}	Wall temperature at thermocouple site, corrected for effect of heating gap
T_1, T_2, T_3, T_4	Viscometer sample temperatures
u	Velocity
V	Average velocity, $\dot{m}/\rho A$
w_i	Uncertainty (error) in variable i
x	Axial position measured from inlet
$X_1, X_2, X_3, \ldots$	Independent variables
Y	Dependent variable
Z	Dummy variable
β	Coefficient of thermal expansion
$\dot{\gamma}$	Shear rate, $\lvert du/dr \rvert$
$\dot{\gamma}_p$	Shear rate defined in Figure 5.4
$\dot{\gamma}_1, \dot{\gamma}_2$	Shear rate at respective positions, R_1 and R_2
δ	Shear rate ratio, $\dot{\gamma}_w/(8V/D)$
ϵ	Radius ratio, R_2/R_1

η	Apparent viscosity, $\tau/\dot{\gamma}$
η_o	Empirical constant
θ_g	Temperature difference, $T_{wa} - T_{wc}$
λ	Dummy variable
ξ	Dimensionless radial position, $2r/D$
ρ	Fluid density
τ	Fluid shear stress
τ_{max}	Maximum shear stress for which rheological curve is valid
τ_o	Empirical constant
τ_1, τ_2	Shear stress at respective positions, R_1 and R_2
ϕ	Dimensionless heat flux, $q_o''D/kT_o$
χ	Rheological parameter (42)
Ω	Angular speed of viscometer rotor

Subscripts:

ab	Average bulk condition
af	Average film temperature condition, $\overline{(T_w + T_b)}/2$
b	Local bulk condition
ℓ	Local position, L
ℓm	Log mean temperature difference
m	Arithmetic mean temperature difference, $\overline{(T_w - T_b)}$
o	Entrance condition
w	Local wall condition
wa, wb, wc, wd	Wall condition at positions a, b, c, and d
x	Position, x

BIBLIOGRAPHY

1. Bader, H. J., A. A. McKillop, J. C. Harper. An experimental and analytical study of entrance flow of non-Newtonian fluids. Head Transfer 1970 4:Rhl. 1970.

2. Benedict, R. P. Fundamentals of temperature, pressure, and flow measurements. New York, McGraw-Hill, 1969. 353 p.

3. Bergles, A. E. and R. R. Simonds. Combined forced and free convection for laminar flow in horizontal tubes with uniform heat flux. International Journal of Heat and Mass Transfer 14: 1989-2000. 1971.

4. Bird, R. B. Zur theorie des warmeubergangs an nicht-Newtonsche flussigkeiten bei laminarer rohrstromung. Chemie-Ingenieur-Technik 31:569-572. 1959.

5. Bird, R. B. Polymer fluid dynamics. Chemical Engineering Progress Symposium, ser. 58, 61:86. 1965.

6. Brown, A. R. and M. A. Thomas. Combined free and forced convection heat transfer for laminar flow in horizontal tubes. Journal of Mechanical Engineering Science 7:440-448. 1965.

7. Charm, S. E. and E. W. Merrill. Heat transfer coefficients in straight tubes for pseudoplastic food materials in streamline flow. Food Research 24:319-331. 1959.

8. Cheng, K. C., S. W. Hong, and G. J. Hwang. Buoyancy effects on laminar heat transfer in the thermal entrance region of horizontal rectangular channels with uniform wall heat flux for large Prandtl number fluid. International Journal of Heat and Mass Transfer 15:1819-1836. 1972.

9. Christiansen, E. B. and S. E. Craig. Heat transfer to pseudoplastic fluids in laminar flow. Journal of the American Institute of Chemical Engineers 8:154-160. 1962.

10. Christiansen, E. B. and G. E. Jensen. Energy transfer to non-Newtonian fluids in laminar flow. In: Progress in International Research on Thermodynamic and Transport Properties, ed. by J. F. Masi and D. J. Tsai. New York, Academic Press, 1962. p. 738-747.

11. Christiansen, E. B., G. E. Jensen, and F. S. Tao. Laminar flow heat transfer. Journal of the American Institute of Chemical Engineers 12:1196-1201. 1966.

12. Cochrane, G. F. A numerical solution for heat transfer to non-Newtonian fluids with temperature-dependent viscosity for arbitrary conditions of heat flux and surface temperature. Ph. D. Thesis. Corvallis, Oregon, Oregon State University, 1969. 169 numb. leaves.

13. Cochrane, G. F. Cooling of Newtonian and non-Newtonian fluids with temperature-dependent viscosity. Albuquerque, 1972. 13 numb. leaves. (University of New Mexico. College of Engineering. Bureau of Engineering Research. Technical report ME-61(71)SAN-183-2 on Sandia contract 51-0059, task 2).

14. Colburn, A. P. A method of correlating forced convection heat transfer data and a comparison with fluid friction. Transactions of American Institute of Chemical Engineers 29:174. 1933.

15. Collins, E. A. and F. E. Filisko. Temperature profiles for polymer melts in tube flow. Journal of the American Institute of Chemical Engineers 16:339. 1970.

16. Del Casal, E. and W. N. Gill. A note on natural convection effects in fully developed horizontal tube flow. Journal of the American Institute of Chemical Engineers 8:570-574. 1962.

17. Depew, C. A. and S. E. August. Heat transfer due to combined free and forced convection in a horizontal and isothermal tube. Transactions of the American Society of Mechanical Engineers, Journal of Heat Transfer, ser. C, 93:380-384. 1971.

18. Deyoung, S. H. and G. F. Scheele. Natural convection distorted non-Newtonian flow in a vertical pipe. Journal of the American Institute of Chemical Engineers 16:712-717. 1970.

19. Ede, A. J. The heat transfer coefficient for flow in a pipe. International Journal of Heat and Mass Transfer 4:105-110. 1961.

20. Etchart, D. Y. A pipe entry length solution for heat transfer and flow in Powell-Eyring fluids with temperature-dependent viscosity and constant flux boundary condition. M. S. Thesis.

Corvallis, Oregon, Oregon State University, 1971. 96 numb. leaves.

21. Eubank, C. C. and W. S. Proctor. M. S. Thesis in Chemical Engineering. Massachusetts Institute of Technology, Cambridge, Massachusetts, 1951.

22. Faris, G. N. and R. Viskanta. An analysis of laminar combined forced and free convection heat transfer in a horizontal tube. International Journal of Heat and Mass Transfer 12:1295-1309. 1969.

23. Fischer, E. K. Colloidal dispersions. New York, Wiley, 1950. 387 p.

24. Foraboschi, F. P. and I. de Federico. Heat transfer in laminar flow of non-Newtonian heat-generating fluids. International Journal of Heat and Mass Transfer 7:315-325. 1964.

25. Forrest, G. and W. L. Wilkinson. Laminar heat transfer to temperature-dependent Bingham fluids in tubes. International Journal of Heat and Mass Transfer 16:2377-2391. 1973.

26. Forsyth, T. H. and N. F. Murphy. Temperature profiles of molten flowing polymers in a heat exchanger. Journal of the American Institute of Chemical Engineers 15:758-763. 1969.

27. Fredrickson, A. G. Principles and applications of rheology. Englewood Cliffs, N. J., Prentice-Hall, 1964. 326 p.

28. Gee, R. E. and J. B. Lyon. Nonisothermal flow of viscous non-Newtonian fluids. Industrial and Engineering Chemistry 49:956-960. 1957.

29. Gill, W. N. Heat transfer in laminar power law flows with energy sources. Journal of the American Institute of Chemical Engineers 8:137-138. 1962.

30. Graetz, L. Ueber die warmeleitungsfahigkeit von flussigkeiten. Annalen der Physik und Chemie 25:337-357. 1885.

31. Grigull, U. Warmeubergang an nicht-Newtonsche flussigkeiten bei laminarer rohrstromung. Chemie-Ingenieur-Technik 28: 553-558. 1956.

32. Griskey, R. G. and I. A. Wiehe. Heat transfer to molten flowing polymers. Journal of the American Institute of Chemical Engineers 12:308-312. 1966.

33. Griskey, R. G. and R. G. Green. Rheological behavior of dilatant (shear-thickening) fluids. Part I. Experimental and data. Transactions of the Society of Rheology 12:13-25. 1968.

34. Griskey, R. G. and R. G. Green. Flow of dilatant (shear-thickening) fluids. Journal of the American Institute of Chemical Engineers 17:725-728. 1971.

35. Hanks, R. W. and E. B. Christiansen. The laminar nonisothermal flow of non-Newtonian fluids. Journal of the American Institute of Chemical Engineers 7:519-523. 1961.

36. Henning, C. D. and W. J. Yang. Laminar forced convection to Bingham plastic flowing through a circular tube with internal heat generation. Applied Scientific Research, sec. A, 18:336-352. 1968.

37. Hirai, E. Theoretical explanation of heat transfer in laminar region of Bingham fluid. Journal of the American Institute of Chemical Engineers 5:130-133-9M. 1959.

38. Huang, C. R. Determination of the shear rates of non-Newtonian fluids from rotational viscometric data. Transactions of the Society of Rheology 15:25-37. 1971.

39. Hwang, G. J. and K. C. Cheng. Boundary vorticity method for convective heat transfer with secondary flow--Application to the combined free and forced laminar convection in horizontal tubes. Heat Transfer 1970 4:NC3.5. 1970.

40. Inman, R. M. Heat transfer to laminar non-Newtonian flow in a circular tube with variable circumferential wall temperature or heat flux. Cleveland, Ohio, 1965. 22 p. (U. S. National Aeronautics and Space Administration. Technical Note D-2674.)

41. Jackson, T. W., J. M. Spurlock, and K. R. Purdy. Combined free and forced convection in a constant temperature horizontal tube. Journal of the American Institute of Chemical Engineers 7:38-45. 1961.

42. Khabakhpasheva, E. M., V. I. Popov, and B. V. Perepelitsa. Heat transfer in viscoelastic fluids. Heat Transfer 1970 4:Rh2. 1970.

43. Knudsen, J. G. and D. L. Katz. Fluid dynamics and heat transfer. New York, McGraw-Hill, 1958. 576 p.

44. Korayem, A. Y. Non-isothermal laminar flow of non-Newtonian fluids in the entrance region of a pipe. Ph. D. Thesis. Davis, California, University of California at Davis, 1964. 121 numb. leaves.

45. Kreiger, I. M. and H. Elrod. Direct determination of the flow curves of non-Newtonian fluids. II. Shearing rate in the concentric cylinder viscometer. Journal of Applied Physics 24:134. 1953.

46. Kumar, R. Heat transfer in laminar flow of Bingham material through circular pipe. Applied Scientific Research, sec. A, 15:87. 1965.

47. Kutateladze, S. S., et al. Hydraulic resistance and heat transfer in stabilized flow of non-Newtonian fluids. Heat Transfer--Soviet Research 2(6):114-123. 1970.

48. Leveque, J. Annales des Mines, ser. 12, 13:201, 305, and 381. 1928.

49. Lyche, B. C. and R. B. Bird. The Graetz-Nusselt problem for a power-law non-Newtonian fluid. Chemical Engineering Science 6:35-41. 1956.

50. Lyon, R. N. Liquid metal heat transfer coefficients. Chemical Engineering Progress Symposium, ser. 2, 47:75-79. 1951.

51. McComas, S. T. and E. R. G. Eckert. Combined free and forced convection in a horizontal circular tube. Transactions of the American Society of Mechanical Engineers, Journal of Heat Transfer, ser. C, 88:147-149. 1966.

52. McKillop, A. A. Heat transfer for laminar flow of non-Newtonian fluids in entrance region of a tube. International Journal of Heat and Mass Transfer 7:853-861. 1964.

53. McKillop, A. A., et al. Variable viscosity entrance-region flow of non-Newtonian liquids. International Journal of Heat and Mass Transfer 13:901-909. 1970.

54. McKillop, A. A., et al. Heat transfer in entrance-region flow with external resistance. International Journal of Heat and Mass Transfer 14:863-866. 1971.

55. Martinelli, R. C. and L. M. K. Boelter. University of California Publications in Engineering 5:23. 1942.

56. Matsuhisa, S. and R. B. Bird. Analytical and numerical solutions for laminar flow of the non-Newtonian Ellis fluid. Journal of the American Institute of Chemical Engineers 11:588-595. 1965.

57. Metzner, A. B. and D. F. Gluck. Heat transfer to non-Newtonian fluids under laminar flow conditions. Chemical Engineering Science 12:185-190. 1960.

58. Metzner, A. B. and M. Whitlock. Flow behavior of concentrated (dilatant) suspensions. Transactions of the Society of Rheology 2:239-254. 1958.

59. Metzner, A. B., R. D. Vaughn, and G. L. Houghton. Heat transfer to non-Newtonian fluids. Journal of the American Institute of Chemical Engineers 3:92-100. 1957.

60. Michiyoshi, I. Heat transfer of slurry flow with internal heat generation. Bulletin of the Japanese Society of Mechanical Engineers 5:315-319. 1962.

61. Michiyoshi, I. and R. Matsumoto. Heat transfer of slurry flow with internal heat generation. Bulletin of the Japanese Society of Mechanical Engineers 7:376-384. 1964.

62. Michiyoshi, I., R. Matsumoto, and M. Hozumi. Heat transfer of slurry flow with heat generation. Bulletin of the Japanese Society of Mechanical Engineers 6:496-504. 1963.

63. Mitsuishi, N. and O. Miyatake. Laminar heat transfer to non-Newtonian Ellis model fluids in cylindrical tubes. Chemical Engineering, Japan 5:82-86. 1967.

64. Mitsuishi, N. and O. Miyatake. Heat transfer of non-Newtonian laminar flow in tubes with constant wall heat flux. Kagaku Kogaku 32:1222-1227. 1968.

65. Mitsuishi, N. and O. Miyatake. Heat transfer with non-Newtonian laminar flow in a tube having a constant wall heat flux. International Chemical Engineering 9:352-357. 1969.

66. Mizushina, T., et al. Laminar heat transfer to non-Newtonian fluids in a circular tube (constant heat flux). Kagaku Kogaku 31:250-255. 1967.

67. Mori, Y. and K. Futagami. Forced convective heat transfer in uniformly heated horizontal tubes, 2nd Report, theoretical study. International Journal of Heat and Mass Transfer 10:1801-1813. 1967.

68. Mori, Y., et al. Forced convective heat transfer in uniformly heated horizontal tubes, 1st report--experimental study on the effect of buoyancy. International Journal of Heat and Mass Transfer 9:453-463. 1966.

69. Morton, B. R. Laminar convection in uniformly heated horizontal pipes at low Rayleigh numbers. Quarterly Journal of Mechanics and Applied Mathematics 12:410. 1959.

70. Newell, P. H. and A. E. Bergles. Analysis of combined free and forced convection for fully developed laminar flow in horizontal tubes. Transactions of the American Society of Mechanical Engineers, Journal of Heat Transfer, ser. C, 92:83-93. 1970.

71. Oliver, D. R. The effect of natural convection on viscous-flow heat transfer in horizontal tubes. Chemical Engineering Science 17:335-350. 1962.

72. Oliver, D. R. and V. G. Jenson. Heat transfer to pseudoplastic fluids in laminar flow in horizontal tubes. Chemical Engineering Science 19:115-129. 1964.

73. Orr, C. and J. M. Dallavalle. Heat transfer properties of liquid-solid suspensions. Chemical Engineering Progress Symposium, ser. 9, 50:29-45. 1954.

74. Pattison, D. A. Motionless inline mixers stir up broad interest. Chemical Engineering, May 19, 1969, p. 94-96.

75. Pawlek, R. A. and C. Tien. Laminar heat transfer to non-Newtonian fluids in entrance region of circular conduit. Canadian Journal of Chemical Engineering 42:222. 1964.

76. Petukhov, B. S. and A. F. Polyakov. Experimental investigation of heat transfer during viscous gravitational flow of liquid in horizontal pipe. Teplofizika Vysokikh Temperatur 5:87-95. 1967.

77. Petukhov, B. S. and A. F. Polyakov. Effect of free convection on heat transfer during forced flow in a horizontal pipe. Teplofizika Vysokikh Temperatur 5:384-387. 1967.

78. Petukhov, B. S. and A. F. Polyakov. Flow and heat transfer in horizontal tubes under combined effect of forced and free convection. Heat Transfer 1970 4:NC3.7. 1970.

79. Petukhov, B. S., A. F. Polyakov, and B. K. Strigin. Heat transfer in tubes with viscous-gravity flow. Heat Transfer--Soviet Research 1:24-31. 1969.

80. Pigford, R. L. Nonisothermal flow and heat transfer inside vertical tubes. Chemical Engineering Progress Symposium, ser. 17, 51:79-92. 1955.

81. Roberts, A. S. Measurement of the dilatant flow properties of some non-Newtonian suspensions. Journal of Chemical and Engineering Data 8:440-444. 1962.

82. Samant, A. B. and W. J. Marner. Heat transfer to a Bingham plastic in the entrance region of a circular tube. Nuclear Engineering Science 43:241-246. 1971.

83. Schechter, R. S. and E. H. Wissler. Heat transfer to Bingham plastics in laminar flow through circular tubes with internal heat generation. Nuclear Science and Engineering 6:371-375. 1959.

84. Schenck, H. Theories of engineering experimentation. 2nd ed. New York, McGraw-Hill, 1968. 284 p.

85. Schenk, J. and J. Van Laar. Heat transfer in non-Newtonian laminar flow in tubes. Applied Scientific Research, sec. A, 7:449-462. 1958.

86. Sellars, J. R., M. Tribus, and S. J. Klein. Heat transfer to laminar flow in a round tube or flat conduit--the Graetz problem extended. Transactions of the American Society of Mechanical Engineers 78:441-448. 1956.

87. Sestak, J. and M. E. Charles. Limiting values of Nusselt number for heat transfer to pipeline flow of non-Newtonian fluids with arbitrary internal heat generation. Chemical Engineering Progress Symposium, ser. 82, 64:212-218. 1968.

88. Shannon, R. L. and C. A. Depew. Combined forced and free laminar convection in horizontal tube with uniform heat flux. Transactions of the American Society Mechanical Engineers, Journal of Heat Transfer, ser. C, 90:353-357. 1968.

89. Shannon, R. L. and C. A. Depew. Forced laminar flow convection in a horizontal tube with variable viscosity and free-convection effects. Transactions of the American Society of Mechanical Engineers, Journal of Heat Transfer, ser. C, 91:251-258. 1969.

90. Shulman, Z. P., et al. Convective heat transfer to a non-linear visco-plastic medium in a circular tube, allowing for dissipation. International Chemical Engineering 11:325. 1971.

91. Sieder, E. N. and G. E. Tate. Heat transfer and pressure drop of liquids in tubes. Industrial and Engineering Chemistry 28:1429-1436. 1936.

92. Siegel, R., E. M. Sparrow, and T. M. Hallman. Steady laminar heat transfer in a circular tube with prescribed wall heat flux. Applied Scientific Research, sec. A, 7:386-392. 1958.

93. Siegwarth, D. P. and T. J. Hanratty. Computational and experimental study of the effect of secondary flow on the temperature field and primary flow in a heated horizontal tube. International Journal of Heat and Mass Transfer 13:27-42. 1970.

94. Siegwarth, D. P., et al. Effect of secondary flow on the temperature field and primary flow in a heated horizontal tube.

International Journal of Heat and Mass Transfer 12:1535-1552. 1969.

95. Skelland, A. H. P. Non-Newtonian flow and heat transfer. New York, Wiley, 1967. 469 p.

96. Stephan, K. Warmetransport in viskosen nicht-Newtonschen flussigkeiten. Chemie-Ingenieur-Technik 39:243-250. 1967.

97. Test, F. L. Laminar flow heat transfer and fluid flow for liquids with temperature dependent viscosity. Transactions of the American Society of Mechanical Engineers, Journal of Heat Transfer, ser. C, 90:385-393. 1968.

98. Thomas, D. G. Heat and momentum transport characteristics of non-Newtonian aqueous thorium oxide suspensions. Journal of the American Institute of Chemical Engineers 6:631-639. 1960.

99. Toor, H. L. Energy equation for viscous flow. Effect of expansion on temperature profiles. Industrial and Engineering Chemistry 48:922-926. 1956.

100. Toor, H. L. Heat generation and conduction in the flow of a viscous compressible liquid. Transactions of the Society of Rheology 1:177-190. 1957.

101. Toor, H. L. Heat transfer in forced convection with internal heat generation. Journal of the American Institute of Chemical Engineers 4:319-323. 1958.

102. Union Carbide Corporation, New York. How to dissolve Polyox water-soluble resins. New York, 1970. 12 p. (pamphlet F-42933).

103. Van Wazer, J. R., et al. Viscosity and flow measurements: A laboratory handbook of rheology. New York, Interscience, 1963. 406 p.

104. Weast, R. C. (ed.). Handbook of chemistry and physics. 50th ed. Cleveland, Chemical Rubber Company, 1969. 2356 p.

105. Whiteman, I. R. and D. B. Drake. Heat transfer to flow in a round tube with arbitrary velocity distribution. Transactions

of the American Society of Mechanical Engineers 80:728-732. 1958.

106. Wissler, E. H. and R. S. Schechter. The Graetz-Nusselt problem (with extension) for a Bingham plastic. Chemical Engineering Progress Symposium, ser. 29, 55:203-208. 1959.

107. Yang, K. T. Laminar forced convection of liquids in tubes with variable viscosity. Transactions of the American Society of Mechanical Engineers, Journal of Heat Transfer, ser. C, 84: 353-362. 1962.

APPENDIX A

AXIAL CONDUCTION IN TUBE WALL

Consider the model shown in Figure A.1 for the heat balance on an incremental segment Δx located at axial position, x. Balancing the energy transfer for the model:

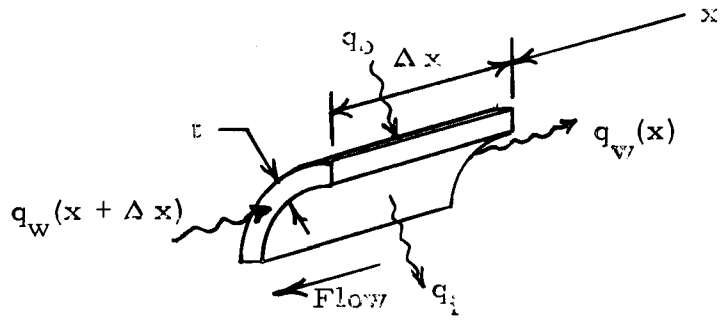

Figure A.1. Model for heat balance on tube wall segment.

$$q_o + q_w(x + \Delta x) - q_w(x) - q_i = 0 \qquad (A.1)$$

More specifically,

$$q_o'' \pi D \Delta x + k_w \pi Dt \frac{\partial T}{\partial x}(x + \Delta x) - k_w \pi Dt \frac{\partial T}{\partial x}(x)$$

$$- h_x \pi D \Delta x (T - T_b) = 0 \qquad (A.2)$$

where q_o'' is the applied heat flux, k_w is the thermal conductivity of the wall, T is the local wall temperature, h_x is the local convective

conductance inside the tube, and T_b is the local bulk temperature. Dividing by $\pi D \Delta x$ and taking the limit as $\Delta x \rightarrow 0$,

$$q_o'' + k_w t \frac{\partial^2 T}{\partial x^2} - h_x (T - T_b) = 0 \qquad (A.3)$$

The second term is obviously the heat flux conducted in the axial direction. It will be labeled q_w''.

Near the entrance, the data are correlated by:

$$Nu_x = C_1 Gz_x^{1/3} \qquad (A.4)$$

where C_1 is a constant. But the Nusselt number is:

$$Nu_x = \frac{h_x D}{k} = \frac{q_o'' D}{k(T - T_b)} \qquad (A.5)$$

if the axial conduction loss is neglected. Solving Equations (A.4) and (A.5) for the temperature difference, one obtains:

$$T - T_b = q_o'' D/k\, C_1 Gz_x^{1/3} \qquad (A.6)$$

But T_b is a linear function of x; hence, differentiating Equation (A.6) twice results in:

$$\frac{\partial^2 T}{\partial x^2} = -\frac{2}{9} \frac{q_o'' D}{k C_1 Gz_x^{1/3} x^2} \qquad (A.7)$$

Then the ratio q_w''/q_o'' is given by:

$$\frac{q''_w}{q''_o} = \frac{2}{9} \frac{k_w}{k} (C_1 Gz_x^{1/3})^{-1} \frac{Dt}{x^2} = \frac{2}{9} \frac{k_w}{k} Nu_x^{-1} \frac{Dt}{x^2} \qquad (A.8)$$

Since the local Graetz numbers for each test section were comparable, the largest axial conduction came from the large test section. The lowest Nusselt number at the first axial position of 3 inches was 35.02 for run number 91. So for $k_w/k = 611$ and $Dt/x^2 = 0.00410$, the ratio is:

$$\left(\frac{q''_w}{q''_o}\right)_{max} = 0.01590 \qquad (A.9)$$

Clearly, even if the Nusselt number was in error, say 10%, the maximum axial flux was not greater than 1.8% of the input flux.

APPENDIX B

EFFECT OF HEATING GAPS ON WALL TEMPERATURE

Consider a pipe flow in which a uniform heat flux is applied at the boundary. A simple energy balance gives:

$$T_b - T_o = \pi D x q''/\dot{m}C_p \tag{B.1}$$

where T_b is the local bulk temperature, T_o is the entrance temperature, and q'' is the applied heat flux. Using the definition of the Graetz number, Equation (B.1) becomes:

$$T_b - T_o = \frac{q''D}{k} \frac{\pi}{Gz_x} \tag{B.2}$$

From the definition of the local Nusselt number, one can write:

$$T_w - T_b = q'' \frac{D}{k} \frac{1}{Nu_x} \tag{B.3}$$

where T_w is the local wall temperature. Adding Equation (B.2) and Equation (B.3), the result is:

$$T_w - T_o = \frac{q''D}{k} \left(\frac{\pi}{Gz_x} + \frac{1}{Nu_x} \right) \tag{B.4}$$

In the absence of a substantial secondary flow, the empirical relationship,

$$Nu_k = C_1 Gz_x^m \tag{B.5}$$

is very good. For a particular set of flow conditions, C_1 and m are constant. Substituting into Equation (B.4), one obtains:

$$T_w - T_o = \frac{q''D}{k}\left(\frac{\pi}{Gz_x} + \frac{1}{C_1 Gz_x^m}\right) \qquad (B.6)$$

Now, consider a boundary condition of uniform heating everywhere except at a certain number of small intervals where no radial flux is applied. Taking advantage of the linearity of the energy equation, superposition can be used to model this boundary condition. The model, shown in Figure B.1, allows for a flow of heat into the gap due to tube wall conduction. This heat is assumed to be uniformly transferred to the fluid (probably not exactly true) and is given by:

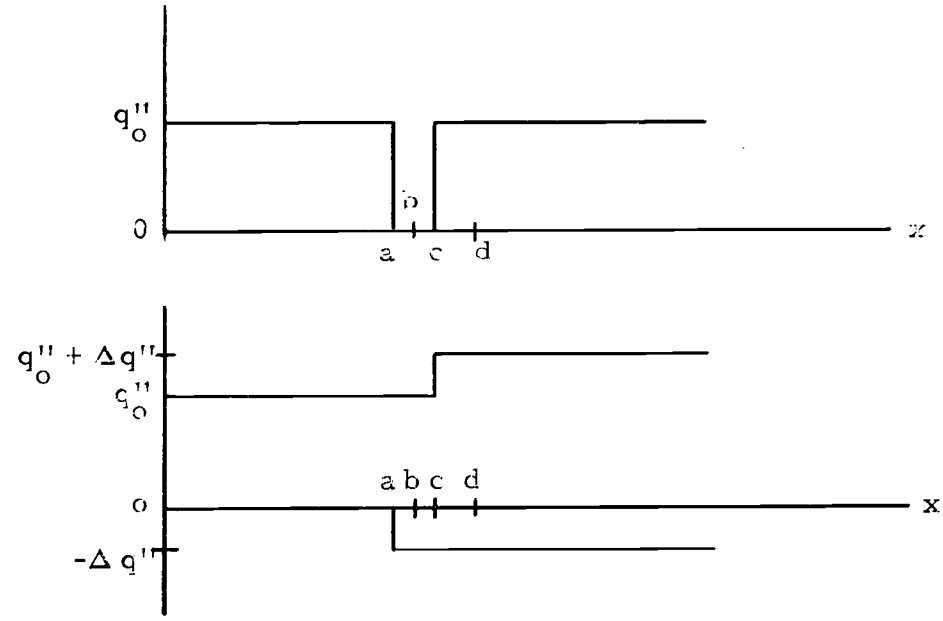

Figure B.1. Model of uniform heat flux with gaps (above) and its equivalent below.

$$q_g'' = q_o'' - \Delta q'' \tag{B.7}$$

where q_g'' is the heat flux into the fluid in the gap. Making use of superposition and Equation (B.6), the following equations give the relationship for the wall temperature within the region specified:

$$T_w - T_o = F(x) \quad , x \leq a \tag{B.8}$$

$$T_w - T_o = F(x) - G(x-a) \quad , a \leq x \leq c \tag{B.9}$$

$$T_w - T_o = F(x) - G(x-a) + G(x-c), \quad x \geq c \tag{B.10}$$

where,

$$F(\lambda) = \frac{q_o'' D}{k}\left(\frac{\pi}{Gz_\lambda} + \frac{1}{C_1 Gz_\lambda^{\,m}}\right) \tag{B.11}$$

$$G(\lambda) = \frac{\Delta q'' D}{k}\left(\frac{\pi}{Gz_\lambda} + \frac{1}{C_1 Gz_\lambda^{\,m}}\right) \tag{B.12}$$

Figure B.2 shows a plot of these functions. At any x, the difference, $T_w - T_o$, is the algebraic sum of the function values. If the wall conduction were negligible, $\Delta q'' \simeq q_o''$, and the temperature drop in the gap would be substantial. However, high axial gradients in the wall cannot be maintained if an adequate thermal path exists.

Using the curve through the measured data, the difference between the measured wall temperature and the wall temperature which would occur at the thermocouple site (position b) if no gaps were

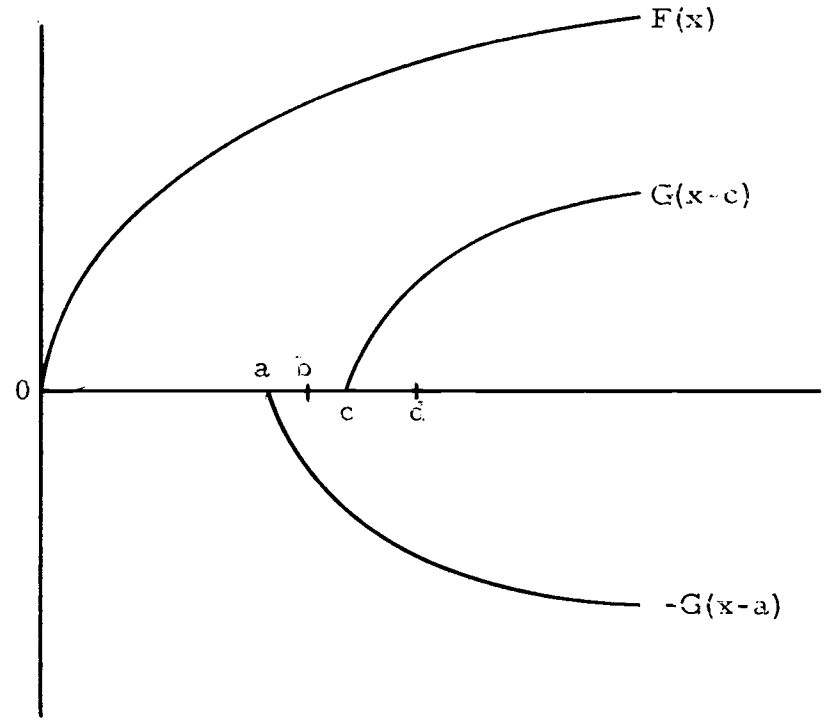

Figure B.2. Plot showing behavior of functions which, when superimposed, give $T_w - T_o$.

present can be approximated. This approximation can be obtained from the following iterative process, making use of Equations (B.8) through (B.12).

1. Obtain C_1 for m for the data point using the measured data for that point and the next point downstream and Equation (B.5).

2. Guess a temperature drop across the gap,

$$\Theta_g = T_{wa} - T_{wc} \tag{B.13}$$

3. Calculate $T_{wc} - T_o$ using:

$$T_{wc} - T_o = F(a) - \Theta_g \tag{B.14}$$

4. Obtain $G(c - a)$ from:

$$G(c - a) = F(c) - F(a) + \Theta_g \tag{B.15}$$

5. Obtain $G(d - c)$ and $G(d - a)$ from:

$$G(d - c) = \left[\frac{G(c - a)}{F(c - a)}\right] F(d - c) \tag{B.16}$$

$$G(d - a) = \left[\frac{G(c - a)}{F(c - a)}\right] F(d - a) \tag{B.17}$$

6. Calculate $T_{wd} - T_o$ by:

$$T_{wd} - T_o = F(d) + G(d - c) - G(d - a) \tag{B.18}$$

7. Obtain the flux conducted into the gap from the upstream side using the approximation:

$$q''_{wa} \simeq \frac{k_w \Theta_g}{c - a} \tag{B.19}$$

8. Obtain the flux conducted into the gap from the downstream side:

$$q''_{wc} \simeq \frac{k_w (T_{wd} - T_o) - (T_{wc} - T_o)}{d - c} \tag{B.20}$$

9. Determine the flux into the fluid from the gap walls from:

$$q''_g = q''_o \left[1 - \frac{G(c - a)}{F(c - a)}\right] \tag{B.21}$$

10. Compare the energy into the gap walls from conduction,

$$q_w = \pi D t (q''_{wa} + q''_{wc}), \tag{B.22}$$

where t is the wall thickness, with the energy convected out of the gap walls,

$$q_g = \pi D(c - a) q''_g \tag{B.23}$$

11. Iterate on Θ_g until $q_w = q_g$.

12. Calculate the difference sought:

$$T_{wb} - T'_{wb} = G(b - a) = \left[\frac{G(c - a)}{F(c - a)}\right] F(b - a) \tag{B.24}$$

where T'_{wb} is the temperature at point b if there were no gap.

APPENDIX C. LISTING OF COMPUTER PROGRAMS

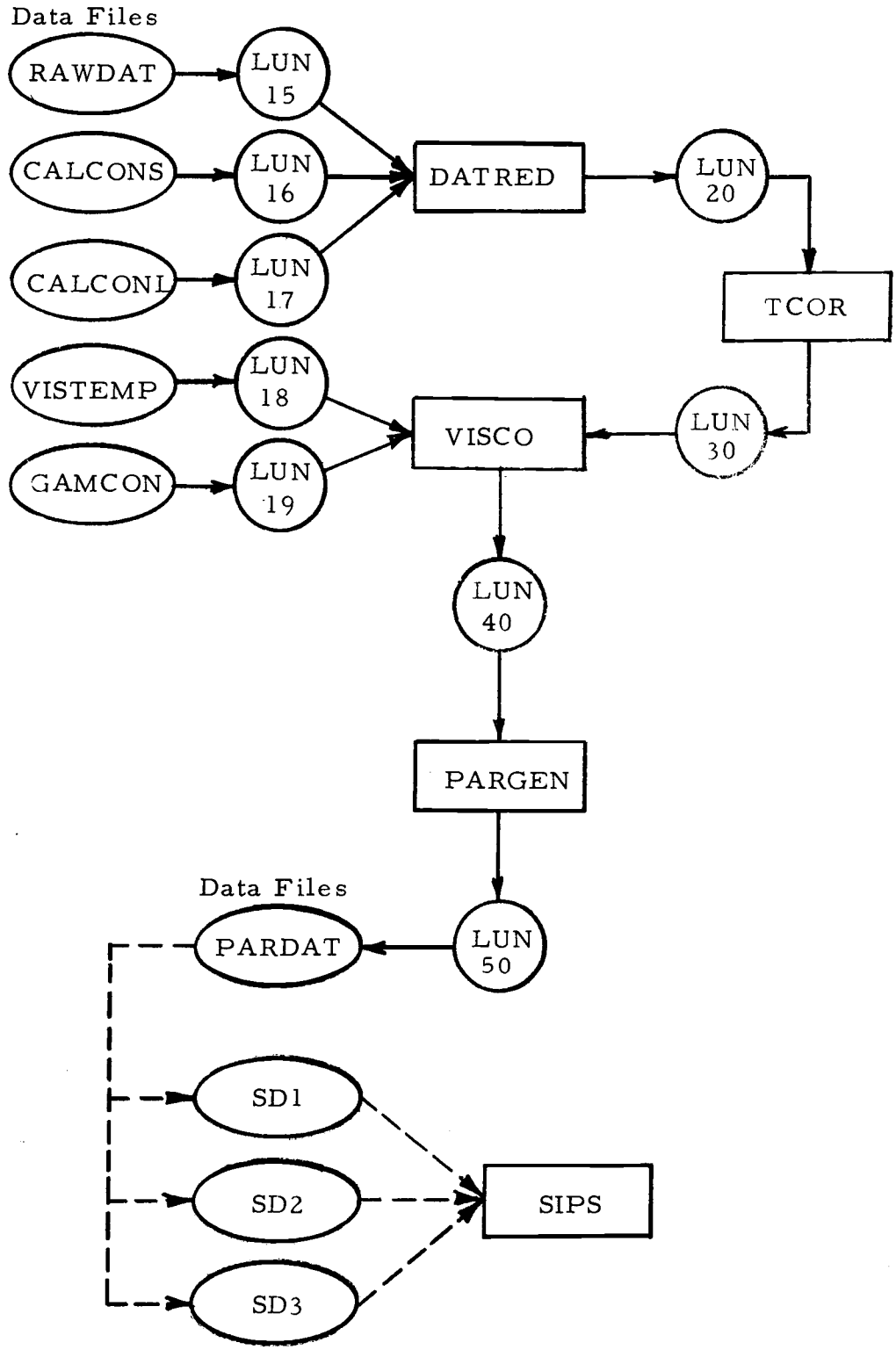

Figure C.1. Flow chart.

```
      PROGRAM *COMPRED
      DIMENSION TW(19),TB(2),X(2),Q(9),ETC(18),DELT(9),R(9),
     *XNUM(9),GZ(9),AS(16),BS(16),AL(18),BL(18)
      REAL MFR,L,K
      INTEGER DATANO
      PI=3.14159
C     L IS TOTAL HEATED LENGTH,CM
      L=303.53
C     READ CALLIBRATION CONSTANTS,AS AND BS FOR SMALL TEST SECTION,
C     AL AND BL FOR LARGE TEST SECTION
      DO 6 I=3,16
      AS(I)=FFIN(16)
06    BS(I)=FFIN(16)
      DO 7 I=3,18
      AL(I)=FFIN(17)
07    BL(I)=FFIN(17)
C     READ RAW DATA
C     DATANO IS THE RUN NUMBER
C     D IS DIAMETER,CM
C     P IS POWER,WATTS (CHANGED TO CAL/SEC)
C     MFR IS MASS FLOW RATE,LB/SEC (CHANGED TO GM/SEC)
C     TB(1) IS INLET BULK TEMP,C
C     ETC IS EMF READING FROM TC NUMBER I,MICROVOLTS
03    DATANO=FFIN(15)
      IF(EOF(15)) CALL EXIT
      D=FFIN(15)
      P=.2389*FFIN(15)
      MFR=FFIN(15)
      TB(1)=FFIN(15)
      NN=18
      IF(D.LT.2) NN=16
      DO 5 I=3,NN
05    ETC(I)=FFIN(15)
C     CORRECT WALL TC EMF AND TRANSFORM TO DEGREES C
C     TW IS MEASURED VALUE CORRECTED FOR TC ERROR,C
C     TW(I) NUMBERED TOP,ODD--BOTTOM,EVEN FROM ENTRANCE
      DO 11 I=3,NN
      IF(NN.EQ.18) GO TO 9
      A=AS(I)
      B=BS(I)
      GO TO 10
09    A=AL(I)
      B=BL(I)
10    DE=A+B*ETC(I)
      EM=ETC(I)+DE
11    TW(I)=TEMP(EM)
      TW(1)=TB(1)
      TW(2)=TW(1)
C     REDUCE RAW DATA
C     Q IS VOLUME FLOW RATE,CUBIC CM/SEC
C     DELT IS DIFFERENCE BETWEEN WALL AND BULK TEMP,C
C     XNUM IS LOCAL NUSSELT NUMBER USING DELT AND K AT
C     BULK TEMP
C     GZ IS LOCAL GRAETZ NUMBER
C     X IS POSITION MEASURED FROM ENTRANCE,CM
C     FL IS FLUX,CAL/SEC-CM**2
      N=NN/2
      Q(1)=MFR/RHO(TB(1))
      DELT(1)=0
      FL=P/(PI*D*L)
      X(1)=0.
      X(2)=7.62
```

```
      X(3)=22.65
      X(4)=53.72
      X(5)=76.2
      X(6)=121.92
      X(7)=182.88
      IF(N.EQ.8) GO TO 12
      X(8)=243.84
      X(9)=297.18
      GO TO 15
12    X(8)=297.18
15    DO 50 I=2,N
      J=I-1
      TB(I)=TB(1)+X(I)*P/(L*MFR*CP(TB(J)))
      D(I)=MFR/RHO(TB(I))
      M=2*I
      JJ=M-1
      ATW=(TW(M)+TW(JJ))/2.
      DELT(I)=ATW-TB(I)
      CAY=K(TB(I))
      XNUM(I)=FL*D/(CAY*DELT(I))
50    GZ(I)=MFR*CP(TB(I))/(CAY*X(I))
      WRITE(20)D,DATANG,DELT,FL,GZ,L,MFR,N,XNUM,P,Q,TB,TW,X
      WRITE(61,101)DATANG,D,MFR,FL
      WRITE(61,102)TB
      WRITE(61,102)TW
      GO TO 3
101   FORMAT(1X,I3,1X,F7.4,1X,F7.3,1X,F6.4)
102   FORMAT(9(1X,F7.3))
      END
      FUNCTION K(T)
C     THERMAL CONDUCTIVITY, CAL/CM-SEC-C, AS FUNCTION OF TEMP,
      REAL K
      K=4.8273+(1.0070E-02)*T-(1.6674E-06)*T**3+
     X(2.3225E-08)*T**4-(1.0341E-10)*T**5
      K=K/3600.
      RETURN
      END
      FUNCTION CP(T)
C     HEAT CAPACITY, CAL/G-C, AS FUNCTION OF TEMP,C
      CP=1.0069-(6.7042E-04)*T+(1.6972E-05)*T**2-(1.7171E-07)
     X*T**3+(6.8316E-10)*T**4
      RETURN
      END
      FUNCTION RHO(T)
C     DENSITY, G/CUBIC CM, AS FUNCTION OF TEMP,C
      RHO=.99997+(5.0299E-05)*T-(7.8164E-06)*T**2+(5.4549E-08)
     X*T**3-(3.1046E-10)*T**4+(6.0397E-13)*T**5
      RETURN
      END
      FUNCTION TEMP(E)
C     THIS FUNCTION CONVERTS CU-CON TC READINGS TO DEGREES C
C     E IS MV,MILLIVOLTS
C     T IS TEMP,F
      IF(E.GT.1.516) GO TO 50
      T=31.9637869+.0466149042*E-1.1762776E-06*E**2
      GO TO 60
50    T=32.8462869+.0455413389*E-6.5840391E-07*E**2
60    TEMP=(T-32.)/1.8
      RETURN
      END
```

```
      PROGRAM PIOOR
C     THIS PROGRAM CORRECTS WALL TEMP READINGS FOR EFFECT OF
C     HEATER GAPS
C     X IS DISTANCE FROM ENTRANCE,CM
C     XA IS DISTANCE TO UPSTREAM EDGE OF GAP FROM ENTRANCE,CM
C     XC IS DISTANCE TO DOWNSTREAM EDGE OF GAP FROM ENTRANCE,CM
C     XD IS DISTANCE TO POINT DOWNSTREAM OF THE GAP FROM ENT-
C     RANCE,CM
C     XAB IS HALF THE GAP WIDTH,CM
C     XAC IS THE GAP WIDTH,CM
C     XAD IS THE DISTANCE TO DOWNSTREAM POINT FROM THE UP-
C     STREAM EDGE OF GAP,CM
C     DELT IS THE MEASURED DIFFERENCE IN LOCAL WALL AND LOCAL
C     BULK TEMP,C
C     EN IS EXPONENT IN MODEL NU=C*GZ**EN
C     C IS CONSTANT IN ABOVE MODEL
C     F IS FUNCTION BASED ON UNIFORM HEAT FLUX WHICH GIVES
C     VALUE OF DIFFERENCE BETWN LOCAL WALL TEMP AND THE
C     ENTRANCE TEMP,C
C     THC IS DIFFERENCE BETWN WALL TEMP AND ENTRANCE TEMP AT
C     XC,C
C     THD IS DIFFERENCE BETWN WALL TEMP AND ENTRANCE TEMP AT
C     XD,C
C     DTW IS THE DROP IN WALL TEMP ACROSS THE GAP,C
C     FW1 IS HEAT FLUX CONDUCTED INTO GAP WALL FROM UPSTREAM
C     SIDE,CAL/SEC-CM**2
C     FW2 IS DITTO FW1 FROM DOWNSTREAM SIDE
C     T IS WALL THICKNESS,CM
C     FGAP IS FLUX INTO FLUID FROM GAP WALL,CAL/SEC-CM**2
C     DT IS THE PREDICTED DIFFERENCE BETWN THE MEASURED VALUE
C     DELT AT X AND THE VALUE AT X WITHOUT A GAP,C
C     XNUM IS THE LOCAL NUSSELT NUMBER BASED ON MEASURED VALUE
C     DELT
C     GZ IS THE LOCAL GRAETZ NUMBER
C     R IS THE RUN NUMBER
      DIMENSION X(9),DELT(9),XNUM(9),GZ(9),DT(9),QGAP(9),
     *QWALL(9),FLW1(9),FLW2(9),FLG(9),DTG(9),R(9),Q(9),TB(9),TW(18)
      COMMON X(9),DELT(9),XNUM(9),GZ(9),C1,EN,I
      REAL L,MFR
      INTEGER DATANO
      XC)=FTYIN(5MXCD= )
05    READ(20)Q,DATANO,DELT,FL,GZ,L,MFR,N,XNUM,F,Q,TB,TW,X
      IF(EOF(20))CALL EXIT
      T=.1016
      IF(N.EQ.9)T=.0889
      DO 100 I=2,N
      TEST=0
      R(I)=DATANO
      DTW=1.
      K=0
      KK=0
      XA=X(I)-.508
      XC=X(I)+.508
      XD=XC+XCD
      XAB=.508
      XAC=1.016
      XAD=XAC+XCD
      IF(I.EQ.N) GO TO 20
      M=I+1
      EN=ALOG(XNUM(I)/XNUM(M))/ALOG(GZ(I)/GZ(M))
20    C=XNU*(I)/(GZ(I)**EN)
      C1=C
```

```
      DTO=F(X(I))
25    KK=KK+1
      IF(KK.GT.40)GO TO 31
      THO=F(XA)-DTW
      GAO=F(XO)-F(XA)+DTW
      THO=F(XO)+GAO*(F(XOB)-F(XAO))/F(XAO)
      FW1=.9091*DTW/XAO
      FW2=.9091*(THO-THO)/XOB
      FGAP=(1.-(GAO/F(XAO)))*FL
      QW=(FW1+FW2)*T
      QG=FGAP*XAO
      IF(FGAP.LT.0)GO TO 31
      IF(QW-QG)30,31,32
30    TEST=DTW
      IF(K.GT.0)GO TO 31
      DTW=DTW+1.
      GO TO 25
32    K=K+1
      IF(TEST.EQ.DTW.OR.TEST.GT.DTW)GO TO 31
      DTW=DTW-.1
      GO TO 25
31    DT(I)=-GAO*F(XAB)/F(XAO)
      DTG(I)=DTW
      QGAP(I)=QG
      QWALL(I)=QW
      FLW1(I)=FW1
      FLW2(I)=FW2
      FLG(I)=FGAP
100   CONTINUE
      WRITE(30)D,DATANO,DELT,DT,FL,GZ,L,MFR,N,F,G,TB,TW,X
      WRITE(25,200)(R(I),DELT(I),DT(I),DTG(I),QGAP(I),QWALL(I),
     *I=2,N)
200   FORMAT(1X,F3.0,1X,F6.2,2(1X,F5.2),2(1X,E16.8))
      GO TO 5
      END
      FUNCTION F(Y)
      COMMON X(9),DELT(9),XNUM(9),GZ(9),C1,EN,I
      F=DELT(I)*XNUM(I)*(3.14159/((X(I)/Y)*GZ(I))+1./(C1
     **((X(I)/Y)*GZ(I))**EN))
      RETURN
      END
```

```
      PROGRAM *VISCO
      DIMENSION A(7,6),TV(14),TA(2),G(9),GAMW(9),GN(9),
     *ETAW(9),ETAS(9),GAMMA(1000),UM(9),TAU(1000),U(1000),
     *T(7),CC(9),TAUM(7),DELT(9),DT(9),GZ(9),ATW(9),X(9)
      COMMON A(7,6)
      INTEGER DATANO
      REAL IGRD1,IGRD2,INT,L,MFR
C     MATCH IS CODE FOR CALLING NEW VISCOSITY CONSTANTS
      MATCH=1
3     READ(30)D,DATANO,DELT,DT,FL,GZ,L,MFR,N,P,G,TB,TW,X
      IF(EOF(30)) CALL EXIT
      MATCH=MATCH-1
      IF(MATCH.NE.0) GO TO 17
      MATCH=6
      WRITE(61,107)D
C     INPUT OF VISTEMP,TV(I),AND MAX TAU FOR WHICH VIS CURVE
C     IS VALID,TAUM
      NT=FFIN(16)
      DO 5 I=1,NT
      TAUM(I)=FFIN(18)
5     TV(I)=FFIN(18)
C     INPUT OF VIS CONSTANTS AND WRITE CHECK
      READ(19)A
      W=TTYIN(4HWR= )
      IF(W.GT.0) WRITE(61,15)((A(I,J),J=1,6),I=1,NT)
15    FORMAT(1X,6(E10.4,1X))
C     INPUT OF STEPSIZE, DTAU, DYNE/SQ CM
17    DTAU=TTYIN(4HDT= )
      DO 100 I=1,N
C     START CALC FOR VALUES AT LOCAL POSITION
C     GN, NEWTONIAN WALL SHEAR RATE, 8V/D, 1/SEC
C     ATW, AVE LOCAL WALL TEMP (CORRECTED), C
      GN(I)=32.*G(I)/(3.14159*D**3)
      WRITE(61,104)GN(I)
      IF(I.NE.1) GO TO 16
      DTAU1=DTAU
16    ATW(I)=TB(I)+DELT(I)-DT(I)
C     THIS LOOP CHOOSES CORRECT VIS CURVES FOR INTERPOLATION
      DO 20 J=1,NT
      IF(ATW(I).GT.TV(J).AND.J.LT.NT) GO TO 20
      II=J-1
      IJ=J
      IF(J.EQ.1) II=J+1
      GO TO 25
20      CONTINUE
C     TR, TEMP RATIO USED IN INTERPOLATION
25    TR=((ATW(I)-TV(II))/(TV(IJ)-TV(II)))*(TV(IJ)+273.)
     X/(ATW(I)+273.)
      WRITE(61,106)TV(II),TV(IJ)
      TAUL2=0.
      TAUU2=0.
      INT=0.
      G2=0.
      IGRD2=0.
      R=8.*G(I)/(3.14159*D**3)
      IF(I.GT.1) GO TO 70
      DTAU2=DTAU
      DGG=GN(I)*.005
C     THIS LOOP ITERATES AND INTEGRATES FOR WALL SHEAR STRESS,
C     TAUW AND WALL SHEAR RATE,GAMW(I) AT THE INLET TEMP
C     TAUU IS TAU ON UPPER TEMP CURVE
C     TAUL IS TAU ON LOWER TEMP CURVE
```

```
C     TAU1 AND TAU2 ARE INTERPOLATED VALUES OF TAU BETWEEN
C     CURVES
C     G1 AND G2 ARE VALUES OF SHEAR RATE FOR TAU1 AND TAU2
C     GAM IS SHEAR RATE FUNCTION AT DISCRETE VIS TEMP
C     GAMP IS DERIVATIVE OF GAM W/RESPECT TO SHEAR STRESS, TAU
C     ETAW IS APPARENT WALL VISCOSITY, POISE
C     ITER IS NUMBER OF INDEXED ITERATIONS (PLANNED)
C     ERROR IS MEASURE OF OVERSHOOT OF THE INTEGRATION
      DO 46 J=1,999,2
      JK=J+1
      DTAU=DTAU2
      GO TO 37
31    DTAU=(.9*DTAU/DG)*DGG
37    TAUU1=TAUU2+DTAU
      G1=GAM(IJ,TAUU1)
      DG=G1-G2
      IF(DG.GT.DGG) GO TO 31
      IF(DG.GT.0) GO TO 39
38    DTAU=DTAU*2.
      TAUU1=TAUU2+DTAU
      G1=GAM(IJ,TAUU1)
      DG=G1-G2
      IF(DG.LT.0) GO TO 38
39    TAUL1=TAUL2+DG/GAMP(II,TAUL2)
      TAU1=TAUL1*(TAUU1/TAUL1)**TR
      IGRD1=TAU1**3
      INT=INT+(DG/2.)*(IGRD1+IGRD2)
      Y=(G1-INT/IGRD1)/3.
      IF(R.GT.Y) GO TO 42
      TAUW=TAU1
      GAMW(I)=G1
      ETAW(I)=TAU1/G1
      ITER=J
40    ERROR=(Y-R)/R
      GO TO 47
41    DTAU=(.9*DTAU/DG)*DGG
42    TAUL2=TAUL1+DTAU
      G2=GAM(II,TAUL2)
      DG=G2-G1
      IF(DG.GT.DGG) GO TO 41
      IF(DG.GT.0) GO TO 44
43    DTAU=DTAU*2.
      TAUL2=TAUL1+DTAU
      G2=GAM(II,TAUL2)
      DG=G2-G1
      IF(DG.LT.0) GO TO 43
44    TAUU2=TAUU1+DG/GAMP(IJ,TAUU1)
      TAU2=TAUL2*(TAUU2/TAUL2)**TR
      IGRD2=TAU2**3
      INT=INT+(DG/2.)*(IGRD1+IGRD2)
      Y=(G2-INT/IGRD2)/3.
      IF(J.EQ.999) GO TO 45
      IF(R.GT.Y) GO TO 46
45    TAUW=TAU2
      GAMW(I)=G2
      ETAW(I)=TAU2/G2
      ITER=JK
      GO TO 40
46    CONTINUE
47    WRITE(61,103)TAUW,ITER,ERROR
C     THIS LOOP SELECTS VIS CURVES FOR INTERPOLATION AT BULK TEMP
48    DO 49 J=1,NT
      IF(TB(I).GT.TV(J)) GO TO 49
```

```
      II=J-1
      IJ=J
      IF(J.EQ.1) II=J+1
      GO TO 50
49    CONTINUE
50    TAU(1)=0
      TAUL2=0.
      TAUU2=0.
      GAMMA(1)=0.
      IGRD2=0.
      DTAU=DTAU1
      INT=0.
      TR=((TB(I)-TV(II))/(TV(IJ)-TV(II)))*(TV(IJ)+273.)/
     X(TB(I)+273.)
C     THIS LOOP FINDS WALL TAU AND WALL GAM AT ELEM TEMP AND
C     GENERATES TAU AND GAM VALUES ACROSS CROSS SECTION
C     TAU(J) IS TAU AT JTH STEP ACROSS CROSS SECTION
C     GAMMA(J) IS CORRESPONDING GAM
      DO 60 J=2,1000,2
      JI=J-1
      JK=J+1
      GO TO 53
52    DTAU=(.9*DTAU/DG)*DGG
53    TAUU1=TAUU2+DTAU
      GAMMA(J)=GAM(IJ,TAUU1)
      DG=GAMMA(J)-GAMMA(JI)
      IF(DG.GT.DGG) GO TO 52
      IF(DG.GT.0) GO TO 55
54    DTAU=DTAU*2.
      TAUU1=TAUU2+DTAU
      GAMMA(J)=GAM(IJ,TAUU1)
      DG=GAMMA(J)-GAMMA(JI)
      IF(DG.LT.0) GO TO 54
55    TAUL1=TAUL2+DG/GAMP(II,TAUL2)
      TAU(J)=TAUL1*(TAUU1/TAUL1)**TR
      IGRD1=TAU(J)**3
      INT=INT+(DG/2.)*(IGRD1+IGRD2)
      Y=(GAMMA(J)-INT/IGRD1)/3.
      IF(R.LT.Y) GO TO 61
      GO TO 57
56    DTAU=(.9*DTAU/DG)*DGG
57    TAUL2=TAUL1+DTAU
      GAMMA(JK)=GAM(II,TAUL2)
      DG=GAMMA(JK)-GAMMA(J)
      IF(DG.GT.DGG) GO TO 56
      IF(DG.GT.0) GO TO 59
58    DTAU=DTAU*2.
      TAUL2=TAUL1+DTAU
      GAMMA(JK)=GAM(II,TAUL2)
      DG=GAMMA(JK)-GAMMA(J)
      IF(DG.LT.0) GO TO 58
59    TAUU2=TAUU1+DG/GAMP(IJ,TAUU1)
      TAU(JK)=TAUL2*(TAUU2/TAUL2)**TR
      IGRD2=TAU(JK)**3
      INT=INT+(DG/2.)*(IGRD1+IGRD2)
      Y=(GAMMA(JK)-INT/IGRD2)/3.
      IF(R.LT.Y) GO TO 62
      IF(J.EQ.998) GO TO 63
60    CONTINUE
61    NN=J
      GO TO 64
62    NN=JK
      GO TO 64
```

```
63    WRITE(61,105)TAU(JK),GAMMA(JK),DTAU
      GO TO 100
64    NM=NN-1
      U(NN)=0.
      C=D/(TAU(NN)*2.)
      E=TAU(NN)*GAMMA(NN)
      INT=0.
C     THIS LOOP GENERATES VELOCITIES, U(J), AT EACH TAU(J)
C     UM IS MAX VELOCITY CALCULATED
      DO 65 J=1,NM
      K=NN-J+1
      KK=K-1
      DG=GAMMA(K)-GAMMA(KK)
      INT=INT+(DG/2.)*(TAU(K)+TAU(KK))
65    U(KK)=C*((E-TAU(KK)*GAMMA(KK))-INT)
      UM(I)=U(1)
      QC(I)=0.
      IGRD2=0.
      B=(6.28306*C**2)/Q(I)
C     THIS LOOP CALC QC(I), VOLUME FLOW RATE FOR CHECK
      DO 66 J=2,NN
      JI=J-1
      DTAU=TAU(J)-TAU(JI)
      IGRD1=IGRD2
      IGRD2=U(J)*TAU(J)
66    QC(I)=QC(I)+(DTAU/2.)*(IGRD1+IGRD2)
      QC(I)=QC(I)*B
      WRITE(61,102)QC(I)
      IGRD2=0.
      ETAB(I)=0.
C     THIS LOOP CALC ETAB, VIS AT BULK CONDITIONS
      DO 67 J=2,NN
      JI=J-1
      DTAU=TAU(J)-TAU(JI)
      IGRD1=IGRD2
      IGRD2=U(J)*(TAU(J)**2)/GAMMA(J)
67    ETAB(I)=ETAB(I)+(DTAU/2.)*(IGRD1+IGRD2)
      ETAB(I)=ETAB(I)*B
      WRITE(61,101)ATW(I),TB(I),U(1),GAMW(I),ETAW(I),ETAB(I)
      GO TO 100
C     THIS LOOP CALCULATES WALL SHEAR RATES IN THE HEATED
C     SECTION USING TAUW AND ATW(I)
C     IF TAUW EXCEEDS CURVE LIMIT,TAUM,POWER LAW EXTRAPOLATION
C     IS USED
70    ALT=ALOG(5./9.)
      IF(TAUW.GT.TAUM(II)) GO TO 71
      GL=GAM(II,TAUW)
      IF(TAUW.GT.TAUM(IJ)) GO TO 72
      GU=GAM(IJ,TAUW)
      GO TO 73
71    TAU1=.5*TAUM(II)
      G1=GAM(II,TAU1)
      TAU2=.9*TAUM(II)
      G2=GAM(II,TAU2)
      RN=ALOG(G1/G2)/ALT
      GL=G1*(TAUW/TAU1)**RN
72    TAU1=.5*TAUM(IJ)
      G1=GAM(IJ,TAU1)
      TAU2=.9*TAUM(IJ)
      G2=GAM(IJ,TAU2)
      RN=ALOG(G1/G2)/ALT
      GU=G1*(TAUW/TAU1)**RN
73    GAMW(I)=GL*(GU/GL)**TR
```

```
      ETAW(I)=TAUW/GAMW(I)
      GO TO 48
100   CONTINUE
      WRITE(6,1)AIW,Q,QAT/NO,DI,ETAW,ETAW,FL,GAMW,CW,GZ,L,
     *MER,N,P,O,TAUW,TB,IW,LM,X
      GO TO 3
101   FORMAT(1X,3(F6.2,1X),F7.3,2(1X,F7.4))
102   FORMAT(1X,E16.8)
103   FORMAT(1X,F7.2,1X,I3,1X,F6.4)
104   FORMAT(1X,F7.2)
105   FORMAT(1X,'BULK CALC ITER GT 1000'/,1X,2(F7.2,2X),F7.5)
106   FORMAT(1X,2(F6.2,1X))
107   FORMAT('-',' DIA= ',F6.4,' CM')
      END
      FUNCTION GAM(MO,SS)
      COMMON A(7,6)
      GAM=A(MO,1)*SS+A(MO,2)*SS**2+A(MO,3)*SS**3+A(MO,4)*SS**4+
     XA(MO,5)*SS**5+A(MO,6)*SS**6
      RETURN
      END
      FUNCTION GAMP(MP,SS)
      COMMON A(7,6)
      GAMP=A(MP,1)+2.*A(MP,2)*SS+3.*A(MP,3)*SS**2+
     X4.*A(MP,4)*SS**3+5.*A(MP,5)*SS**4+6.*A(MP,6)*SS**5
      RETURN
      END
```

```
      PROGRAM *PARGLN
C     ATW IS LOCAL AVG WALL TEMP, CORRECTED FOR EFFECT OF
C     GAP IN HEATING,C
C     BR, BRINKMAN NO EVAL AT INLET WALL COND
C     RE, LOCAL REYNOLDS NO EVAL AT BULK COND
C     PRB, LOCAL PRANDTL NO EVAL AT BULK COND
C     PRW, LOCAL PRANDTL NO EVAL AT WALL COND
C     DEL, LOCAL RATIO OF NEWTONIAN TO NEWT WALL SHEAR RATE
C     ETAR, LOCAL RATIO OF VISCOSITY AT BULK TO WALL COND
C     GZ, LOCAL GRAETZ NO EVAL AT BULK COND
C     PHIW, LOCAL DIMENSIONLESS FLUX W/K EVAL AT WALL TEMP
C     PHIB, LOCAL DIMENSIONLESS FLUX W/K EVAL AT BULK TEMP
C     GRMB, LOCAL MODIFIED GRASHOF NO EVAL AT BULK COND
C     GRMW, LOCAL MODIFIED GRASHOF NO EVAL AT WALL COND
C     RAMB, LOCAL MODIFIED RAYLEIGH NO EVAL AT BULK COND
C     RAMW, LOCAL MODIFIED RAYLEIGH NO EVAL AT WALL COND
C     HA, LOCAL CONVECTIVE CONDUCTANCE EVAL AT CIRC AVE WALL
C     TEMP, CAL/SQ CM-SEC
C     DT IS CORRECTION IN LOCAL WALL TEMP DUE TO EFFECT OF
C     GAP IN HEATING,C
C     HT, LOCAL CONVECTIVE CONDUCTANCE EVAL AT TOP WALL TEMP,
C     CAL/SQ CM-SEC
C     HB, LOCAL CONVECTIVE CONDUCTANCE EVAL AT BOTTOM WALL
C     TEMP, CAL/SQ CM-SEC
C     NUAW, LOCAL NUSSELT NO EVAL AT CIRC AVE WALL COND
C     NUAB, LOCAL NUSSELT NO EVAL AT CIRC AVE WALL TEMP AND
C     W/K EVAL AT LOCAL BULK TEMP
C     NUT, LOCAL NUSSELT NO EVAL AT TOP WALL TEMP AND W/K EVAL
C     AT LOCAL BULK TEMP
C     NUB, LOCAL NUSSELT NO EVAL AT BOTTOM WALL TEMP AND W/K
C     EVAL AT LOCAL BULK TEMP
C     GRW, LOCAL GRASHOF NO EVAL AT WALL CONDITIONS
C     GRB, LOCAL GRASHOF NO EVAL AT BULK CONDITIONS
      DIMENSION ATW(9),DEL(9),DT(9),ETAB(9),ETAR(9),ETAW(9),
     *GAMW(9),GN(9),GRB(9),GRMB(9),GRMW(9),GRW(9),GZ(9),HA(9),
     *HB(9),HT(9),NUAB(9),NUAW(9),NUB(9),NUT(9),PHIB(9),
     *PHIW(9),PRB(9),PRW(9),Q(9),RAMB(9),RAMW(9),RE(9),
     *TB(9),TW(18),UM(9),X(9),R(9)
      REAL K,MFR,L,NUAB,NUAW,NUB,NUT
      INTEGER DATANO
05    READ(40)ATW,C,DATANO,DT,ETAB,ETAW,FL,GAMW,GN,GZ,L,MFR,
     *N,P,Q,TAUW,TB,TW,UM,K
      IF(EOF(40)) CALL EXIT
      C2=1.273240
      G=980.7
      BR=(ETAW(1)*Q(1)**2)/((TB(1)+273.)*.785*(C**2)*K(TB(1))
     **4.186E07)
      DO 100 I=1,N
      M=2*I
      J=M-1
      R(I)=DATANO
      CAYW=K(ATW(I))
      CAYB=K(TB(I))
      RE(I)=C2*MFR/(C*ETAB(I))
      PRB(I)=CP(TB(I))*ETAB(I)/CAYB
      PRW(I)=CP(ATW(I))*ETAW(I)/CAYW
      DEL(I)=GAMW(I)/GN(I)
      ETAR(I)=ETAB(I)/ETAW(I)
      PHIW(I)=FL*Q/(CAYW*(TB(I)+273.))
      PHIB(I)=PHIW(I)*CAYW/CAYB
      GRMB(I)=G*(D**4)*(RHO(TB(I))**2)*FL*B(TB(I))/(CAYB*
     *ETAB(I)**2)
```

```
      GRAW(I)=G*(D**4)*(RHO(ATW(I))**2)*BL*E(ATW(I))/(CAYW*
     *ETAW(I)**2)
      RAAW(I)=GRAW(I)*PRW(I)
      RAMW(I)=GRMW(I)*PRW(I)
      IF(I.GT.1) GO TO 100
      HA(I)=BL/(ATW(I)-TB(I))
      HT(I)=BL/(TW(I)-DT(I)-TB(I))
      HB(I)=BL/(TW(M)-DT(I)-TB(I))
      NUAW(I)=HA(I)*D/CAYW
      NUAB(I)=HA(I)*D/CAYB
      NUT(I)=HT(I)*D/CAYB
      NUB(I)=HB(I)*D/CAYB
      GRW(I)=GRAW(I)/NUAW(I)
      GRB(I)=GRAB(I)/NUAB(I)
100   CONTINUE
      WRITE(50)ATW,BR,C,CATANG,CEL,CT,ETAB,ETAR,ETAR,FL,GAMW,
     *GN,GRB,GRMB,GRMW,GRW,GZ,HA,HB,HT,L,MFR,N,NUAB,NUAW,NUB,
     *NUT,P,PHIB,PHIW,PRB,PRW,Q,RAMB,RAMW,RE,TAUR,TE,TW,UM,X
      WRITE(51,101)(R(I),GZ(I),NUAB(I),NUAR(I),CEL(I),ETAR(I),
     *PHIW(I),PRB(I),RAMW(I),I=2,N)
101   FORMAT(1X,F3.0,1X,F8.2,2(1X,F6.3),2(1X,F7.4),1X,F6.4,
     *1X,F8.2,1X,F10.1)
      GO TO 5
      END
      FUNCTION K(T)
C     THERMAL CONDUCTIVITY, CAL/CM-SEC-C, AS FUNCTION OF TEMP,
     C
      REAL K
      K=4.8273+(1.6070E-02)*T-(1.8674E-06)*T**3+
     X(2.3225E-08)*T**4-(1.0341E-10)*T**5
      K=K/3600.
      RETURN
      END
      FUNCTION B(T)
C     THERMAL EXPANSIVITY,1/C, AS FUNCTION OF TEMP, C
      B=-61.034+16.947*T-.22374*T**2+(2.6036E-03)*T**3-
     X(1.7805E-05)*T**4+(5.3328E-08)*T**5
      B=B*1.0E-06
      RETURN
      END
      FUNCTION CP(T)
C     HEAT CAPACITY, CAL/G-C, AS FUNCTION OF TEMP,C
      CP=1.0069-(6.7042E-04)*T+(1.6972E-05)*T**2-(1.7171E-07)
     X*T**3+(6.9316E-10)*T**4
      RETURN
      END
      FUNCTION RHO(T)
C     DENSITY, G/CUBIC CM, AS FUNCTION OF TEMP,C
      RHO=.99997+(5.0299E-05)*T-(7.8164E-06)*T**2+(5.4549E-08)
     X*T**3-(3.1046E-10)*T**4+(8.0997E-13)*T**5
      RETURN
      END
```

APPENDIX D

LISTING OF VISCOMETER DATA

3.[illegible]% CMC
MV SYSTEM ROT DIA= 40.03 MM BEAK DIA= 42.00 MM

ROTOR VEL., RAD/S	SHEAR STRESS, DYNES/SQ CM AT - 22.0 C	32.3 C	44.1 C	55.4 C	67.[illegible] C		
.38	15.4	0	0	0	0	0	0
.75	30.4	12.4	0	0	0	0	0
1.13	42.9	25.6	17.0	0	0	0	0
2.26	77.6	51.3	38.4	19.0	0	0	0
3.39	105.0	72.5	42.9	27.5	15.2	0	0
6.79	168.0	125.0	79.4	50.6	35.2	0	0
10.15	2[illegible]1.0	1[illegible]2.0	110.0	71.3	42.9	0	0
20.30	41[illegible].0	305.0	193.0	122.0	75.4	0	0
30.45	[illegible]	410.0	2[illegible]7.0	177.3	107.[illegible]	0	0
61.07	[illegible]	[illegible]	449.0	306.0	193.[illegible]	0	0

5.4% CMC
MV SYSTEM ROT DIA= 40.08 MM BEAK DIA= 42.00 MM

ROTOR VEL., RAD/S	SHEAR STRESS, DYNES/SQ CM AT - 20.0 C	30.0 C	40.0 C	51.0 C	60.0 C	70.0 C	83.2 C
.38	71.0	54.5	37.3	27.5	17.0	0	0
.75	130.5	90.7	64.0	46.6	32.0	22.3	15.0
1.13	174.5	121.5	85.9	63.2	45.0	31.4	23.1
2.26	290.0	200.0	142.5	105.5	77.0	52.2	39.3
3.39	372.5	264.1	192.[illegible]	140.8	102.1	70.9	53.5
6.79	554.3	428.9	320.8	243.0	175.6	121.5	89.1
10.15	769.7	602.2	416.9	320.7	230.3	162.0	121.5
20.30	1196.6	845.0	661.5	521.1	392.9	275.4	204.1
30.44	1597.7	1154.5	881.9	689.5	525.1	365.5	273.6
61.07	2277.0	1763.9	1379.0	1090.4	833.3	589.3	441.0

1.[illegible]% POLYOX
MV SYSTEM ROT DIA= 40.08 MM BEAK DIA= 42.00 MM

ROTOR VEL., RAD/S	SHEAR STRESS, DYNES/SQ CM AT - 20.0 C	30.0 C	40.0 C	50.0 C	60.0 C	70.0 C	83.2 C
.38	10.1	0	0	0	0	0	0
.75	19.4	12.8	0	0	0	0	0
1.13	27.5	19.0	13.4	0	0	0	0
2.26	47.0	34.2	24.3	17.6	0	0	0
3.39	62.8	47.4	35.2	24.7	17.4	0	0
6.79	100.4	77.5	61.5	47.0	34.4	24.3	13.4
10.15	109.6	104.7	77.5	63.2	47.4	38.2	19.5
20.30	149.3	1[illegible].4	128.0	103.7	81.0	61.6	36.5
30.44	253.7	212.7	165.5	130.1	105.3	81.0	53.1
61.07	354.6	31[illegible].3	260.5	210.4	159.[illegible]	171.2	95.1

1.?% POLYOX
MV SYSTEM ROT DIA= [illegible] MM BEAK DIA= [illegible] MM

ROTOR VEL, RAD/S	SHEAR STRESS, DYNES/SQ CM AT – 20.0 C	30.0 C	40.0 C	50.0 C	60.0 C	70.0 C	83.2 C
.38	67.7	51.0	38.5	27.4	[illegible]	12.2	0
.75	102.1	79.4	62.4	47.0	33.2	22.7	10.1
1.13	125.4	102.1	79.4	61.4	45.4	31.6	16.2
2.26	161.4	149.0	119.9	97.2	72.5	54.3	30.6
3.39	221.9	164.7	150.7	121.5	93.1	64.7	42.9
6.79	310.7	259.2	223.5	181.4	143.9	110.2	71.7
10.18	364.6	305.7	267.3	225.2	175.6	146.1	95.6
20.36	535.1	425.0	364.3	312.7	254.3	205.0	150.7
30.54	613.0	521.1	445.0	354.5	303.7	250.0	191.2
61.07	551.9	753.6	641.4	541.2	437.0	364.6	260.6

2.4% POLYOX
MV SYSTEM ROT DIA= 40.06 MM BEAK DIA= 42.00 MM

ROTOR VEL, RAD/S	SHEAR STRESS, DYNES/SQ CM AT – 20.0 C	30.0 C	40.0 C	50.0 C	60.0 C	70.0 C	83.2 C
.38	225.0	181.4	147.4	119.9	94.0	49.6	29.2
.75	293.6	251.1	212.7	176.6	140.9	76.1	47.4
1.13	340.7	295.6	254.3	217.1	175.6	97.2	63.8
2.26	437.0	355.5	332.7	296.6	233.3	140.9	94.0
3.39	509.1	437.0	364.6	333.7	204.6	173.3	119.9
6.79	661.4	573.3	509.1	445.0	380.8	241.4	176.6
10.18	759.7	669.5	569.3	521.1	449.0	288.4	217.1
20.36	994.2	821.9	769.7	685.5	597.3	372.8	302.9
30.54	1186.6	1025.2	914.0	817.8	709.5	441.0	348.6
61.07	1603.5	1411.1	1234.7	1090.4	962.1	633.4	513.1

2.4% POLYOX (DEGRADED)
MV SYSTEM ROT DIA= 40.06 MM BEAK DIA= 42.00 MM

ROTOR VEL, RAD/S	SHEAR STRESS, DYNES/SQ CM AT – 20.0 C	30.0 C	40.0 C	50.0 C	60.0 C	70.0 C	84.0 C
.38	59.7	50.2	36.5	25.1	17.3	0	0
.75	113.4	85.9	64.8	49.4	34.8	24.3	16.2
1.13	158.7	113.4	87.5	67.2	49.6	34.6	24.3
2.26	230.0	181.4	142.6	113.4	84.2	63.2	43.7
3.39	283.6	234.9	187.9	150.7	113.4	87.5	62.4
6.79	412.9	344.6	265.1	234.9	161.4	140.9	108.5
10.18	505.1	420.9	356.8	296.6	236.5	187.5	145.8
20.36	701.5	559.3	509.1	430.3	344.6	243.3	234.9
30.54	849.9	721.5	621.4	533.2	433.9	365.6	296.6
61.07	1136.6	1010.2	865.9	753.6	605.4	533.2	437.0

APPENDIX E

LISTING OF REDUCED TEST DATA

3.0% CMC RUN NO 68 DIA= 1.384 CM
MASS F R= 106.95 G/SEC POW= 4049.5 WATTS FLUX= 3.006 WATTS/SQ CM

X, CM	TWALL TOP, C	TWALL BOT, C	TWALL, C COR	C	TBULK, C	H SH RATE, 1/SEC	W SS, D/SQCM	VIS,GK POISE
0	21.64	21.64	21.64		21.64	4.8342E 02	410.5	1.1834
7.62	36.04	37.92	40.79		21.67	9.1055E 02	410.5	1.1749
22.86	45.27	45.27	47.47		22.32	1.4428E 03	410.5	1.1548
45.72	52.00	52.30	54.23		23.00	1.7278E 03	410.5	1.1285
76.20	56.72	54.57	60.95		23.91	1.9140E 03	410.5	1.0940
121.92	65.96	66.53	68.97		25.28	1.9426E 03	410.5	1.0410
182.88	72.59	72.36	76.64		27.10	2.6366E 03	410.5	.9735
297.16	82.99	81.07	84.77		30.51	3.9022E 03	410.5	.9166

3.0% CMC RUN NO 71 DIA= 1.384 CM
MASS F R= 242.99 G/SEC POW= 6013.2 WATTS FLUX= 4.385 WATTS/SQ CM

X, CM	TWALL TOP, C	TWALL BOT, C	TWALL, C COR	C	TBULK, C	H SH RATE, 1/SEC	W SS, D/SQCM	VIS,GK POISE
0	22.19	22.19	22.19		22.19	1.0338E 03	731.5	.9507
7.62	40.47	40.39	43.71		22.34	2.1233E 03	731.5	.9466
22.86	47.66	47.66	50.77		22.64	2.5179E 03	731.5	.9380
45.72	54.33	54.39	57.34		23.06	2.7487E 03	731.5	.9261
76.20	61.14	61.09	64.11		23.68	2.9986E 03	731.5	.9042
121.92	68.00	68.04	72.19		24.57	4.3356E 03	731.5	.8798
182.88	73.71	74.54	76.03		25.76	5.7495E 03	731.5	.8476
297.16	82.79	81.04	85.62		27.99	8.3332E 03	731.5	.8157

3.0% CMC RUN NO 72 DIA= 2.680 CM
MASS F R= 109.95 G/SEC POW= 3953.2 WATTS FLUX= 1.947 WATTS/SQ CM

X, CM	TWALL TOP, C	TWALL BOT, C	TWALL, C COR	C	TBULK, C	H SH RATE, 1/SEC	W SS, D/SQCM	VIS,GK POISE
0	22.19	22.19	22.19		22.19	6.1269E 01	88.9	1.6413
7.62	39.56	39.03	40.97		22.41	1.3496E 02	88.9	1.6284
22.86	46.60	46.62	48.18		22.64	1.7346E 02	88.9	1.6016
45.72	53.47	53.57	55.15		23.49	2.1987E 02	88.9	1.5610
76.20	59.98	59.11	61.13		24.35	2.6789E 02	88.9	1.5084
121.92	67.49	65.50	68.26		25.69	3.3916E 02	88.9	1.4321
182.88	74.34	70.35	74.22		27.37	4.1583E 02	88.9	1.3327
243.84	78.69	73.87	78.87		29.10	4.8406E 02	88.9	1.2453
297.16	82.25	76.91	81.17		30.62	5.4234E 02	88.9	1.1741

3.0% CMC RUN NO 73 DIA= 2.680 CM
MASS F R= 276.02 G/SEC POW= 5428.6 WATTS FLUX= 2.124 WATTS/SQ CM

X, CM	TWALL TOP, C	TWALL BOT, C	TWALL, C COR	C	TBULK, C	H SH RATE, 1/SEC	W SS, D/SQCM	VIS,GK POISE
0	22.51	22.51	22.51		22.51	1.5753E 02	183.9	1.4170
7.62	39.88	39.23	41.63		22.63	3.4210E 02	183.9	1.4113
22.86	46.30	46.22	48.04		22.86	4.2358E 02	183.9	1.3994
45.72	52.46	53.09	54.74		23.22	5.2263E 02	183.9	1.3811
76.20	58.25	57.55	60.04		23.69	6.1247E 02	183.9	1.3570
121.92	64.94	64.48	66.84		24.40	7.5579E 02	183.9	1.3161
182.88	71.45	69.99	72.55		25.45	9.3492E 02	183.9	1.2700
243.84	73.12	75.20	73.73		26.39	1.1044E 03	183.9	1.2360
297.16	82.23	78.92	82.66		27.12	1.2334E 03	183.9	1.1884

5.4% CMC RUN NO 61 DIA= 1.324 CM
MASS F R= 48.52 G/SEC POW= 3910.1 WATTS FLUX= 2.984 WATTS/SQ CM

X, CM	TWALL TOP, C	TWALL BOT, C	TWALL, COR, C	TGULK, C	H SH RATE, 1/SEC	H SS, D/SCCM	VIS,EK POISE
0	22.10	22.10	22.10	22.10	4.35[illegible] 02	1067.0	3.7750
7.62	38.04	38.06	40.37	32.34	9.54[illegible] 02	1067.0	3.7473
22.86	45.37	45.37	47.64	22.62	1.20[illegible] 03	1067.0	3.6797
45.72	51.93	51.93	54.08	25.53	1.63718 03	1067.0	3.5337
76.20	58.47	58.53	60.59	24.49	2.09811 03	1067.0	3.4613
121.92	65.92	66.03	68.74	25.93	3.16[illegible]E 03	1067.0	3.3060
182.88	72.53	73.32	75.65	27.83	4.64[illegible] 03	1067.0	3.1946
297.18	82.10	82.22	85.21	31.41	5.49[illegible] 03	1067.0	2.9050

5.4% CMC RUN NO 62 DIA= 1.324 CM
MASS F R= 267.90 G/SEC POW= 6601.6 WATTS FLUX= 5.001 WATTS/SQ CM

X, CM	TWALL TOP, C	TWALL BOT, C	TWALL, COR, C	TGULK, C	H SH RATE, 1/SEC	H SS, D/SCCM	VIS,EK POISE
0	21.30	21.30	21.30	21.30	1.20[illegible] 03	1990.4	2.7666
7.62	33.89	33.72	43.25	21.45	2.37[illegible] 03	1990.4	2.7550
22.86	47.36	47.36	50.89	21.74	3.76[illegible] 03	1990.4	2.7305
45.72	54.20	54.20	57.41	22.19	4.65[illegible] 03	1990.4	2.6931
76.20	60.31	60.99	64.18	22.78	6.25[illegible] 03	1990.4	2.6437
121.92	67.72	68.65	72.33	23.67	8.39[illegible] 03	1990.4	2.5704
182.88	73.64	74.93	78.31	24.65	1.08[illegible] 04	1990.4	2.4703
297.18	82.75	81.66	86.34	27.07	1.39[illegible] 04	1990.4	2.3799

5.4% CMC RUN NO 63 DIA= 2.660 CM
MASS F R= 102.74 G/SEC POW= 3681.4 WATTS FLUX= 1.440 WATTS/SQ CM

X, CM	TWALL TOP, C	TWALL BOT, C	TWALL, COR, C	TGULK, C	H SH RATE, 1/SEC	H SS, D/SCCM	VIS,EK POISE
0	21.35	21.35	21.35	21.35	6.11[illegible]E 01	305.3	7.0109
7.62	37.52	37.30	39.09	21.57	1.4444E 02	305.3	6.9570
22.86	44.39	44.56	45.95	22.00	1.8790E 02	305.3	6.8455
45.72	50.40	51.31	52.65	22.64	2.4476E 02	305.3	6.6420
76.20	56.93	56.84	58.38	23.50	3.1023E 02	305.3	6.4232
121.92	63.52	63.69	65.30	24.79	4.2983E 02	305.3	6.1064
182.88	70.95	69.94	71.87	26.51	5.6881E 02	305.3	5.7094
243.84	77.62	75.58	78.15	28.24	6.9957E 02	305.3	5.3445
297.18	82.16	79.42	82.41	29.75	8.0291E 02	305.3	5.0470

5.4% CMC RUN NO 64 DIA= 2.660 CM
MASS F R= 283.80 G/SEC POW= 5703.5 WATTS FLUX= 2.740 WATTS/SQ CM

X, CM	TWALL TOP, C	TWALL BOT, C	TWALL, COR, C	TGULK, C	H SH RATE, 1/SEC	H SS, D/SCCM	VIS,EK POISE
0	21.30	21.30	21.30	21.30	1.70[illegible] 02	801.1	5.2028
7.62	38.22	38.46	41.04	21.42	4.03[illegible] 02	801.1	5.2016
22.86	45.48	45.79	47.62	21.66	5.24[illegible] 02	801.1	5.1875
45.72	52.03	52.61	54.52	22.03	6.90[illegible] 02	801.1	5.0898
76.20	57.37	57.84	59.88	22.51	8.87210 02	801.1	4.9792
121.92	64.57	64.87	66.94	23.24	1.24[illegible] 03	801.1	4.8473
182.88	70.90	70.81	72.70	24.21	1.63[illegible] 03	801.1	4.6706
243.84	77.60	76.84	79.26	25.18	1.90[illegible] 03	801.1	4.5143
297.18	81.67	81.90	83.72	26.13	2.28[illegible] 03	801.1	4.3773

1.0% POL RUN NO 89 DIA= 1.384 CM
MASS F R= 101.47 G/SEC POW= 3529.4 WATTS FLUX= 2.977 WATTS/SQ CM

X, CM	TWALL TOP, C	TWALL BOT, C	TWALL, COR, C	TBULK, C	W SH RATE, 1/SEC	W SS, D/SQCM	VIS,BK POISE
0	22.00	22.00	22.00	22.00	4.93041 02	100.0	.6282
7.62	38.50	38.73	41.90	22.23	5.43038 02	100.0	.6245
22.86	45.87	45.87	48.24	22.70	1.09578 03	100.0	.6170
45.72	52.26	52.26	54.51	23.40	1.36689 03	100.0	.6057
76.20	58.34	58.64	60.93	24.33	1.70394 03	100.0	.5938
121.92	66.15	66.55	68.95	25.72	2.27228 03	100.0	.5690
182.88	72.92	72.60	75.47	27.58	2.80358 03	100.0	.5386
297.18	82.75	80.62	84.35	31.07	3.69408 03	100.0	.5129

1.0% POL RUN NO 90 DIA= 1.384 CM
MASS F R= 202.32 G/SEC POW= 5959.9 WATTS FLUX= 4.919 WATTS/SQ CM

X, CM	TWALL TOP, C	TWALL BOT, C	TWALL, COR, C	TBULK, C	W SH RATE, 1/SEC	W SS, D/SQCM	VIS,BK POISE
0	21.75	21.75	21.75	21.75	1.25444E 03	342.8	.4524
7.62	40.71	41.03	44.27	21.88	2.39555E 03	342.8	.4511
22.86	47.35	47.65	51.15	22.13	3.14928E 03	342.8	.4484
45.72	54.02	54.02	56.95	22.51	3.75208E 03	342.8	.4444
76.20	60.75	60.34	63.44	23.02	4.61225E 03	342.8	.4389
121.92	67.53	66.53	71.67	23.78	5.97055E 03	342.8	.4308
182.88	73.71	74.31	77.08	24.79	6.91438E 03	342.8	.4203
297.18	82.97	81.15	85.75	26.70	8.35159E 03	342.8	.4100

1.0% POL RUN NO 91 DIA= 2.660 CM
MASS F R= 101.83 G/SEC POW= 4426.8 WATTS FLUX= 1.732 WATTS/SQ CM

X, CM	TWALL TOP, C	TWALL BOT, C	TWALL, COR, C	TBULK, C	W SH RATE, 1/SEC	W SS, D/SQCM	VIS,BK POISE
0	21.50	21.50	21.50	21.50	5.82220E 01	49.3	1.0061
7.62	41.19	40.59	42.75	21.76	1.31388E 02	49.3	.9956
22.86	48.56	48.58	50.34	22.28	1.70650E 02	49.3	.9782
45.72	56.03	55.77	57.62	22.07	2.23402E 02	49.3	.9518
76.20	62.64	61.11	63.91	24.11	2.79503E 02	49.3	.9146
121.92	70.59	66.36	70.59	25.66	3.64402E 02	49.3	.8620
182.88	76.28	70.01	75.44	27.77	4.46095E 02	49.3	.7985
243.84	80.38	72.47	78.84	29.66	5.18988E 02	49.3	.7401
297.18	82.47	73.95	80.63	31.69	5.61543E 02	49.3	.6918

1.0% POL RUN NO 92 DIA= 2.660 CM
MASS F R= 202.32 G/SEC POW= 5077.0 WATTS FLUX= 2.300 WATTS/SQ CM

X, CM	TWALL TOP, C	TWALL BOT, C	TWALL, COR, C	TBULK, C	W SH RATE, 1/SEC	W SS, D/SQCM	VIS,BK POISE
0	21.95	21.95	21.95	21.95	1.68960E 02	100.6	.8137
7.62	40.68	40.26	42.80	22.08	3.62381E 02	100.6	.8109
22.86	47.02	47.43	49.45	22.33	4.39533E 02	100.6	.8050
45.72	53.63	54.06	56.16	22.70	5.42398E 02	100.6	.7960
76.20	59.49	58.97	61.45	23.20	6.93006E 02	100.6	.7841
121.92	66.18	65.24	68.13	23.95	8.99156E 02	100.6	.7670
182.88	72.40	70.26	73.48	24.98	1.13973E 03	100.6	.7402
243.84	76.86	74.84	79.23	25.95	1.37588E 03	100.6	.7156
297.18	82.67	78.35	82.75	26.82	1.58121E 03	100.6	.6972

1.6% POL RUN NO 94 DIA= 1.384 CM
MASS F R= 101.24 G/SEC POW= 3907.7 WATTS FLUX= 2.960 WATTS/SQ CM

X, CM	TWALL TOP, C	TWALL BOT, C	TWALL, COR, C	TBULK, C	W SH RATE, 1/SEC	W SS, D/SCCM	VIS,EK POISE
0	21.70	21.70	21.70	21.70	4.69[illegible] 02	499.7	2.4901
7.62	38.36	38.36	40.03	21.93	9.[illegible] 02	499.7	2.4791
22.86	45.54	45.54	47.91	22.40	1.17[illegible] 03	499.7	2.4562
45.72	51.93	51.93	54.17	23.09	1.94[illegible] 03	499.7	2.4219
76.20	58.37	58.39	60.65	24.02	2.87[illegible] 03	499.7	2.3769
121.92	65.64	66.42	68.61	25.41	4.04[illegible] 03	499.7	2.3133
182.88	72.31	72.82	75.12	27.27	5.37[illegible] 03	499.7	2.2278
297.16	82.70	81.89	84.83	30.74	4.39[illegible] 03	499.7	2.1459

1.6% POL RUN NO 95 DIA= 1.384 CM
MASS F R= 276.57 G/SEC POW= 5900.6 WATTS FLUX= 4.470 WATTS/SQ CM

X, CM	TWALL TOP, C	TWALL BOT, C	TWALL, COR, C	TBULK, C	W SH RATE, 1/SEC	W SS, D/SCCM	VIS,EK POISE
0	22.15	22.15	22.15	22.15	1.30[illegible] 03	913.7	1.5129
7.62	40.83	40.76	44.19	22.28	2.96[illegible] 03	818.7	1.5191
22.86	47.66	47.66	50.85	22.53	3.83[illegible] 03	818.7	1.5029
45.72	54.09	54.09	56.96	22.91	5.00[illegible] 03	818.7	1.4909
76.20	60.66	60.69	63.48	23.42	5.95[illegible] 03	818.7	1.4749
121.92	67.70	68.92	71.60	24.18	6.39[illegible] 03	818.7	1.4539
182.88	73.94	74.94	77.87	25.20	6.12[illegible] 03	818.7	1.4226
297.16	83.12	82.39	85.32	27.11	1.1104E 04	818.7	1.3958

1.6% POL RUN NO 96 DIA= 2.680 CM
MASS F R= 102.88 G/SEC POW= 3834.8 WATTS FLUX= 1.501 WATTS/SQ CM

X, CM	TWALL TOP, C	TWALL BOT, C	TWALL, COR, C	TBULK, C	W SH RATE, 1/SEC	W SS, D/SCCM	VIS,EK POISE
0	22.35	22.35	22.35	22.35	6.6[illegible]E 01	195.6	5.3684
7.62	39.00	38.55	40.38	22.57	1.30[illegible] 02	195.6	5.3646
22.86	45.48	45.68	47.14	23.02	1.66[illegible]E 02	195.6	5.3035
45.72	51.62	52.20	53.57	23.69	2.10[illegible] 02	195.6	5.2153
76.20	57.61	57.54	59.14	24.59	2.75[illegible] 02	195.6	5.1054
121.92	64.36	64.16	65.94	25.93	3.59[illegible] 02	195.6	4.9488
182.88	71.27	70.44	72.35	27.72	4.67[illegible] 02	195.6	4.7429
243.84	77.91	76.16	78.66	29.52	6.15[illegible] 02	195.6	4.5501
297.16	82.56	80.36	83.07	31.09	7.4461E 02	195.6	4.3618

1.6% POL RUN NO 97 DIA= 2.680 CM
MASS F R= 250.60 G/SEC POW= 5993.3 WATTS FLUX= 2.345 WATTS/SQ CM

X, CM	TWALL TOP, C	TWALL BOT, C	TWALL, COR, C	TBULK, C	W SH RATE, 1/SEC	W SS, D/SCCM	VIS,EK POISE
0	22.15	22.15	22.15	22.15	1.[illegible]E 02	317.1	3.7253
7.62	40.55	40.11	42.83	22.28	3.87[illegible] 02	317.1	3.7153
22.86	47.09	47.33	49.37	22.53	4.77[illegible] 02	317.1	3.6945
45.72	53.52	54.20	56.16	22.92	6.52[illegible] 02	317.1	3.6625
76.20	59.19	59.39	61.49	23.43	8.14[illegible] 02	317.1	3.6202
121.92	65.67	66.42	68.47	24.20	1.0102E 03	317.1	3.5571
182.88	71.47	72.12	73.82	25.23	1.24[illegible] 03	317.1	3.4750
243.84	77.76	76.02	78.80	26.28	1.40[illegible] 03	317.1	3.3962
297.16	81.98	83.17	84.56	27.15	1.53[illegible] 03	317.1	3.3222

2.4% POL RUN NO 98 DIA= 1.384 CM
MASS F R= 103.19 G/SEC POW= 3946.4 WATTS FLUX= 2.992 WATTS/SQ CM

X, CM	TWALL TOP, C	TWALL BOT, C	TWALL, C COR, C	TBULK, C	H SH RATE, 1/SEC	H SS, D/SCCM	VIS,EK POISE
0	22.45	22.45	22.45	22.45	5.4[illegible]E 02	1017.0	10.2480
7.62	38.71	38.76	41.66	22.66	9.82[illegible]E 02	1017.0	9.3469
22.86	45.96	45.96	46.32	23.14	1.1630E 03	1017.0	9.5204
45.72	52.29	52.29	54.52	23.83	1.4235E 03	1017.0	9.3600
76.20	58.70	58.91	60.82	24.77	1.7233E 03	1017.0	8.9158
121.92	65.96	66.31	68.96	26.13	4.7570E 03	1017.0	7.8171
182.88	72.55	73.32	75.40	27.97	5.6[illegible]E 03	1017.0	7.2903
297.18	83.21	82.81	85.45	31.42	7.0[illegible]E 03	1017.0	6.8194

2.4% POL RUN NO 99 DIA= 1.384 CM
MASS F R= 264.09 G/SEC POW= 5906.2 WATTS FLUX= 4.474 WATTS/SQ CM

X, CM	TWALL TOP, C	TWALL BOT, C	TWALL, C COR, C	TBULK, C	H SH RATE, 1/SEC	H SS, D/SCCM	VIS,EK POISE
0	21.80	21.90	21.80	21.90	1.4399E 03	1562.6	6.7700
7.62	40.50	40.39	43.73	22.02	2.9941E 03	1562.6	6.5174
22.86	47.45	47.45	50.65	22.27	3.4[illegible]E 03	1562.6	6.3215
45.72	53.78	53.75	56.73	22.65	4.2440E 03	1562.6	5.9490
76.20	60.21	60.34	63.06	23.15	5.[illegible]E 03	1562.6	5.5947
121.92	67.20	68.49	71.33	23.90	1.5231E 04	1562.6	5.1171
182.88	73.30	74.49	77.46	24.90	1.6[illegible]E 04	1562.6	4.7350
297.18	82.72	82.15	85.98	26.77	1.7809E 04	1562.6	4.4642

2.4% POL RUN NO 100 DIA= 2.680 CM
MASS F R= 102.51 G/SEC POW= 3909.4 WATTS FLUX= 1.530 WATTS/SQ CM

X, CM	TWALL TOP, C	TWALL BOT, C	TWALL, C COR, C	TBULK, C	H SH RATE, 1/SEC	H SS, D/SCCM	VIS,EK POISE
0	22.15	22.15	22.15	22.15	7.[illegible]E 01	484.3	28.9471
7.62	38.92	38.41	40.28	22.38	1.4913E 02	484.3	28.2110
22.86	45.29	45.56	46.99	22.64	1.8593E 02	484.3	26.8063
45.72	51.66	52.20	53.57	23.52	2.3353E 02	484.3	25.0701
76.20	57.37	57.61	59.04	24.44	2.[illegible]E 02	484.3	23.2130
121.92	64.01	64.73	66.04	25.82	3.[illegible]E 02	484.3	21.0760
182.88	70.45	71.10	72.27	27.65	5.7360E 02	484.3	19.0035
243.84	77.13	77.40	78.65	29.48	1.1980E 03	484.3	17.4367
297.18	82.09	82.73	83.87	31.09	1.4111E 03	484.3	16.5615

2.4% POL RUN NO 101 DIA= 2.680 CM
MASS F R= 275.47 G/SEC POW= 5927.6 WATTS FLUX= 2.320 WATTS/SQ CM

X, CM	TWALL TOP, C	TWALL BOT, C	TWALL, C COR, C	TBULK, C	H SH RATE, 1/SEC	H SS, D/SCCM	VIS,EK POISE
0	22.25	22.25	22.25	22.25	2.0000E 02	696.0	17.9440
7.62	40.73	39.97	42.64	22.38	4.1209E 02	696.0	17.6537
22.86	46.86	47.21	49.25	22.64	4.9374E 02	696.0	17.0976
45.72	53.33	54.04	55.99	23.03	6.1752E 02	696.0	16.3518
76.20	58.38	59.29	61.25	23.54	7.0956E 02	696.0	15.5276
121.92	65.54	66.31	68.24	24.32	1.7575E 03	696.0	14.5502
182.88	71.51	72.16	73.89	25.35	2.3427E 03	696.0	13.5708
243.84	78.23	79.56	80.34	26.39	2.7951E 03	696.0	12.8009
297.18	82.82	83.40	85.13	27.29	3.1613E 03	696.0	12.2603

2.4% POL(D) RUN NO 102 DIA= 1.364 CM
MASS F R= 271.07 G/SEC POW= 3020.8 WATTS FLUX= 2.220 WATTS/SQ CM

X, CM	TWALL TOP, C	TWALL BOT, C	TWALL, COR, C	TBULK, C	W SH RATE, 1/SEC	W SS, D/SCCM	VIS,BK POISE
0	21.69	21.68	20.68	21.68	1.[illegible] 03	1105.4	1.9820
7.62	30.87	30.64	32.36	20.95	1.47[illegible] 03	1105.4	1.9794
22.86	34.96	34.96	36.59	21.08	2.10[illegible] 03	1105.4	1.9739
45.72	38.91	38.91	40.45	21.28	2.94[illegible] 03	1105.4	1.9654
76.20	42.69	42.75	44.19	21.55	3.97[illegible] 03	1105.4	1.9540
121.92	46.82	47.63	49.01	21.95	5.59[illegible] 03	1105.4	1.9366
182.88	50.53	51.15	52.70	22.49	7.81[illegible] 03	1105.4	1.9110
297.18	55.87	56.66	57.62	23.49	3.7[illegible] 03	1105.4	1.8885

2.4% POL(D) RUN NO 103 DIA= 2.680 CM
MASS F R= 277.69 G/SEC POW= 3019.9 WATTS FLUX= 1.182 WATTS/SQ CM

X, CM	TWALL TOP, C	TWALL BOT, C	TWALL, COR, C	TBULK, C	W SH RATE, 1/SEC	W SS, D/SCCM	VIS,BK POISE
0	21.38	21.35	21.36	21.36	1.82[illegible] 02	430.9	4.3860
7.62	31.25	30.94	32.24	21.45	2.69[illegible] 02	430.9	4.3792
22.86	35.06	35.25	36.27	21.59	3.05[illegible] 02	430.9	4.3565
45.72	38.87	39.37	40.27	21.77	3.45[illegible] 02	430.9	4.3347
76.20	42.20	42.56	43.49	22.03	3.84[illegible] 02	430.9	4.3057
121.92	46.01	46.80	47.50	22.42	4.37[illegible] 02	430.9	4.2621
182.88	49.49	50.33	50.97	22.95	4.91[illegible] 02	430.9	4.2048
243.84	52.30	53.78	54.40	23.47	5.69[illegible] 02	430.9	4.1390
297.18	55.38	56.40	56.95	23.93	6.27[illegible] 02	430.9	4.0908

2.4% POL(D) RUN NO 104 DIA= 1.364 CM
MASS F R= 405.02 G/SEC POW= 6040.1 WATTS FLUX= 4.676 WATTS/SQ CM

X, CM	TWALL TOP, C	TWALL BOT, C	TWALL, COR, C	TBULK, C	W SH RATE, 1/SEC	W SS, D/SCCM	VIS,BK POISE
0	21.45	21.45	21.45	21.45	1.96[illegible] 03	1337.4	1.6224
7.62	38.25	37.99	41.35	21.54	3.60[illegible] 03	1337.4	1.6196
22.86	44.42	44.42	47.41	21.72	4.07[illegible] 03	1337.4	1.6136
45.72	50.31	50.31	53.07	21.99	4.69[illegible] 03	1337.4	1.6045
76.20	56.41	56.40	59.11	22.35	5.54[illegible] 03	1337.4	1.5922
121.92	62.75	63.88	66.79	22.88	6.51[illegible] 03	1337.4	1.5738
182.88	68.13	69.16	72.23	23.60	7.16[illegible] 03	1337.4	1.5497
297.18	76.21	75.49	79.41	24.94	7.92[illegible] 03	1337.4	1.5230

2.4% POL(D) RUN NO 105 DIA= 1.364 CM
MASS F R= 405.02 G/SEC POW= 6014.9 WATTS FLUX= 5.338 WATTS/SQ CM

X, CM	TWALL TOP, C	TWALL BOT, C	TWALL, COR, C	TBULK, C	W SH RATE, 1/SEC	W SS, D/SCCM	VIS,BK POISE
0	21.65	21.65	21.65	21.65	1.96[illegible] 03	1332.7	1.6163
7.62	40.57	40.27	44.12	21.75	3.79[illegible] 03	1332.7	1.6130
22.86	47.39	47.36	50.80	21.96	4.34[illegible] 03	1332.7	1.6062
45.72	53.97	53.97	57.07	22.27	5.21[illegible] 03	1332.7	1.5958
76.20	60.75	60.74	63.85	22.68	6.11[illegible] 03	1332.7	1.5789
121.92	67.77	69.08	72.34	23.29	7.13[illegible] 03	1332.7	1.5581
182.88	73.66	74.96	78.29	24.11	7.78[illegible] 03	1332.7	1.5308
297.18	80.12	82.22	86.03	25.65	8.64[illegible] 03	1332.7	1.5040

2.4% POL(C) RUN NO 107 DIA= 2.000 CM
MASS F R= 416.13 G/SEC POW= 6017.4 WATTS FLUX= 2.359 WATTS/SQ CM

X, CM	TWALL TOP, C	TWALL BOT, C	TWALL, COR, C	TBULK, C	W SH RATE, 1/SEC	W SS, D/SEC CM	VIS,EK POISE
0	22.15	22.15	22.15	22.15	2.77[illegible] 02	521.2	3.7150
7.62	38.38	37.95	40.74	22.24	5.17[illegible] 02	521.2	3.7078
22.86	44.25	44.47	46.44	22.43	8.16838E 02	521.2	3.6927
45.72	50.29	50.79	52.73	22.67	7.[illegible] 02	521.2	3.6693
76.20	55.46	55.45	57.47	23.02	9.[illegible] 02	521.2	3.6301
121.92	61.40	61.99	64.32	23.54	1.12599E 03	521.2	3.5836
182.88	66.57	66.97	68.62	24.23	1.[illegible] 03	521.2	3.5227
243.84	72.24	72.33	74.31	24.93	1.46316E 03	521.2	3.4566
297.18	75.68	76.67	78.20	25.54	1.61135E 03	521.2	3.4062

2.4% POL(C) RUN NO 108 DIA= 2.000 CM
MASS F R= 416.13 G/SEC POW= 6939.5 WATTS FLUX= 2.716 WATTS/SQ CM

X, CM	TWALL TOP, C	TWALL BOT, C	TWALL, COR, C	TBULK, C	W SH RATE, 1/SEC	W SS, D/SEC CM	VIS,EK POISE
0	22.15	22.15	22.15	22.15	2.76633E 02	520.7	3.7122
7.62	41.12	40.04	43.21	22.25	5.59295E 02	520.7	3.7039
22.86	47.05	47.29	49.53	22.49	8.76338E 02	520.7	3.6884
45.72	53.78	54.34	56.60	22.75	1.[illegible] 03	520.7	3.6598
76.20	59.52	59.45	61.63	23.15	1.05316E 03	520.7	3.6239
121.92	66.11	66.56	69.01	23.75	1.27699E 03	520.7	3.5626
182.88	71.86	72.21	74.12	24.55	1.45944E 03	520.7	3.4930
243.84	78.34	78.25	80.47	25.36	1.70055E 03	520.7	3.4190
297.18	82.34	83.40	85.14	26.06	1.90245E 03	520.7	3.3618

APPENDIX F

LISTING OF PARAMETERS

RUN NO 68 RE= 53.13 GR= 3.[illegible]E-04

X/D	GZ	NU	DELTA	PRW	PRB	GR*W	GR*B
0	0	0	1.054	534.9	824.5	0E 00	0E 00
5.50	3772.9	36.455	2.212	299.[illegible]	81[illegible].8	5.3[illegible]3E 03	2.9[illegible]91E 02
16.51	3253.5	26.015	2.772	233.4	[illegible]	5.754[illegible]E 03	[illegible].1839E 02
33.03	1523.5	21.055	3.22[illegible]	222.2	753.1	3.4[illegible]E 03	3.4[illegible]E 02
55.05	971.6	17.550	3.689	176.1	757.2	1.1642E 04	3.7465E 02
88.07	665.8	14.753	4.716	135.9	717.9	2.6[illegible]E 04	4.3431E 02
132.11	481.5	13.111	6.390	97.6	671.5	4.6[illegible]E 04	5.2161E 02
214.65	244.6	11.636	9.429	65.5	625.4	9.2365E 04	6.5259E 02

RUN NO 71 RE= 235.10 GR= 1.5727E-03

X/D	GZ	NU	DELTA	PRW	PRB	GR*W	GR*B
0	0	0	1.105	432.2	661.3	0E 00	0E 00
5.50	22172.2	46.635	2.276	227.5	658.1	3.8[illegible]E 03	6.9[illegible]E 02
16.51	7364.4	34.559	2.592	189.5	651.7	1.3663E 04	7.2056E 02
33.03	3667.5	28.351	2.939	171.5	641.5	1.7517E 04	7.5443E 02
55.05	2266.5	23.750	3.205	155.5	627.0	2.217[illegible]E 04	8.0553E 02
88.07	1577.1	19.550	4.032	106.5	607.9	4.9351E 04	8.6114E 02
132.11	915.6	16.026	6.192	79.1	583.5	5.1793E 04	9.8928E 02
214.65	559.6	16.216	5.695	54.6	555.4	1.5657E 05	1.1451E 03

RUN NO 72 RE= 31.63 GR= 1.7616E-04

X/D	GZ	NU	DELTA	PRW	PRB	GR*W	GR*B
0	0	0	1.050	1009.0	1141.7	0E 00	0E 00
2.64	10030.8	35.564	2.314	437.3	1132.0	1.1072E 04	1.1305E 03
5.53	3339.5	25.625	2.973	335.4	1112.0	2.0318E 04	1.1865E 03
17.66	1866.7	20.240	3.766	261.4	1081.8	3.5408E 04	1.2831E 03
25.44	997.6	17.252	4.565	212.6	1042.8	5.5595E 04	1.4165E 03
45.50	621.5	14.721	5.609	166.2	966.6	9.4613E 04	1.6451E 03
66.25	412.3	13.265	7.114	134.6	913.6	1.4803E 05	2.0056E 03
91.66	307.2	12.454	5.295	114.[illegible]	850.1	2.0552E 05	2.4135E 03
110.90	251.6	12.216	6.934	106.5	750.4	2.4514E 05	2.5252E 03

RUN NO 73 RE= 92.55 GR= 6.9627E-04

X/D	GZ	NU	DELTA	PRW	PRB	GR*W	GR*B
0	0	0	1.078	609.9	954.5	0E 00	0E 00
2.64	25164.4	47.507	2.336	356.5	980.5	2.3075E 04	2.0851E 03
5.53	8362.5	35.092	2.694	264.2	971.5	3.8825E 04	2.1465E 03
17.66	4167.0	27.899	3.555	227.6	957.9	6.5930E 04	2.2261E 03
25.44	2565.6	24.600	4.151	192.7	939.8	9.2400E 04	2.3456E 03
45.50	1564.9	20.049	5.150	154.6	909.7	1.4526E 05	2.5632E 03
66.25	1043.6	18.101	6.600	134.1	875.6	2.0649E 05	2.8463E 03
91.66	773.4	16.267	7.945	98.5	843.1	3.6553E 05	3.1479E 03
110.90	637.3	15.236	5.097	86.0	813.4	5.1542E 05	3.4545E 03

RUN NO 61 RE= 24.00 BR= [illegible]

X/D	GZ	NU	DELTA	PRW	PRB	GR*W	GR*B
0	0	0	1.14?	1703.?	[illegible]	0E 00	0E 00
5.50	6353.7	30.215	2.?21	71?.?	[illegible]	[illegible]347E 02	[illegible]942E 01
10.01	2592.5	25.017	[illegible]	[illegible]	[illegible]	1.[illegible]E 03	3.[illegible]E 01
33.03	1?53.2	20.003	4.[illegible]	4[illegible]	[illegible].2	1.5[illegible]E 03	3.70[illegible]E 01
55.05	593.5	17.410	5.50-	327.?	2[illegible]5.9	3.165[illegible]E 03	3.690[illegible]E 01
85.07	550.3	14.494	9.325	210.9	227[illegible]	7.[illegible]21[illegible]E 03	4.2491E 01
132.11	[illegible]69.0	12.?57	10.?40	10[illegible]	[illegible].4	1.[illegible]07E 04	5.14[illegible]E 01
214.03	225.0	11.305	14.335	121.5	1571.5	2.[illegible]E 04	[illegible]4215E 01

RUN NO 62 RE= 39.00 BR= 4.[illegible]E-03

X/D	GZ	NU	DELTA	PRW	PRB	GR*W	GR*B
0	0	0	1.173	1145.4	1929.5	0E 00	0E 00
5.50	24?07.8	50.?3?	2.[illegible]	442.2	[illegible]	2.[illegible]E 03	[illegible]73[illegible]E 01
10.01	5102.?	37.?7?	3.05?	34?.?	19?1.?	4.[illegible]E 03	[illegible]E 01
33.03	4075.9	30.273	4.517	275.4	1873.3	7.4[illegible]E 03	9.430[illegible]E 01
55.05	2441.4	25.471	5.[illegible]	2[illegible]	1[illegible]	1.[illegible]E 04	1.0[illegible]E 02
85.07	1522.0	21.415	8.72?	135.?	1750.5	3.1[illegible]E 04	1.[illegible]E 02
132.11	1011.3	19.343	10.559	114.5	1705.5	4.6151E 04	1.2392E 02
214.03	[illegible]13.0	17.298	13.492	[illegible]	1033.2	5.2727E 04	1.4349E 02

RUN NO 63 RE= 6.90 BR= 5.3159E-04

X/D	GZ	NU	DELTA	PRW	PRB	GR*W	GR*B
0	0	0	1.123	3479.3	4858.7	0E 00	0E 00
2.84	9395.7	35.160	2.650	1409.4	4646.0	9.6967E 02	5.5675E 01
8.53	3126.0	25.352	3.447	1006.3	4704.4	1.0257E 03	5.8556E 01
17.06	1561.1	19.575	4.490	810.1	4614.1	3.3652E 03	6.3857E 01
28.44	934.4	17.014	5.690	633.1	4451.3	5.7451E 03	7.0594E 01
45.50	561.9	14.464	7.681	492.2	4216.4	1.1735E 04	8.1846E 01
68.25	360.1	12.615	10.424	330.0	3923.9	2.1611E 04	9.9099E 01
91.00	265.3	11.153	12.522	273.3	3650.4	3.4159E 04	1.1905E 02
119.50	205.0	10.597	14.701	237.0	3459.5	4.6150E 04	1.3916E 02

RUN NO 64 RE= 25.75 BR= 2.5533E-03

X/D	GZ	NU	DELTA	PRW	PRB	GR*W	GR*B
0	0	0	1.137	2452.3	3642.4	0E 00	0E 00
2.84	25937.3	48.619	2.717	970.8	3626.3	3.2163E 03	1.5392E 02
8.53	8639.0	36.250	3.437	751.1	3595.0	5.0370E 03	1.5620E 02
17.06	4318.0	28.590	4.531	565.5	3542.1	1.0[illegible]E 04	1.[illegible]E 02
28.44	2590.5	24.05?	[illegible]	45[illegible]	34[illegible].3	1.7[illegible]E 04	1.75[illegible]E 02
45.50	1612.0	20.[illegible]	5.[illegible]	30[illegible].2	[illegible]1.7	[illegible]E 04	1.9[illegible]7E 02
68.25	1072.1	18.[illegible]	1[illegible]	2[illegible]	[illegible]	[illegible]E 04	2.1[illegible]E 02
91.00	801.9	16.555	13.[illegible]	191.3	3113.3	1.06[illegible]E 05	2.[illegible]E 02
119.50	605.5	15.44?	15.[illegible]1	155.5	3012.3	1.4525E 05	2.5517E 02

RUN NO 89 RE= 143.97 GR= 1.[illegible]E-[illegible]

X/D	GZ	NU	DELTA	PRW	PRB	GR*W	GR*B
0	0	0	1.1[illegible]	257.0	457.2	0E 00	0E 00
5.50	9201.6	34.511	2.159	148.4	[illegible]	1.3[illegible]E 04	1.0456E 03
16.51	3063.1	[illegible]	[illegible]	111.1	[illegible]	[illegible] 04	1.0[illegible] 03
33.03	1506.5	[illegible]	3.497	[illegible]	[illegible]	4.[illegible]E 04	1.16[illegible] 03
55.05	928.7	17.236	4.392	70.1	405.5	7.[illegible] 04	1.2[illegible] 03
88.07	573.2	14.412	5.510	51.6	391.9	1.35[illegible]E 05	1.4315E 03
132.11	360.2	12.[illegible]	7.136	41.[illegible]	[illegible]	[illegible] 05	1.[illegible]924E 03
214.65	251.5	11.476	9.434	31.4	[illegible]	3.[illegible]E 05	2.0523E 03

RUN NO 90 RE= 574.00 GR= 8.1[illegible]E-04

X/D	GZ	NU	DELTA	PRW	PRB	GR*W	GR*B
0	0	0	1.104	186.5	315.1	0E 00	0E 00
5.50	25795.1	44.[illegible]	2.165	96.0	314.1	4.[illegible]E 04	2.99[illegible]E 03
16.51	8552.1	35.541	2.695	71.0	312.0	9.[illegible]E 04	3.0[illegible]E 03
33.03	4291.3	27.944	3.453	56.[illegible]	308.8	1.4[illegible]E 05	3.1[illegible]E 03
55.05	2571.1	23.579	4.244	47.[illegible]	304.6	2.3[illegible]E 05	3.31[illegible]E 03
88.07	1603.5	19.[illegible]	5.453	38.2	298.3	4.2[illegible]E 05	3.[illegible]E 03
132.11	1056.0	17.004	6.360	31.1	290.2	5.6551E 05	3.8501E 03
214.65	652.6	15.053	7.675	25.[illegible]	281.7	9.0[illegible]E 05	4.3[illegible]E 03

RUN NO 91 RE= 46.00 GR= 8.5436E-05

X/D	GZ	NU	DELTA	PRW	PRB	GR*W	GR*B
0	0	0	1.079	589.9	702.6	0E 00	0E 00
2.04	9307.4	35.023	2.441	247.2	696.2	3.9641E 04	3.2708E 03
6.53	3057.6	25.506	3.155	166.3	680.2	7.3592E 04	3.4905E 03
17.06	1545.4	20.560	4.134	142.0	660.4	1.3079E 05	3.6032E 03
28.44	924.5	17.774	5.172	112.5	632.5	2.2644E 05	4.2831E 03
45.50	575.3	15.430	6.732	85.6	593.8	4.0565E 05	5.0950E 03
68.25	351.4	14.595	8.251	65.3	547.0	5.5152E 05	6.3259E 03
91.00	284.5	14.146	9.507	55.5	504.2	[illegible] 05	7.6[illegible]E 03
113.98	232.4	14.161	10.357	54.5	469.1	1.[illegible]E 06	9.3554E 03

RUN NO 92 RE= 164.50 GR= 4.7740E-04

X/D	GZ	NU	DELTA	PRW	PRB	GR*W	GR*B
0	0	0	1.126	414.5	508.4	0E 00	0E 00
2.04	25750.3	47.097	2.419	183.7	504.2	9.5348E 04	6.6860E 03
6.53	3567.2	35.506	2.910	150.[illegible]	559.6	1.5120E 05	6.8537E 03
17.06	4269.0	28.429	3.754	115.[illegible]	552.9	2.7155E 05	7.1161E 03
28.44	2583.7	24.[illegible]	4.[illegible]	93.4	543.9	4.[illegible]E 05	7.4761E 03
45.50	1562.7	21.[illegible]	6.[illegible]	71.[illegible]	[illegible]	7.[illegible] 05	8.1[illegible] 03
68.25	1085.5	19.[illegible]	7.404	57.1	[illegible]	1.[illegible] 06	8.94[illegible] 03
91.00	790.5	17.[illegible]	9.243	45.[illegible]	492.5	1.[illegible] 06	9.6949E 03
113.98	652.4	16.[illegible]	10.544	39.7	476.5	2.6375E 06	1.0715E 04

RUN NO 94 RE= 37.40 BR= [illegible]

X/D	GZ	NU	DELTA	PRW	PRB	GR*W	GR*B
0	0	0	1.2[illegible]	[illegible]	1734.5	0E 00	0E 00
5.[illegible]	9245.0	64.742	2.441	349.1	1725.7	2.[illegible]13E 03	6.5150E 01
16.51	5576.5	29.174	3.013	276.5	[illegible]	3.99[illegible]E 03	6.7676E 01
33.03	1566.4	20.422	3.571	235.2	1580.8	7.4614E 03	7.1576E 01
55.05	913.4	17.136	5.325	154.4	1647.5	1.4843E 04	7.6663E 01
88.07	572.4	14.355	6.016	135.8	1594.0	1.9604E 04	8.5246E 01
132.11	379.7	12.045	7.617	105.7	1505.0	3.2471E 04	9.7494E 01
214.66	231.6	11.236	11.243	73.5	1455.7	7.5544E 04	1.1963E 02

RUN NO 95 RE= 109.55 BR= 1.5146E-03

X/D	GZ	NU	DELTA	PRW	PRB	GR*W	GR*B
0	0	0	1.231	451.2	1052.4	0E 00	0E 00
5.5[illegible]	25455.6	44.675	2.756	182.[illegible]	1[illegible]49.4	1.3654E 04	2.6545E 02
16.51	5477.3	34.550	3.565	146.6	1044.4	2.2354E 04	2.7445E 02
33.03	4234.5	28.011	4.066	105.5	1034.9	4.5281E 04	2.6314E 02
55.05	2530.6	23.554	5.454	85.3	1022.3	5.9563E 04	2.9563E 02
88.07	1562.1	19.576	5.556	66.6	1005.6	5.6432E 04	3.1236E 02
132.11	1051.6	17.523	7.569	63.1	951.2	1.4146E 05	3.3755E 02
214.66	543.9	15.476	10.334	45.9	957.3	2.7732E 05	3.7325E 02

RUN NO 96 RE= 9.07 BR= 3.0429E-04

X/D	GZ	NU	DELTA	PRW	PRB	GR*W	GR*B
0	0	0	1.251	1991.5	3746.4	0E 00	0E 00
2.64	9300.7	35.936	2.337	996.2	3727.5	2.0460E 03	1.0172E 02
8.53	3122.9	26.166	3.051	770.5	3650.3	3.6955E 03	1.0594E 02
17.06	1553.5	20.668	3.964	566.0	3612.2	6.7550E 03	1.1238E 02
28.44	932.6	17.674	5.050	455.7	3527.2	1.1611E 04	1.2113E 02
45.50	560.6	15.309	6.574	346.5	3406.5	2.0683E 04	1.3491E 02
65.25	385.4	13.562	8.561	265.7	3249.1	3.7255E 04	1.5523E 02
91.00	287.7	12.215	11.276	196.6	3162.6	6.7591E 04	1.7785E 02
118.90	235.1	11.455	13.516	166.5	2952.6	1.0117E 05	2.0093E 02

RUN NO 97 RE= 35.79 BR= 1.3066E-03

X/D	GZ	NU	DELTA	PRW	PRB	GR*W	GR*B
0	0	0	1.290	1145.1	2591.6	0E 00	0E 00
2.64	25607.6	43.301	2.603	541.3	2583.7	1.1213E 04	3.2752E 02
8.53	5529.6	36.593	3.235	434.1	2567.3	1.6563E 04	3.3467E 02
17.06	4266.1	29.154	4.056	313.5	2542.3	3.4478E 04	3.4578E 02
28.44	2552.4	25.266	5.471	245.2	2519.2	5.1562E 04	3.6047E 02
45.50	1561.6	21.455	6.758	195.6	2466.2	1.0072E 05	3.8466E 02
65.25	1055.2	19.436	8.37[illegible]	166.1	2395.5	1.5855E 05	4.1775E 02
91.00	751.4	17.465	10.771	125.6	2355.7	2.7412E 05	4.5237E 02
118.90	547.6	16.235	13.666	101.9	2279.4	4.1152E 05	4.5612E 02

RUN NO 98 RE= 3.25 GR= [illegible]

X/D	GZ	NU	DELTA	PRW	PRB	GR*W	GR*B
0	0	0	1.304	1255.[illegible]	7123.1	0E 00	0E 00
5.60	9460.3	35.500	2.423	701.0	[illegible]7.1	5.[illegible] 02	4.1043E 00
16.[illegible]	3131.[illegible]	[illegible]	[illegible]	[illegible]	[illegible]	[illegible] 02	4.[illegible] 00
33.03	1502.7	20.007	[illegible]	[illegible]	[illegible]	1.[illegible] 03	5.[illegible] 00
55.05	935.2	17.533	4.540	336.3	5011.6	3.0152E 03	6.3636E 00
90.07	562.3	14.522	11.357	130.4	5573.0	1.9?72E 04	7.7242E 00
132.11	305.5	13.155	14.73?	102.2	4963.7	3.1567E 04	9.4372E 00
214.56	235.7	11.360	17.750	55.0	4625.0	4.6571E 04	1.1765E 01

RUN NO 99 RE= 33.60 GR= 6.3115E-03

X/D	GZ	NU	DELTA	PRW	PRB	GR*W	GR*B
0	0	0	1.313	757.6	4713.1	0E 00	0E 00
[illegible].50	25345.6	45.531	2.[illegible]	[illegible].3	4605.2	[illegible] 03	1.3[illegible] 01
16.51	5642.5	34.022	3.159	292.1	4390.1	2.6405E 03	1.5567E 01
33.03	4315.5	26.023	3.915	235.3	4152.6	4.1026E 03	1.7616E 01
55.05	2560.2	23.567	5.335	144.7	[illegible]3.2	[illegible] 04	2.[illegible] 01
90.07	1613.5	15.655	13.520	64.5	3542.2	1.30[illegible] 05	2.457[illegible] 01
132.11	1072.3	17.620	14.777	60.5	3265.0	1.5317E 05	3.0223E 01
214.56	[illegible]650.5	15.497	15.550	55.5	3079.7	1.69[illegible] 05	3.[illegible] 01

RUN NO 100 RE= 1.65 GR= 6.5350E-04

X/D	GZ	NU	DELTA	PRW	PRB	GR*W	GR*B
0	0	0	1.439	4305.6	20137.8	0E 00	0E 00
2.64	9352.9	36.460	2.742	2159.5	19612.7	4.4550E 02	3.7206E 00
8.53	3113.5	25.652	3.416	1708.9	16611.0	7.6562E 02	4.1908E 00
17.06	1553.7	21.154	4.293	1344.5	17372.3	1.3061E 03	4.9267E 00
25.44	929.6	18.196	5.213	1097.0	16044.2	2.0411E 03	5.9421E 00
45.50	579.0	15.482	10.756	520.0	14512.2	5.2465E 03	7.5538E 00
66.25	364.1	13.631	17.650	313.7	13021.1	2.6620E 04	9.6354E 00
91.00	250.7	12.449	21.954	253.2	11591.0	4.2375E 04	1.1306E 01
110.90	234.3	11.131	25.[illegible]	213.5	11248.5	5.6734E 04	1.4269E 01

RUN NO 101 RE= 7.29 GR= 2.5457E-03

X/D	GZ	NU	DELTA	PRW	PRB	GR*W	GR*B
0	0	0	1.423	2327.2	12479.6	0E 00	0E 00
2.64	25132.7	45.597	2.520	1117.7	12273.1	2.5936E 03	1.4406E 01
8.53	5571.4	36.514	3.378	921.0	11677.7	4.0803E 03	1.5519E 01
17.06	4161.0	29.118	4.197	752.6	11346.6	5.7957E 03	1.7228E 01
25.44	2565.0	[illegible]	5.531	551.5	10759.3	1.[illegible] 04	1.9460E 01
45.50	1562.2	21.427	12.02[illegible]	251.1	[illegible]	[illegible] 04	2.2152E 01
66.25	1355.5	19.[illegible]	13.01[illegible]	157.1	[illegible]8.2	1.[illegible] 05	[illegible] 01
91.00	775.7	17.275	19.155	[illegible]	[illegible]	1.[illegible] 05	[illegible] 01
110.90	635.7	15.904	21.605	157.1	5465.6	2.2545E 05	6.5456E 01

RUN NO 102   RE= 125.79   GR= 2.3170E-03

X/D	GZ	NU	DELTA	PRW	PRB	GR*W	GR*B
0	0	0	1.267	561.6	1384.0	0E 00	0E 00
5.50	24634.6	44.926	1.755	356.7	1361.9	1.25[illegible]E 03	7.5735E 01
16.51	6275.0	34.586	[illegible]	351.[illegible]	[illegible]	[illegible]	7.6616E 01
33.03	4135.1	26.323	2.2[illegible]	310.2	1376.7	[illegible]	7.7954E 01
55.05	2479.1	22.096	2.456	266.4	1361.7	2.6616E 03	7.5795E 01
88.07	1547.6	18.566	2.755	256.5	1345.2	3.3078E 03	8.2616E 01
132.11	1330.2	16.264	3.032	226.2	1325.1	[illegible]	8.674[illegible]E 01
214.66	682.1	14.059	3.536	196.2	1306.8	7.1061E 03	9.2356E 01

RUN NO 103   RE= 35.06   GR= 1.3376E-03

X/D	GZ	NU	DELTA	PRW	PRB	GR*W	GR*B
0	0	0	1.239	1046.5	3058.1	0E 00	0E 00
2.34	29464.6	47.590	1.827	1004.7	3032.6	1.0[illegible]67E 03	1.147[illegible]E 02
5.53	9464.9	34.020	2.075	946.5	3039.7	1.0543E 03	1.1659E 02
17.86	4238.0	27.251	2.346	825.[illegible]	3018.6	2.3372E 03	1.1571E 02
29.44	2558.1	23.553	2.66[illegible]	741.1	2996.4	3.0335E 03	1.2154E 02
47.56	1553.6	19.722	2.971	646.2	2962.7	4.1733E 03	1.2615E 02
66.25	1055.9	17.009	3.336	576.9	2916.4	5.4891E 03	1.3234E 02
91.00	785.3	15.152	3.545	492.7	2855.5	7.5717E 03	1.3934E 02
118.90	546.6	14.733	4.236	442.7	2831.5	9.5474E 03	1.4505E 02

RUN NO 104   RE= 229.61   GR= 4.2215E-03

X/D	GZ	NU	DELTA	PRW	PRB	GR*W	GR*B
0	0	0	1.260	474.6	1131.0	0E 00	0E 00
5.50	37042.2	56.763	2.311	246.4	1126.7	7.3623E 03	2.3217E 02
16.51	12341.0	35.677	2.617	215.0	1124.0	1.0343E 04	2.3566E 02
33.03	6165.7	31.629	3.012	184.5	1116.7	1.4664E 04	2.4106E 02
55.05	3695.6	26.462	3.566	154.9	1107.0	2.1627E 04	2.4644E 02
88.07	2366.2	21.555	4.181	136.4	1092.5	3.2159E 04	2.5951E 02
132.11	1554.5	19.663	4.595	117.5	1073.6	4.6025E 04	2.7546E 02
214.66	940.7	17.347	5.651	105.6	1051.2	5.2636E 04	2.9920E 02

RUN NO 105   RE= 236.49   GR= 4.2056E-03

X/D	GZ	NU	DELTA	PRW	PRB	GR*W	GR*B
0	0	0	1.259	473.1	1126.0	0E 00	0E 00
5.50	37019.2	51.167	2.437	231.6	1123.4	9.8780E 03	2.7041E 02
16.51	12332.4	39.157	2.611	196.2	1115.0	1.4355E 04	2.7565E 02
33.03	6163.7	32.111	3.346	164.6	1109.5	2.1613E 04	2.6221E 02
55.05	3652.1	26.543	3.526	139.1	1096.5	3.1542E 04	2.9322E 02
88.07	2363.5	22.292	4.377	117.3	1076.4	[illegible] 04	3.0228E 02
132.11	1552.1	19.592	4.977	107.6	1059.3	5.7151E 04	3.2936E 02
214.66	988.9	17.666	5.569	95.4	1035.0	7.5331E 04	3.5976E 02

RUN NO 107 RE= 53.22 GR= 3.2[illegible]E-03

X/D	GZ	NU	DELTA	PRW	PRB	GR*W	GR*B
0	0	0	1.23[illegible]	1307.4	25[illegible]4.5	0E 00	0E 00
2.54	37961.6	54.[illegible]	2.344	[illegible]	2573.5	7.1[illegible]32E 03	3.29[illegible]1E 02
5.83	12654.2	41.[illegible]	2.75[illegible]	[illegible]	[illegible]	1.1[illegible]E 04	3.5[illegible]E 02
17.3[illegible]	6322.4	3[illegible]	[illegible]	44[illegible].1	[illegible]	1.[illegible]E 04	3.4[illegible]E 02
25.44	5759.7	26.206	4.171	364.5	2519.1	2.6106E 04	3.547[illegible]E 02
45.50	2365.0	23.756	5.055	295.3	24[illegible]5.2	4.40[illegible]1E 04	3.7134E 02
63.25	1573.6	21.509	5.734	266.6	24[illegible].2	[illegible]E 04	3.9424E 02
91.00	1177.5	19.154	6.623	224.2	25[illegible].6	5.1[illegible]11E 04	4.15[illegible]E 02
110.90	364.5	17.562	7.292	2[illegible]	[illegible]7.2	1.[illegible]E 05	4.4109E 02

RUN NO 103 RE= 53.26 GR= 3.2727E-03

X/D	GZ	NU	DELTA	PRW	PRB	GR*W	GR*B
0	0	0	1.254	1366.6	2552.5	0E 00	0E 00
2.54	37300.2	54.526	2.533	615.4	2575.9	1.6679E 04	3.6113E 02
5.83	12652.5	41.362	3.605	502.5	2562.3	1.6667E 04	3.8769E 02
17.35	6320.9	35.157	4.031	377.4	2541.5	3.6[illegible]21E 04	3.9[illegible]E 02
25.44	3766.2	26.764	4.614	310.4	2513.6	4.5154E 04	4.1265E 02
45.59	2363.6	24.314	5.782	256.3	2457.1	5.9115E 04	4.3677E 02
63.25	1572.2	22.044	6.554	222.4	2413.5	5.5[illegible]E 04	4.6776E 02
91.00	1176.6	19.675	7.096	191.5	2557.2	1.02[illegible]E 05	5.0151E 02
110.90	963.5	16.263	5.609	176.4	2613.3	1.7674E 05	5.3117E 02